A NUMERICAL SIMULATION AND EXPERIMENTAL STUDY OF VORTEX RINGS

A NUMERICAL SIMULATION AND EXPERIMENTAL STUDY OF VORTEX RINGS

By:

JIANQIN WANG, B. ENG

A Thesis

Submitted to the School of Graduate Studies

in Partial fulfilment of the Requirements

for the Degree Master of Engineering

McMaster University

February 1999

MASTER OF ENGINEERING (1999) McMaster University
(Mechanical Engineering) Hamilton, Ontario

TITLE: A Numerical Simulation and Experimental Study of Vortex Rings.

AUTHOR: Jianqin Wang, B. Eng.

SUPERVISOR: Dr. B. Latto

NUMBER OF PAGES: xv, 100.

ABSTRACT

The objective of this research was to investigate parameters affecting vortex ring formation and propagation and their application to mixing of fluids. To this end both empirical and numerical simulation experiments were conducted.

The empirical experiments involved observations and measurement of the volume, displacement and velocity of vortex rings generated from a 5 cm diameter tube. The results revealed that there is an optimal range of generation injection velocity for various mixing requirements.

The numerical simulations were done using a commercial package, FLUENT. Both tube type and plate orifice type vortex ring generators were investigated. Also the affects of a central shaft and various projections on the control of the motion of a vortex ring. All models considered a polar model cylindrical tank with a diameter to height ratio of 3:10. The average injection velocity was in the range of 0.7 m/s to 3 m/s.

When simulating the tube type generator various injection velocity profiles and value were investigated, which resulted in a fitted correlations of non-dimension displacement versus non-dimension time as a function of infection profile. In order to control the forward motion of vortex rings some obstructions were considered. It was found that the trajectory and energy of a vortex ring can

be controlled with shape and geometries of baffles.

In the simulations for the orifice plate type generator, a moving mesh technique was used. As expected a pair of vortex rings were produced per half cycle of the plate oscillation, but they did not travel as fast as expected. Recommendations have been made to improve the simulation accuracy.

It has also been found that the FLUENT package will not properly simulate turbulent vortex rings. However, this may be because a vortex ring is not truly homogeneously turbulent. The use of a laminar model appears to give quite good agreement with empirical data for tube type vortex ring generator.

The results of this research are expected to be useful for the optimization of the design of vortex ring mixing systems.

ACKNOWLEDGMENTS

I would like to ex press my sincere appreciation to my supervisor Dr. B. Latto for giving me the opportunity to work on this project and for his guidance, assistance and encouragement throughout this study. I would also like to thank the technicians in the Department of Mechanical Engineering for their valuable help in setting the experimental apparatus and repairing computer. I would especially like to thank Dr. Y. Sheng for the helpful discussions of using FLUENT and GeoMesh.

TABLE OF CONTENTS

LIST OF FIGURES

LIST OF TABLES

NOMENCLATURE

A, B, C, a, b, c - constants

D - diameter of the injection orifice

D_d - diameter of baffle

D_i - orifice equivalent diameter of plate

D_o - overall diameter of plate

D_r - diameter of vortex ring

K - correction

k - fraction of the displaced volume passing through the orifice

L - length of theoretical fluid slug

n - speed of motor (rpm)

P_{min} - pressure at the eye of vortex ring

R - radius of the injection orifice

Re - injecting Reynolds number

Ri - Richardson number

R_r - radius of vortex ring

S - piston stroke

s - plate moving distance

t - time from beginning of injection

T_i - period of injection

U - velocity of vortex ring (axial component)

U_i - injection velocity

U^* - average injection velocity

$U_i(t)$ - injection velocity profile

V - volume of vortex ring

V_i - theoretical volume of vortex ring

X - displacement of vortex ring during propagation (axial component)

X_m - Maximum penetration depth of a vortex ring into a stratified layer

Γ - circulation

CHAPTER 1

INTRODUCTION

Mixing of liquids is one of most common energy intensive operation in the industries involved with the manufacture and processing of liquids and solid suspension. The majority of industries currently use rotary or static type mixers. A number of factors determine the efficiency of a particular mixing process, such as mixing time, ability to produce a homogeneous or dispersed liquid, and the power consumption. Latto[1] has pioneered the development of a new group of mixers which he calls vortex ring mixers (VRM's), and have wide applications. These mixers generate fluid vortex rings in a controlled manner and eject them into through the fluid being mixed / agitated. In this manner controlled mass transfer within the fluid can be achieved. Both theoretical and empirical experiments have clearly demonstrated the value of these novel fluid mixers (1987, 1989, 1990, 1992, 1994), which normally comply with the requirements of homogeneity, maintenance and energy. Two main types of vortex ring mixer have been developed by Latto: (1) tube type in which a vortex ring is generated by the controlled ejection of a mass of fluid through a tube, and (2) plate type in which a plate is oscillated in a

---

[1]Department of Mechanical Engineering at McMaster University and MIXIS Corporation Dundas Ontario Canada.

controlled manner to eject a mass of fluid through an orifice to create a vortex ring.

A vortex ring is a rotating toroidal ring of fluid which has an overall oblate spheroid shape. The streamlines of the internal flow can be thought of as closed curves to the same degree that the flow can be thought of as steady in a translating coordinate system, (see Figure 1.1 and 1.2). The internal rotation of the fluid about its "eye" results in the highest fluid shear at the eye, with almost zero shear at the outer surface where the fluid velocity relative to the ambient fluid is very low. Due to the fluid motion around a vortex ring as it translates, both viscous shear and the form drag on the vortex ring are quite low. This permits a vortex ring to travel considerable distances after it is formed. As a vortex ring travels through a fluid there is some mass transfer between the ambient fluid and the vortex ring. This results in a wake of discharged fluid. The combination of the wake and the transport of mass within a vortex ring creates an excellent mass transport mechanism. The continuous generation of vortex rings within a fluid can therefore create both vortex ring mass and convective mass transfer within the bulk of the fluid. This can result in an efficient mixing process with low energy input.

Another property of vortex rings is that they usually have linear motion and are therefore directionally stable. The trajectory of a vortex ring can be affected by their proximity to solid boundaries or to other vortex rings. Also, a vortex ring trajectory can be controlled by obstructions in its path. A convenient geometry for a vortex ring mixer is the use of a central drive shaft. It may also be necessary to use flow deflectors or baffles. These two aspects can be used to control the

direction and motion of vortex rings and therefore the motion of the bulk of the fluid. An example of such application is the mixing of fluids, such as paint, when energetic agitation is often required but without the ingestion of air which may occur due to excessive surface agitation.

In order to be able to design practical vortex ring mixers for specific application either empirical experiments or numerical analysis must be done. It is sometimes difficult to perform empirical experiments due to the size of the proposed system or the type of fluids being used, such as slurries or highly non-Newtonian fluids. The use of numerical analysis has been proven to be of considerable value in predicting the behaviour of particular system geometries.

A number of papers have been published concerning the use of numerical analysis for predicating vortex ring behaviour, but these were mainly concerned with the formation of vortex rings. Of considerable concern from a practical aspect are the life and behaviour of vortex rings after they have been generated and the behaviour of the fluid around the generating device. Latto (1990), Papple (1991), and Hua (1994) developed a program which included Bousinesq approximation for buoyancy effects. Although the computer program gave what appeared to be excellent and interesting results, at the time it was developed it did require the computational power of a super computer.

Although a great deal of effort has been put into fundamental studies of vortex rings, there are a number of practical problems associated with the design and operation of vortex ring mixers, which need to be investigated, such as the

vortex ring behaviour with different injection velocity profiles and values; and the practical methods for controlling vortex ring behaviour within the fluid being mixed by introducing obstructions on the path of a vortex ring. This thesis attempts to address these aspects.

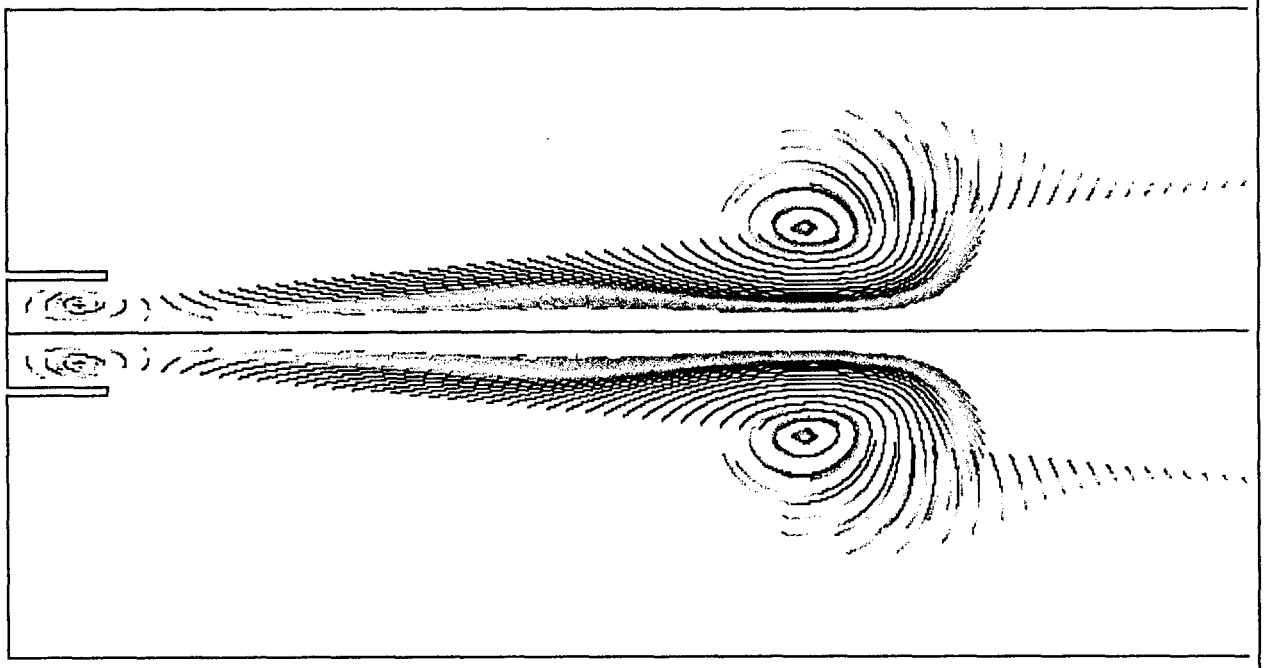

Figure 1.1
Streaklines

Feb 01 1999
Fluent 4.47
Fluent Inc.

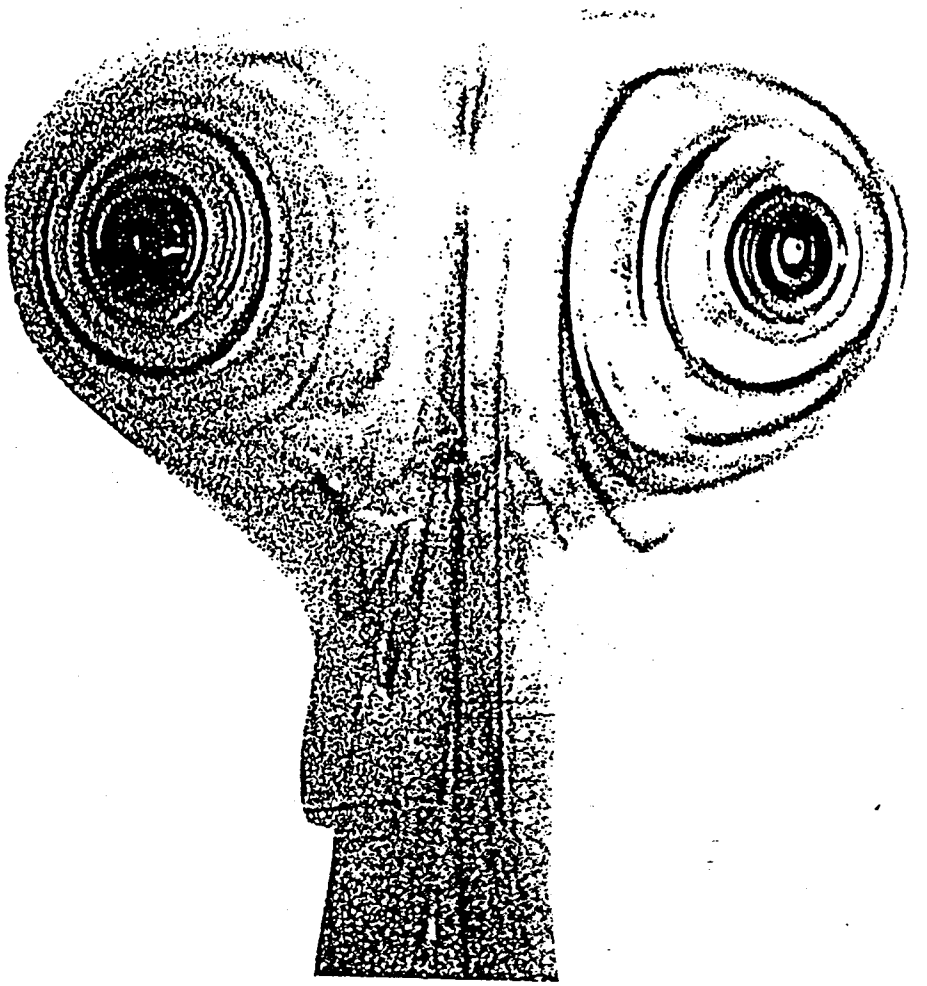

Figure 1.2 A vortex ring

CHAPTER 2

LITERATURE REVIEW

Vortex rings are a particularly fascinating fluid mechanics phenomenon. They can be observed at the commencement of a jet of fluid passing through an orifice; volcanic eruptions; the resulting mushroom cloud from a nuclear explosion, or when raindrops impact a water surface in which vortex rings can be identified as playing a major role. The generation, formation, and propagation of vortex rings have been the subject of numerous experimental, analytical and numerical studies. Since the first recorded observation of vortex rings were made by Rogers (1858), various aspects of vortex ring have been studied extensively by a number of researchers over the last century.

The earlier studies were primarily on flow visualization or inviscid flow analyses. The earliest mathematical model is "Hill's Spherical Vortex" (1894), which assumed that an inviscid fluid occupies a spherical envelope. Another model was developed by Lamb (1933), whose premise was that the primary vorticity is contained in a torus whose core is smaller than that of the circumscribing torus. Recently, the scope of the research on vortex rings is much wider than before, but the topic has become specialized, such as: the formation and motion of vortex rings

(Maxworthy (1977), Didden (1979), Glezer (1988), Nitsche (1994), Heeg (1997), and Gharib, et al. (1998)); the impact of a vortex ring on a wall (Walker (1987) and Carnevale, et al. (1997)); vortex rings traversing a fluid with a step change in density (Linden (1973) and Hecht (1980)); the dynamics of a vortex ring moving orthogonally to the rotation vector of a uniformly rotating fluid (Eisenga, et al. (1998)), and fluid mixing using vortex rings (Baird, et al (1979, 1992) and Latto (1987, 1989, 1992)).

In view of the spectrum of research that has been done thus far, the focus of this literature review will be mainly concentrated on two particular areas: (1) the formation and development of a vortex ring; and (2) the application of vortex rings for mixing of fluids.

2.1 The Fundamentals of the Formation and Development of A Vortex Ring

A vortex ring can be generated by impulsively ejecting a slug of fluid through an orifice. As the jet of fluid passes through the orifice, vorticity begins to accumulate in the boundary layer of the jet. When this jet of fluid leaves the orifice, the vorticity in the boundary layer causes the fluid to roll up to form a vortex ring that has a toroidal core and the overall shape of an oblate spheroid. The rolling up process is discussed by Maxworthy (1977) and depicted in Figure 2.1.

The important parameters for a fully formed vortex ring are its diameter D_r,

circulation Γ and its translation velocity U, which were considered in Irdmusa and Garris's (1987) experimental investigation. It is generally agreed that vortex ring properties mainly depend on two criteria:(1) the type of generator and its geometric configuration; and (2) the initial conditions which include stroke L and the fluid injection velocity history Ui(t). Some of these parameters can be combined into the Reynold number for identifying generation and flow conditions.

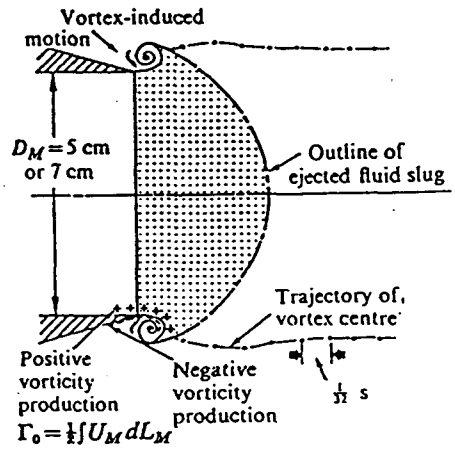

Figure 2.1 Rolling up process of a vortex ring during its generation at a tube. Maxworthy (1977)

The duration of a jet plays an important role in the successful formation of a vortex ring. If the volume of fluid pulsed is not enough, the vortex ring does not accumulate enough vorticity in its core and is unable to form properly and travel away from the orifice. On the other hand, if the volume of fluid ejected is too large an initial primary vortex ring develops and leaves the orifice when it has reached an optimum size and the forming jet will continue and may produce a second vortex ring. This second vortex ring usually interacts with the primary vortex ring and may

destroy it. By studying the unsteady velocity field in the nozzle-exit plane during the rolling up process, Didden (1979) found that the diameter and circulation of the formed vortex ring depend on the parameter L/D, and are independent of the average injecting velocity U_i within a certain Reynolds number range. Baird et al (1979) recommended that for a most efficient laminar vortex ring the L/D ratio should preferably be the range 0.7 to 2.8. Later Latto (1987) suggested that this range should be 1.5 to 3.5 with an optimum value of L/D of about 2.8. Virtually any value of L/D will result in the generation of a vortex ring, but as stated previously the volume of fluid ejected will affect the formation of a vortex ring. When L/D <1.5, a vortex ring may be weak , and when L/D > 3.5 an initial primary vortex ring develops and leaves the orifice as it reaches an optimum size and another vortex ring is formed immediately behind the primary vortex ring. The following ring may result in an instability of the primary ring. Recently, Gharib, et al (1998) studied experimentally the effects of a wide range of L/D ratios using digital particle image velocimetry (DPIV). They found that the flow field generated by large L/D consisted of a leading vortex ring followed by a trailing jet, and flow fields generated by small stroke ratios showed only a single vortex ring, as shown in Figure 2.2. The transition between these two distinct states was observed to occur at a stroke ratio in the range of 3.6 - 4.5 for a broad range of flow conditions. This is in agreement with the deductions of Latto over a decade ago.

The characteristics of a vortex ring depend strongly on the geometry boundary condition. Since all of the vorticity essential to the existence of a vortex

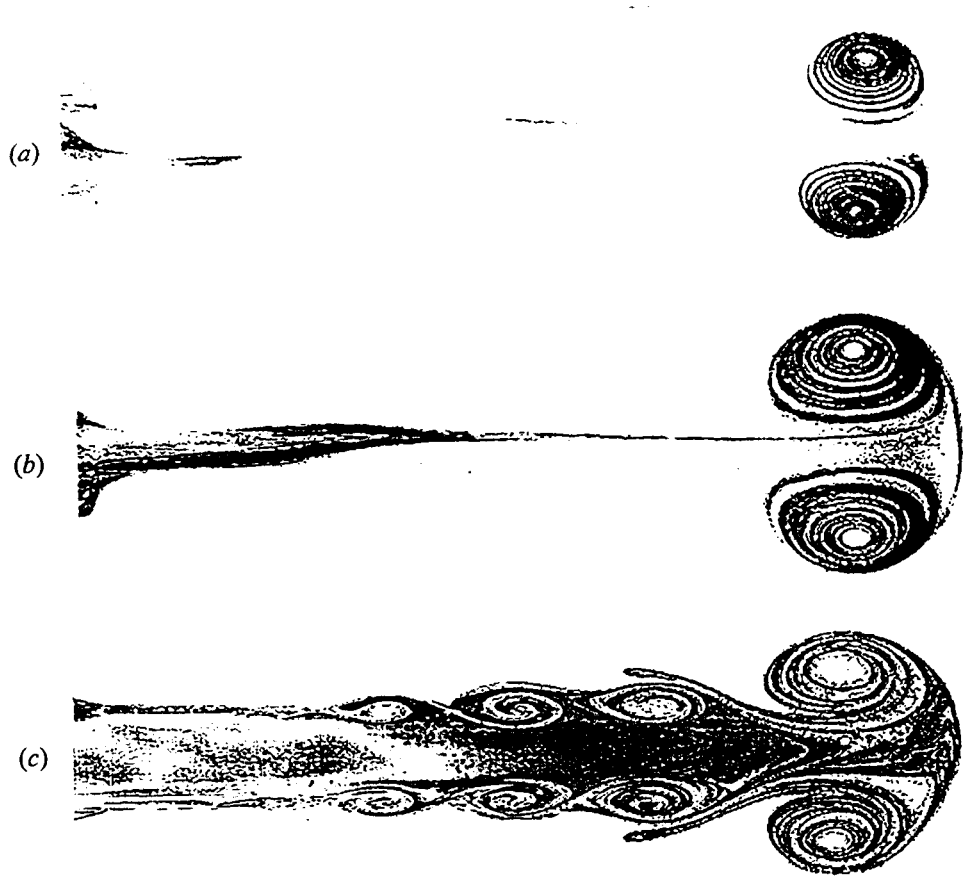

Figure 2.2 Visualization of vortex rings at X/D ≈ 9 for (a) L/D = 2, Re ≈ Γ/ν ≈ 28; (b) L/D = 3.8, Re ≈ 6000; and (c) L/D = 14.5. All the cases were generated by an impulsive piston. Gharib, et al (1998)

ring is generated in the boundary layer prior to the formation of the ring, different geometries will produce different amounts of vorticity. Two very common structures of vortex ring generation and boundary conditions are shown in Figure 2.3. The data of Irmusa and Garris (1987) show that tube generated vortex rings tend to have a slower translation velocity and larger volume than orifice generated vortex rings for a given injection condition and orifice diameter. Another strong effect on the formation and developing of a vortex ring is the injection velocity history $U_i(t)$.

Didden's (1977) work shows that different injecting velocity programs will lead to different characteristics of vortex rings, see Figure 2.4.

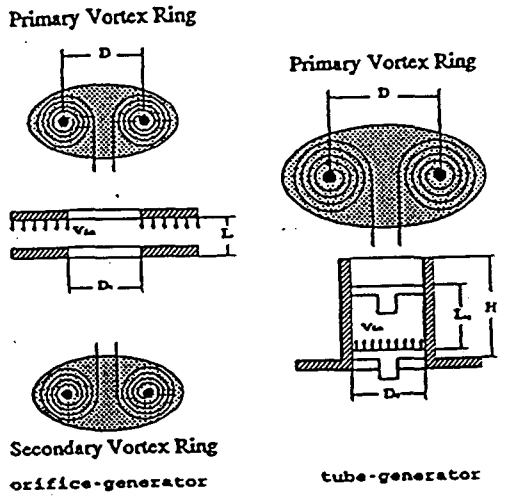

Figure 2.3 Two types of vortex ring generators. Hua (1994)

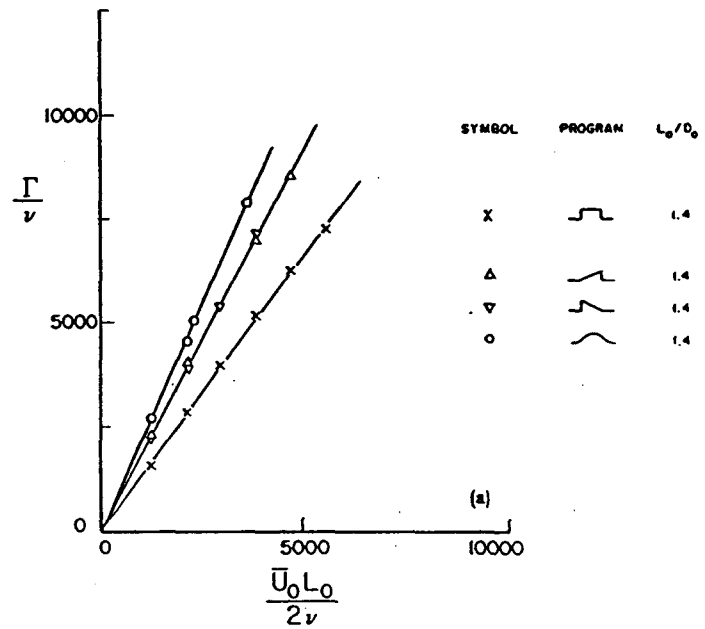

Figure 2.4 Circulation for the laminar vortex rings produced with various injection velocity profiles. Didden (1977)

Both Honji (1976) and Maxworthy (1977) investigated the penetration of vortex rings through stratified fluid layers. Honji observed how a vortex ring behaved as it passed upward through a relatively sharp density gradient. It was observed that, as a vortex ring reached an interface, it elongates considerably in the direction of motion. Maxworthy investigated vortex rings travelling downwards through a stratified fluid with a density gradient that nearly extended all the way to the bottom of the tank. He observed a decrease in the diameter of the vortex ring as it passed through the stratified layers. He also noticed a decrease in the velocity of the vortex ring, leading to its eventual destruction. He explained that the decrease in the vortex ring diameter was a consequence of layers of the vortex ring core being stripped away and mixing into the outer flow regions of the ring. This occurs because buoyancy forces destabilize the interface between the core and the outer flow.

Didden's (1979) work has been very popular among vortex ring researchers, since it provides a clear picture of the role of internal and external boundary layers in the formation process and circulation of the vortex ring. Utilizing similarity theory, Saffman (1978) and Pullin (1979) obtained expressions for the vortex ring trajectory, circulation and its vorticity distribution. Weigand & Gharib (1997) revisited the vortex ring problem using digital particle image velocimetry (DPIV). They showed that vortex rings generated by a tube type generator possess a Gaussian vorticity distribution in their core region.

Numerical simulation and development of computer codes have a

considerable value in the prediction and understanding of the behavior of a vortex ring. Due to the complexity of the problem and the lack of the required high-speed computer technology numerical studies of vortex rings started much later than empirical studies. Until about 1970, publications on numerical studies were primarily concerned with the behavior of vortex rings traversing a fluid.

Friebel and Rath (1987) simulated the behavior of laminar vortex rings from the formation phase to the viscous decay by solving the two dimensional Navier-Stokes equations in cylindrical coordinates. They investigated the influence of various parameters on the vortex generation process, and simulated the behavior of vortex rings in the vicinity of different obstacles, such as walls and free surfaces. Their numerical simulation results are in good agreement with their experimental data.

The formation and transport of vortex rings in a thermally stratified fluid was studied numerically by Latto et al. (1990) and Papple et al. (1991) using a control-volume based finite difference method. The formation of vortex ring was simulated by single or periodical injection of a quantity of the fluid through a tube centrally located near a free surface in a tank initially containing a stably stratified fluid. Their results showed that the criteria for the penetration of a buoyant vortex ring through a fluid having a step change in density is a function of the Richardson number Ri (the Ri number is the ratio of buoyant force and inertia force). They showed that when $Ri < 0.1$ buoyant vortex rings can penetrate from the lower density into the higher density fluid, creating significant mixing in the bulk of the fluids. However,

for Ri > 0.1, a vortex ring cannot penetrate the high density fluid and mixing can only occur at the interface. That is, when Ri > 0.1 the fluid interface behaves as though it were a solid boundary.

Based on the work of Latto and Papple, Hua (1994) further developed several numerical models to carry out the numerical simulations of vortex ring penetrating in both stratified Newtonian fluid and non-Newtonian fluid. His results showed that the penetration and trajectory of a vortex ring through a density gradient are independent of the defined injection Reynolds number (Re), but as previously indicated primarily dependent on the Richardson number (Ri). Laminar vortex rings in a power law fluids behave inviscidly and the same as in Newtonian fluids for a certain range of injection Reynolds numbers. The trajectories and velocities of a vortex ring are basically the same for non-Newtonian and Newtonian fluids. However at a distance from the generating orifice or after a certain time which is a function of the injection time, for shear thinning fluids notably more motion and vorticity are created in the central column and at locations remote from the generating orifice and the actual vortex ring, than shear thickening fluids.

More recently, James & Madnia (1996) presented a numerical study of vortex ring formation for different velocity-time generator configurations. They concluded that the total circulation and impulse in the flow field of the ring are approximately the same when using nozzles with and without a vertical wall at the nozzle exit plane. Heeg and Riley (1997) presented the results from numerical calculations based upon the Navier-Stokes equations at relatively high Reynolds numbers, for

the formation of a vortex ring when the fluid is ejected from a circular tube. Their results basically agree with the experiments of Didden (1979) except for the rate of shedding of circulation during the initial stages of ring formation, which was substantially higher than that predicted by Didden.

2.2 Mixing Application of Vortex Rings

Although there have been a notable number of publications on the theory and basic experiments pertinent to the formation and development of vortex rings, only a few publications have addressed the use of vortex rings for practical applications. In 1972 Mattingly suggested a number of applications for vortex rings (Kendig, 1972), but these applications were not tried until Baird, et al. (1979) investigated mixing of stratified fluids using vortex rings both in his laboratory and the Hamilton Harbour. The tests indicated that a vortex ring mixer is considerably more efficient than rotary impellers in mixing stratified liquids. A little later, Latto developed vortex ring mixers for a wide range of applications, such as the mixing of sedimentary slurries, Newtonian and non-Newtonian liquids and the gasification of liquids. Latto (1987, 1988, 1989, 1990, 1991, 1992) and Baird et al. (1979, 1992) have demonstrated the practical use of vortex ring mixers for wide range of applications.

In order to efficiently design vortex ring mixers an accurate assessment of the vortex ring behavior for various types for generator and the prediction of mass transfer is very important. Perrons (1995) empirically investigated the life of vortex

ring generated from a tube and observed how variations in the stroke speed and stroke length of a tube type vortex ring mixer, affect the vortex ring it generated.

Ho (1991) did an experimental study of the penetration and propagation of vortex rings in stratified hot/cold water and water/aqueous saline solution, and numerically simulated the behavior of vortex rings adjacent to a solid flat boundary. His experiments showed that after a vortex ring penetrated through the interface of the stratified layer, the fluid inside the ring mixed with the surrounding fluid. The amount of mixing depended on the depth of penetration of the ring into the stratified layer. He obtained the following empirical relationship to predict the maximum penetration depth of a vortex ring into a stratified layer:

$$X_m/R = -29.7 \log_{10} Ri - 22.7 \qquad (2.1)$$

Ho also attempted a relatively simple analytical prediction of the trajectory of a vortex ring traveling parallel to a flat plate. His results showed that a vortex ring would slow down and turn away from its original path towards a solid boundary. In order to minimize the effect of the wall, Ho suggested that the center of the generation orifice should be 7.5 times the radius of the injection orifice from the wall.

Later Latto proposed the use of various obstructions to control the trajectory of a vortex ring and has applied for a patent for such devices. Lumley (1997) under Latto's supervision investigated practical methods for causing premature vortex ring decay by introducing obstructions in the path of the vortex ring, which may be used in mixing applications where it is undesirable that vortex rings break through the free surface of the mixture. Lumley used a commercial Computational Fluid Dynamics

(CFD) software package FLUENT to simulate vortex rings with baffles in the way. His results showed the rate of deceleration and the growth rate of the vortex ring radius both depend on the diameter of the obstruction involved.

Hua (1994) performed experiments and numerical simulations for primary and secondary vortex rings generated by a plate type generator. Figure 2.5 shows a series of vorticity contour plots for an orifice plate. When an orifice plate moves down a primary vortex ring is ejected up, and when the plate is abruptly stopped the inertial force of the fluid behind the generating plate produces a secondary vortex ring which travels in an opposite direction to that of the first one. Two vortex rings are generated radially if there is a gap between the plate and the wall of a tank. Consequently, a plate type generator can produce at least four times as many vortex rings as a tube type generator. Even though the size of the vortex rings is smaller than that of those generated by a tube, the total volume contained by these vortex rings during one cycle of the plate generator is much larger than that of a vortex ring formed by a tube generator. Therefore, a plate can create more mass transfer and mixing than a similar size tube generator.

Over the period 1978 to 1998 Latto has devoted a great deal of effort to the study of vortex ring mixing and mixers, and made considerable advancements in this field. The research by Latto over the past nearly two decades has been primarily concerned with various aspects of vortex ring generation, such as an attempt to obtain useful data for the design of vortex ring generators and

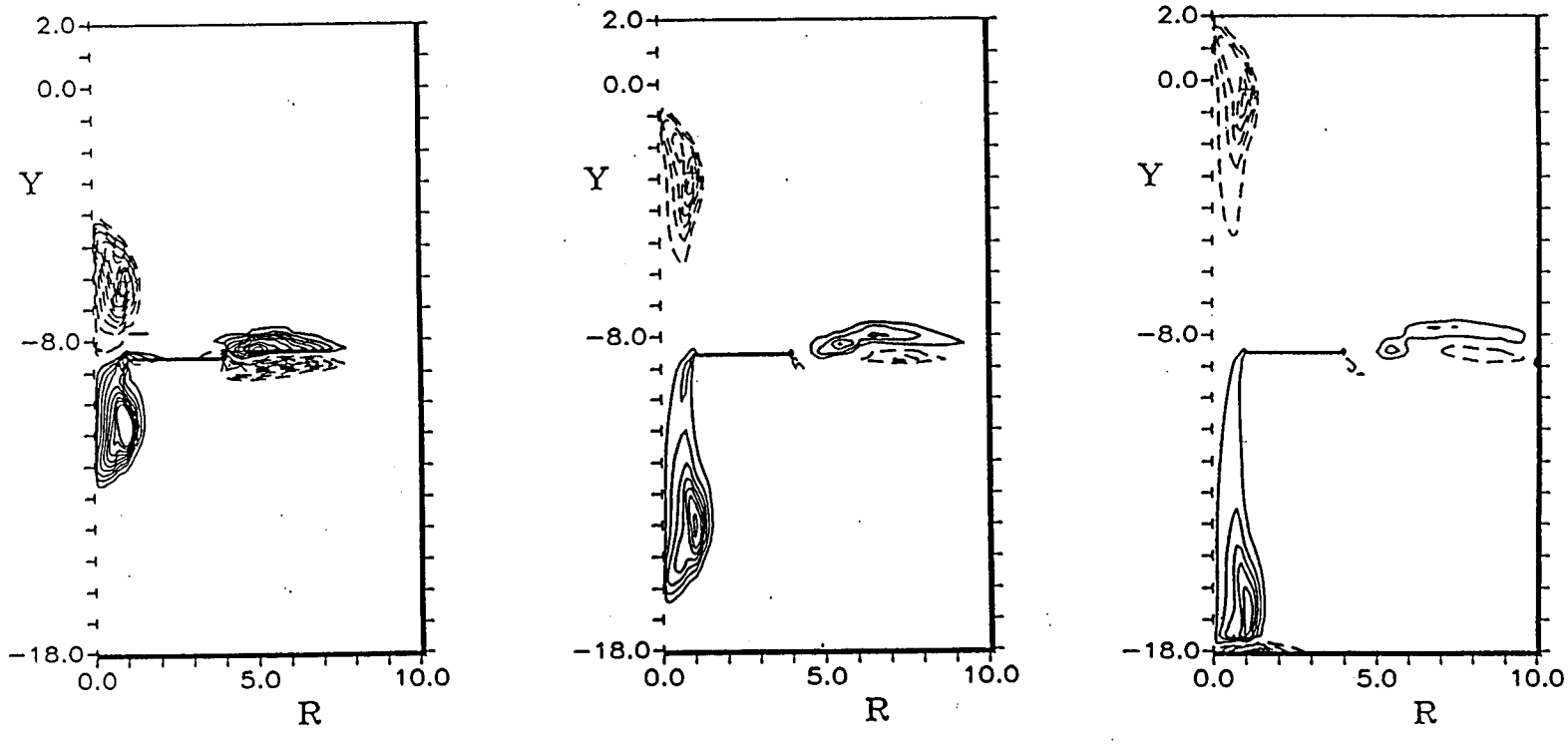

Figure 2.5 A series of vorticity contour plots for an orifice plate. Hua (1994)

consequently mixing equipment using the vortex ring phenomena. This was done to achieve optimal generation of vortex rings and investigate the affects of frequency of generation of vortex rings and adjacent walls and baffles on the trajectories of and decay of vortex rings. The theoretical analysis and subsequent empirical research on the optimal spacing of generators and generator to wall distance has resulted in some general conditions for the designing of mixing systems. The two main types of vortex ring mixers developed by Latto are tube type mixers Figure 2.6 and various plate type mixers Figure 2.7.

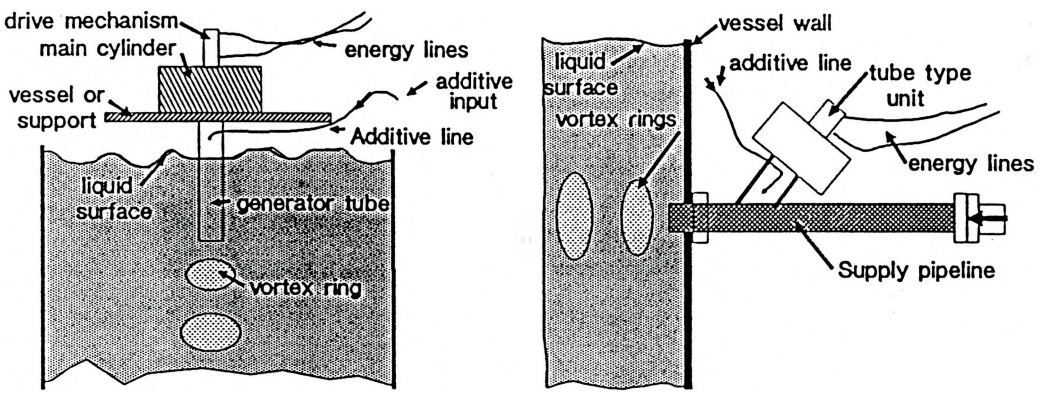

Figure 2.6 Typical tube type vortex ring mixers: (a) self contained unit with fluid addition; (b) unit installed in a pipeline. Latto (1992)

Of primary interest to users of a mixer is the homogeneity of the mixing, low maintenance and low energy consumption amongst others. Although the majority of industries currently use rotary or static type mixers, vortex ring mixers are beginning to be utilized because of the low energy consumption and the relative

ease of application and control. Investigations conducted by Latto (1997) have demonstrated the usefulness of vortex rings to a wide range of mixing applications, such as the mixing of non-Newtonian substances, polymer solutions, aeration of large tanks of water agitation of digester liquid, and so on.

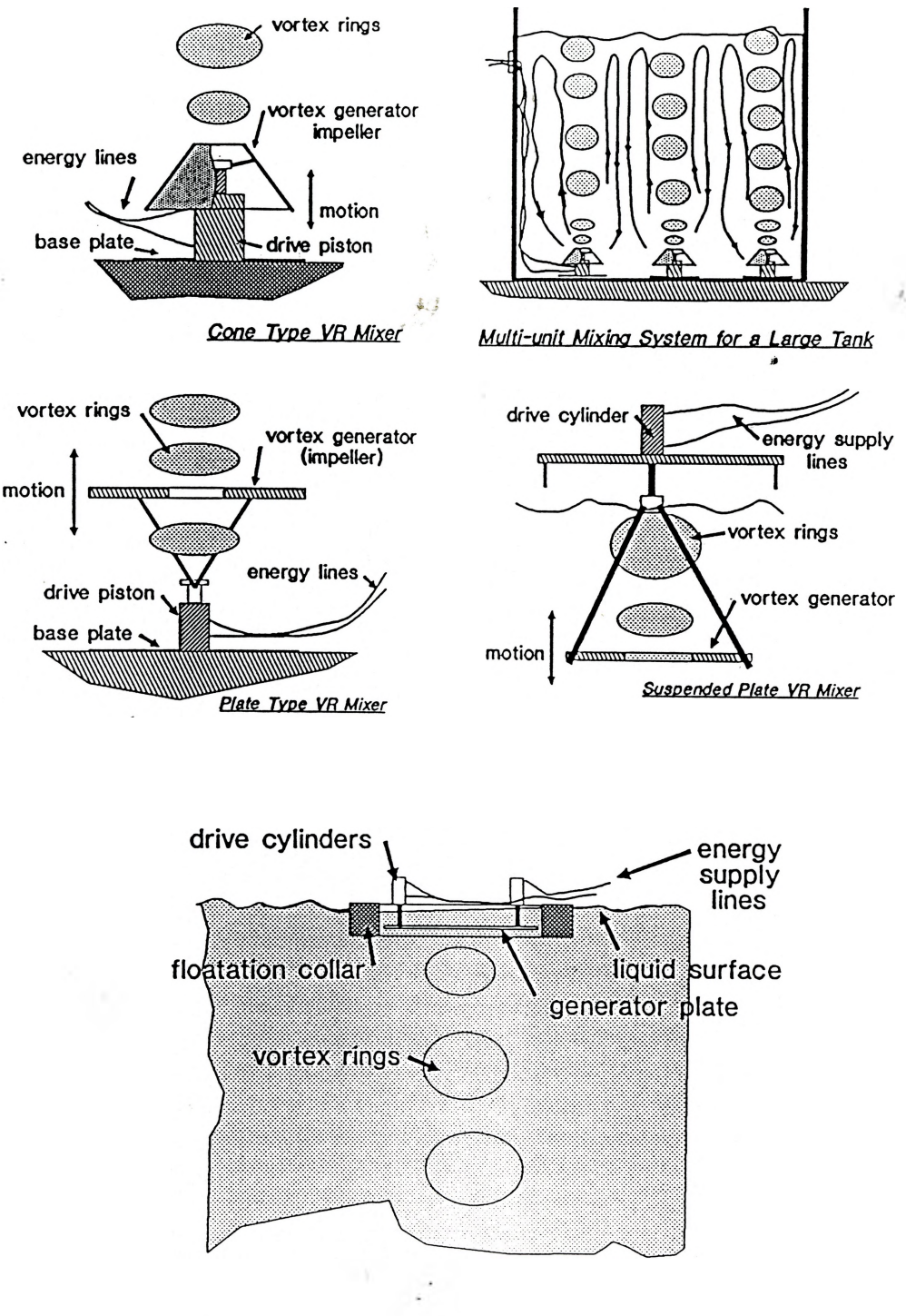

Figure 2.7 Typical plate type vortex ring mixers showing flat plate, conical, suspended plate, and multi-unit installations and a plate unit with a floatation collar. Latto (1992)

CHAPTER 3

EXPERIMENTAL STUDY OF VORTEX RINGS

3.1 Introduction

As previously stated, a vortex ring primarily creates transport of mass within the vortex ring itself, the fluid being mixed due to the mass transported within, but also some mass transfer between the ambient fluid and the vortex ring (wake), which also creates fluid convection within the bulk of the fluid. Thus the mixing efficiency of a vortex ring mixer depends on the combination of the mass transport of a vortex ring and the wake together with convected mass transfer. Therefore, from a design aspect, it is important to know the mass or volume of a vortex ring at the generation phase. It is also useful to be able to predict the life and behaviour of a vortex ring as it travels through a fluid. Unfortunately, very few publications have referred to this subject. Some researchers have made contributions on measurement and calculation of the circulation of a vortex ring, such as Didden (1977) who measured the circulation for laminar vortex rings produced with various velocity programs; and Glezer (1981) who derived an equation to calculate the initial circulation. However, there appears to be very few publications pertinent to the

mass or volume of a vortex ring for mixing application.

It is difficult to calculate or measure the mass or volume of a vortex ring using numerical simulation, since it is difficult to determine the exact boundary of a vortex ring. Consequently, an empirical experiment was designed to fulfill this task. An important aspect in the generation of vortex rings is the injection velocity profile. In order to investigate the effect of the injection velocity profile for the propagation of a vortex ring and compare the numerical results with empirical data, it was necessary to observe and measure a vortex ring during its progress, that is its position and apparent size as a function of time. In order to do this an existing dye injection system had to be modified for this study.

3.2 Experimental Apparatus

The experiments were carried out in water contained in a plexiglass tank having a 0.3 m square cross section and a 2 m depth. The tank is supported on a steel frame, as indicated schematically in Figure 3.1. Vortex rings are generated using a tube type vortex ring generator having an inside diameter of 5 cm and the tube exit orifice suspended just below the free water surface. A generated ring moved vertically downward in the tank, and could be illuminated and viewed from the four vertical sides of the tank. A mirror system located below the floor of the tank, permitted the axial observation of a vortex ring as it progresses towards the bottom of the tank, and therefore the cross section shape change of a vortex ring.

As previously stated, when generating a vortex ring, the injection velocity

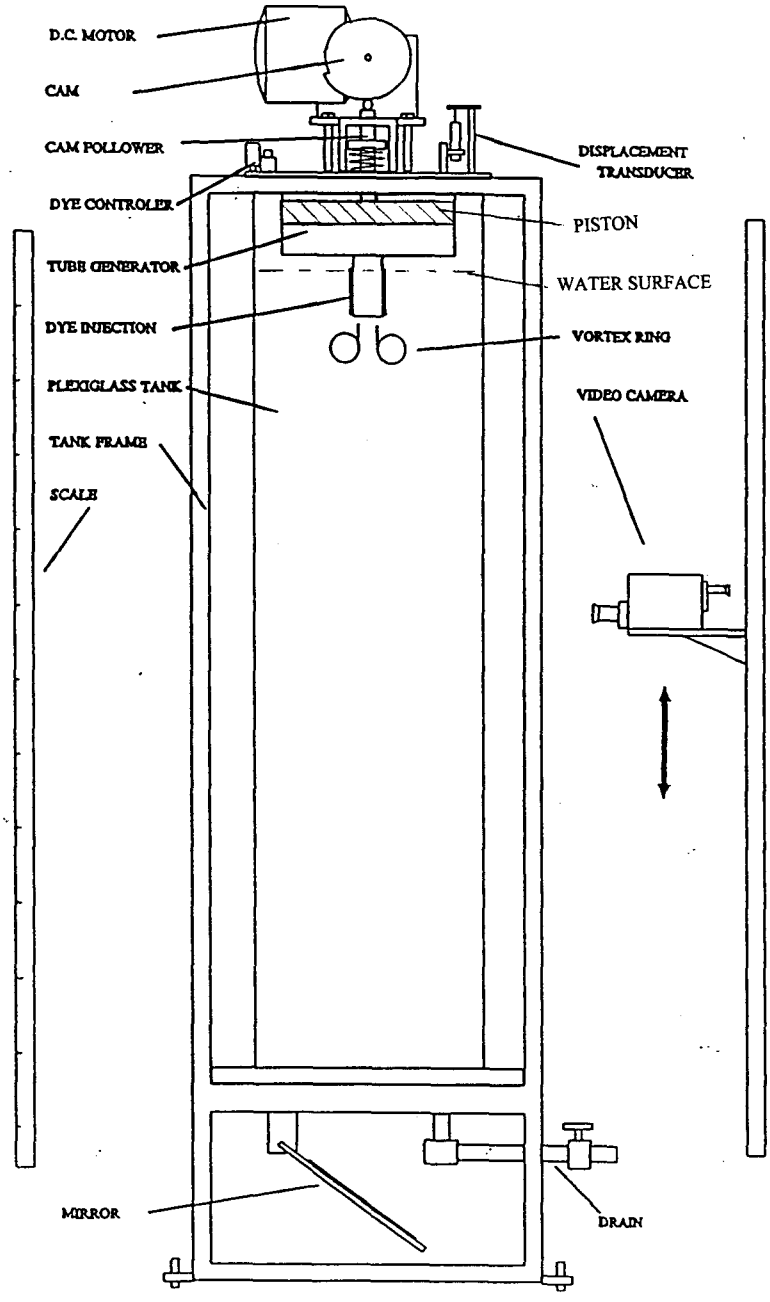

Figure 3.1 Schematic of the apparatus with tube generator.

profile is very important. In this case the motion of the water being injected through the tube type orifice is controlled by a cam mechanism having a particular profile, which is driven by a variable speed D.C. motor. The cam pushes the piston of the vortex ring generator down and a slug of fluid is ejected through the tube and a vortex ring forms. The displacement and velocity of the piston are measured using a displacement transducer which is either connected to an oscilloscope or a data acquisition system, where the displacement of the displacement of the plate versus time is recorded. The diameter of the piston D_p and injection tube D are 24.5 cm and 5 cm respectively, as shown in Figure 3.3. If the stroke of the piston is S, theoretical length of the pulse for each injection is

$$L = (D_p/D)^2 S = 24.01\ S \qquad (3.1)$$

or

$$S = L/24.01 \qquad (3.2)$$

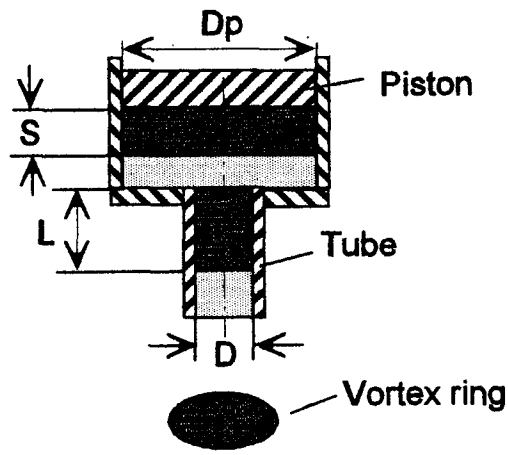

Figure 3.3 Diagram of a tube injector

An optimal value for the ratio L/D of 2.8, suggested by Latto (1989), which

is comparable to that obtained by others, was used in these experiments. Thus for a D= 5 cm, the optimal length L is 14 cm. Therefore from equation 3.2, the stroke S was set at 0.58 cm to satisfy the optimal condition.

A video camera is used to record the process of generation and the path of a vortex ring until it reaches the bottom of the tank or disintegrates. The camera is mounted on a platform which can be moved axially up and down manually, to follow and record the displacement of the vortex ring with respect to the opening of the tube. A measuring tape is put on the side of the tank to indicate the scale of the displacement.

In order to examine the effect of various injection profiles, several cams with different shapes and sizes are used. The initial cam was made of steel which had durability, but it is not convenient to manufacture or modify frequently . However, it was found to be very convenient to produce wood (oak) cams which are easy to manufacture and modify and have sufficient durability to last for the duration of the experiments.

A dye injection system is set up for the flow visualization of a vortex ring. The original design of the dye injection system utilized two capillary injection tubes attached to the outside of the mouth of the generating tube. During an injection period, food dye is injected into the shear layer of a vortex ring, and traces out the formation and propagation of the vortex ring. This design is very suitable for the flow visualization of a vortex ring during the vortex ring formation and propagation though two plastic capillary tubes, as shown in Figure 3.2 (A). However, it is not

adequate for the measurement of overall size of a vortex ring, when the outline of the periphery of the vortex ring needs to be observed. In order to observe the full volume of a vortex ring, an additional dye injection tube was added inside of the generating tube though the piston, as shown in Figure 3.2 (B). This permitted sufficient quantities of dye to be injected into the vortex ring. Thus when a fully formed vortex ring is ejected from the generating orifice it is completed filled with a dyed solution, and the volume of a vortex ring could be observed and measured according to the region occupied by the dyed water.

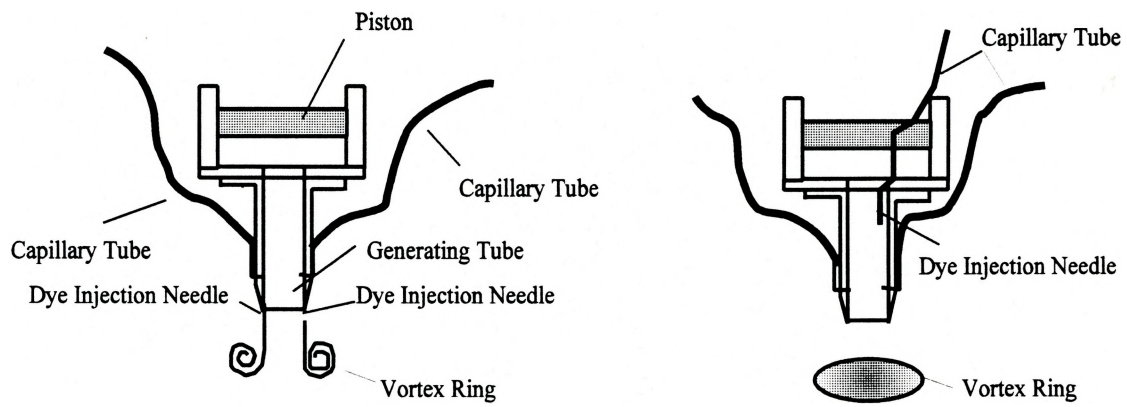

(A) The original system (B) The modified system

Figure 3.2 The Dye Injection System

3.3 Experimental Results

Several experiments were performed using the tube type generator system as shown in Figure 3.1. In order to observe the vortex ring formation, before the

injection of fluid, food dye was ejected from the two dye injection capillaries, as shown in Figure 3.2 (A). Figure 3.4 (A - D) are a series of pictures of a vortex ring formation, which were made using a Kodak Ektapro EM digital high speed camera at 125 frames per second. These pictures clearly show the formation process when fluid was ejected out of the generator tube orifice, and indicate flow separation at the boundary layer causing the rolling up process which forms the vortex ring core at the sharp edge of the tube outlet. As the injection is accelerated, the rolled spiral vortex ring core moves away from the outlet. Initially, the dyed vortex ring core was in a plane parallel to the direction of motion through the centroid of the vortex ring. The dye at the vortex ring core has a rotating motion about a circle, in a counterclockwise direction when viewed from above. The motion quickly results in a vortex ring with a completely dyed annular core, as shown in Figure 3.4 (D). A typical fully developed laminar vortex ring is stable and travels downwards as shown in Figure 3.5. As the vortex ring travels vertically downwards, its diameter increases gradually, until the vortex ring impacts the bottom of the tank and breaks up.

A triangular injection velocity profile with six different injection velocities were used in the experiments, (from 30% to 80% of the maximum input 120 volt voltage to the motor). On the basis of measurement data and calculation of the shape and motion of the cam, a table of the relationship between the percentage voltage supplied to the motor and the theoretical injection velocity is given below in Table 3.1:

Voltage (%)	30	40	50	60	70	80
N (rpm)	25	35	45	57	68	80
Injection time T_i (s)	0.14	0.10	0.078	0.061	0.051	0.044
Calculated injection velocity U_i (m/s)	1.00	1.40	1.80	2.28	2.72	3.20

Table 3.1 Injection Velocity Data

The first part of the experiments was measuring the displacement and velocity of vortex rings, for various injection velocities. Figure 3.6 presents data on the displacement of vortex rings vs. time, which were obtained by measuring the distance from the injection tube orifice to the core of a vortex ring. The velocity of vortex rings vs. time are presented on Figure 3.7. These graphs indicate that as injection velocity increases, the forward velocity of a vortex ring increases. The data also reveal that the velocity of a vortex ring is not linearly related to the injection velocity. As the injection velocity was raised from 1 m/s to 3.2 m/s, the vortex ring velocity at 0.5 s after injection grew only from 0.31 m/s to 0.56 m/s. On the other hand, the higher the injection velocity, the faster the vortex ring velocity reduces. In all cases, the velocity of a vortex ring on reaching the bottom of the tank are about 50% of the initial velocity. The relationship between injection velocity and vortex ring velocity shows in Table 3.2:

Voltage (%)	30	40	50	60	70	80
U_i (m/s)	1	1.4	1.8	2.28	2.72	3.2
U (m/s)	0.31	0.40	0.45	0.49	0.53	0.56
U/U_i (%)	32.5	30.0	26.2	22.5	20.4	18.3

Table 3.2 Vortex Ring Velocity with Various Injection Velocity at 0.5 s

The second part of the experiments was measuring the volume of vortex rings. The modified dye injection system as shown in Figure 3.2 (B) was used to eject dye into the generating tube, prior to fluid ejection from the orifice, resulting a vortex ring completely filled with dye, thus permitting the observation and measurement of the outline or periphery of the vortex ring produced. Figure 3.8 gives a series of pictures which shows the change of the outline of a vortex ring as it travels downwards. The outline of a vortex ring has an elliptic side view and a circular top view, that is, it is an oblate spheroid, as depicted in the diagram in Figure 3.9.

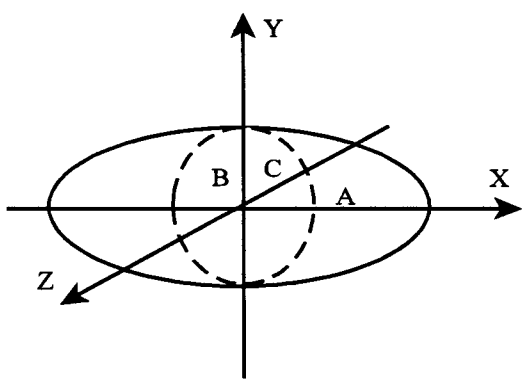

Figure 3.9 Diagram of an ellipsoid

The volume for an ellipsoid is

$$V = 4\pi/3*ABC \qquad (3.3)$$

For a spheroid, where A = C,

$$V = 4\pi/3*A^2B \qquad (3.4)$$

Figure 3.10 shows the volume of vortex rings vs. time in various injection velocities, which was obtained by measuring the distance A and B of a vortex ring, and calculating using formula (3.4). All the plots in Figure 3.10 show that a vortex ring expands as it moves forward. This is because after its generation, during its forward motion the vortex ring entrains more ambient fluid than it rejects in its wake which in turn increases its volume. Thus its volume increases, but not at the rate of entrainment. Due to the mass transfer between the ambient fluid and a vortex ring, the vortex ring's contents are diluted and the ring's outline periphery becomes difficult to observe. Consequently, the measurements were taken only during the first one second period after the vortex ring is formed.

Theoretically, the volume of a fully formed vortex ring has the same volume of fluid ejected from the generating orifice before the ring propagation. Thus, theoretical volume is

$$Vi = \pi/4*D_p{}^2S = \pi/4*24.5^2*0.583 = 274.8\ (cm^3) \qquad (3.5)$$

The first point of each plot in Figure 3.10 presents the volume of a vortex ring 0.2 s after ejection has started, which is the condition for a vortex ring immediately after it has been fully formed. However, the volume is only about 250 cm^3 for most injection velocities, which is slightly lower than the theoretical volume 274.8 cm^3

based on equation (3.5). Figure 3.11 shows the dimensionless volume V/V_i vs. time.

Latto (1987) believed the growth of a vortex ring is virtually independent of the fluid properties, and used a modified sphericity equation to calculate the volume of a vortex ring at the formative stage:

$$V = K\pi/6D_r^{\ 3} \qquad (3.6)$$

where K is the correction for non-sphericity of the vortex ring and is approximately equal to 1.45 for the majority of vortex rings; D_r is the diameter of a vortex ring as shown in Figure 3.12. At the optimal condition L/D = 2.8, for plate type injection generator $D_r/D = 1.282$, then an approximate empirical equation was derived:

$$V = 1.6\ D^3 \qquad (3.7)$$

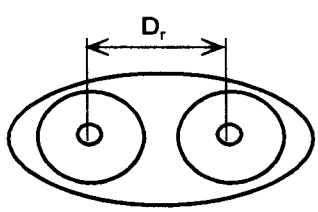

Figure 3.12 Diagram of a vortex ring

When D = 5 cm equation (3.7) gives V = 200 cm^3, which is much lower than the theoretical volume 274.8 cm^3. It appears that equation (3.4) (for spheroid) more accurately represents the volume of a vortex ring than equation (3.6) (for sphericity).

3.4 Analysis and Discussion

The results of the experiments presented above reveal that the injection velocity is one of the primary factors which determine the behaviors of a vortex ring. The first experiment has shown that the translational velocity of a vortex ring is a function of the injection velocity, that is the vortex ring velocity increasing as injection velocity rising. But the increase in the velocity of a vortex ring is not a linear function of the injection velocity, for example, while the injection velocity was raised from 1 to 3.2 m/s, the vortex ring velocity grew only from 0.31 to 0.56 m/s at 0.5 s after it injected, which means the rate of vortex ring velocity to injection velocity drops from 32.5% to 18.3%. Furthermore, the higher the injection velocity, the faster a vortex ring velocity decreases during the propagation stage. In the experiment, after a vortex ring traveled about 170 cm and before it reached the tank bottom, the velocity of a vortex ring decreased to about 50% of the initial velocity. See Figures 3.6 and 3.7.

The second experiment showed that the volume of a vortex ring did not have a significant change and the plots of volume vs. time have a quite similar tendency, when the injection velocity was varied from 1.4 to 3.2 m/s, (i.e. the voltage supplied to the motor changed from 40% to 80%). However there is a difference when injection velocity is equal or lower than 1 m/s (or 30% of full voltage) and the volume of a vortex ring has a notable increase, as the ring travels forward. For instance, at one second after the start of the fluid injection, the volume of a vortex ring grew

up to 25 - 39% larger than the theoretical volume. See Figure 3.10 and 3.11.

The above analysis implies that the higher the injection velocity (or power input) does not necessarily cause more effective mass transfer of a vortex ring. It would appear that there should be a optimal range of injection velocities for different fluid properties and mixing processes, which can lead to an effective vortex ring transfer with a minimal power input. That is to minimize the power density for a given mixing requirement.

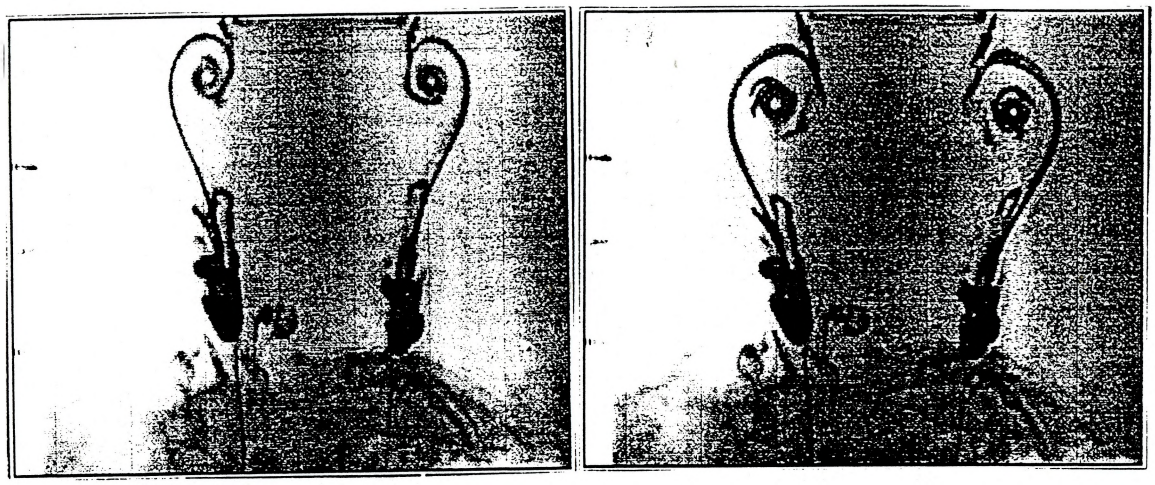

(A) (B)

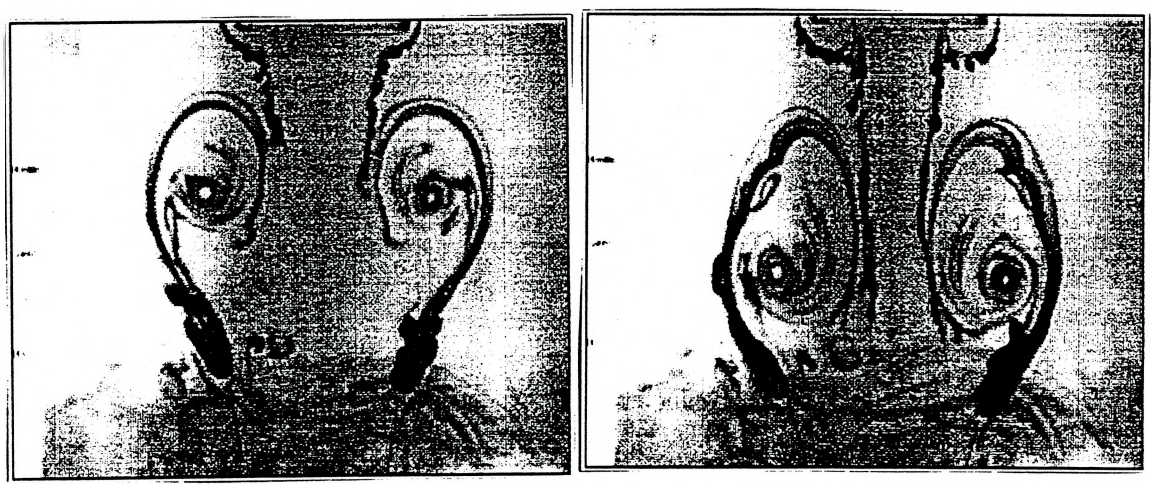

(C) (D)

Figure 3.4 A series of pictures of the formation of a vortex ring.

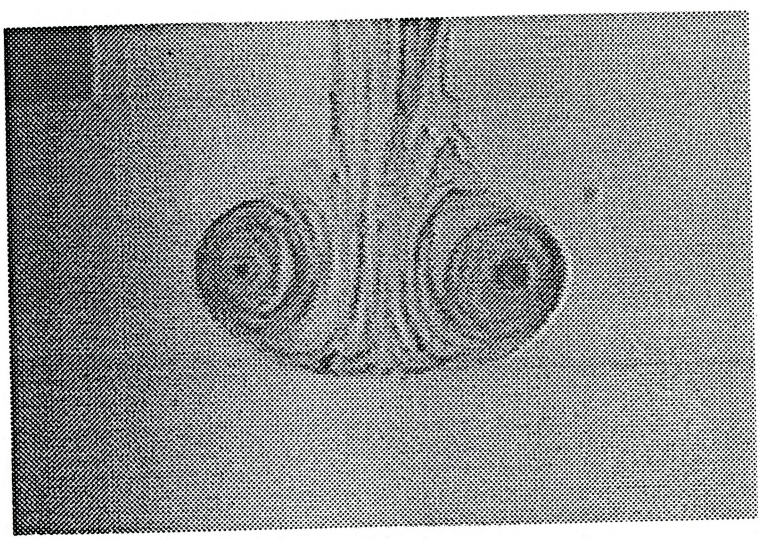

Figure 3.5 A typical fully developed laminar vortex ring.

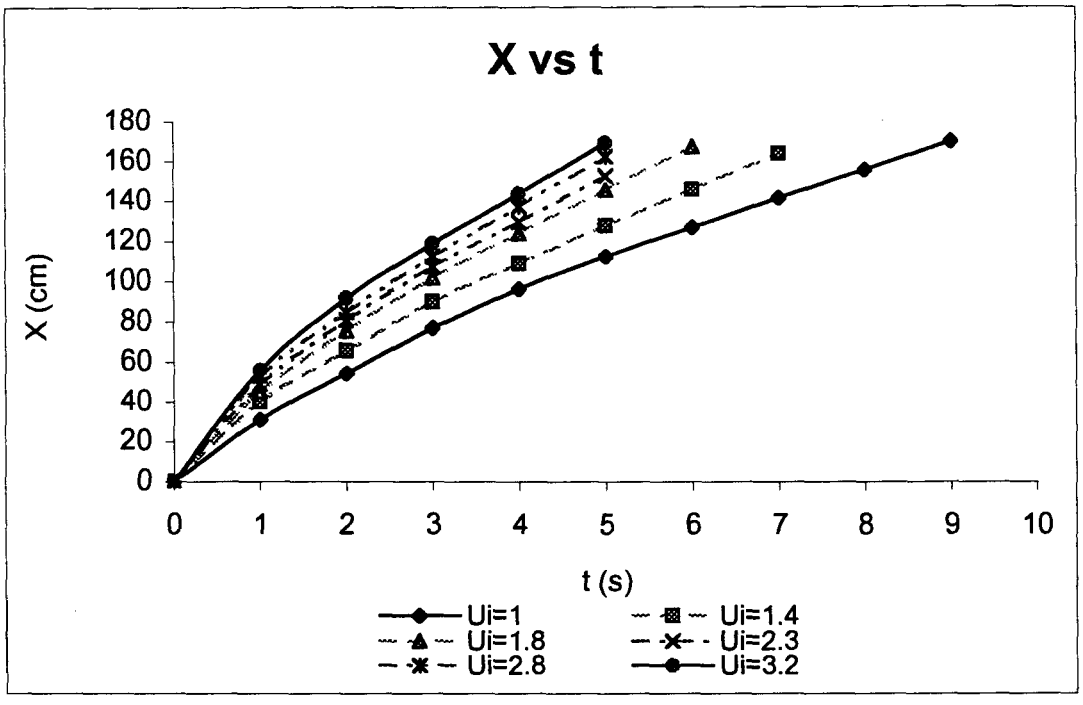

Figure 3.6 Displacement of a vortex ring vs. time

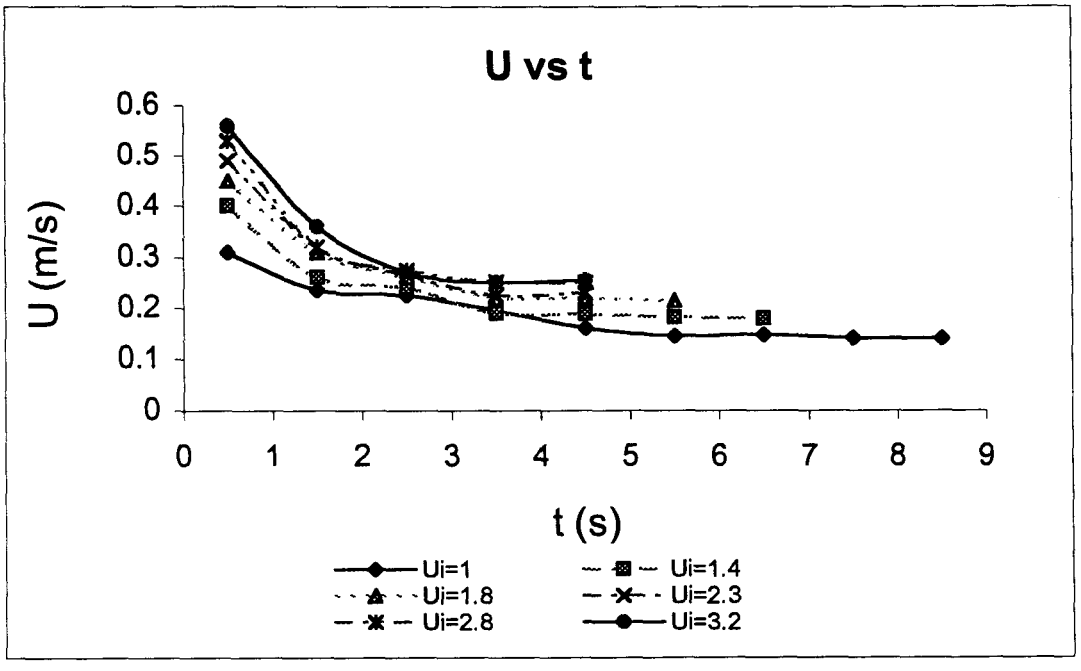

Figure 3.7 Velocity of a vortex ring vs. time

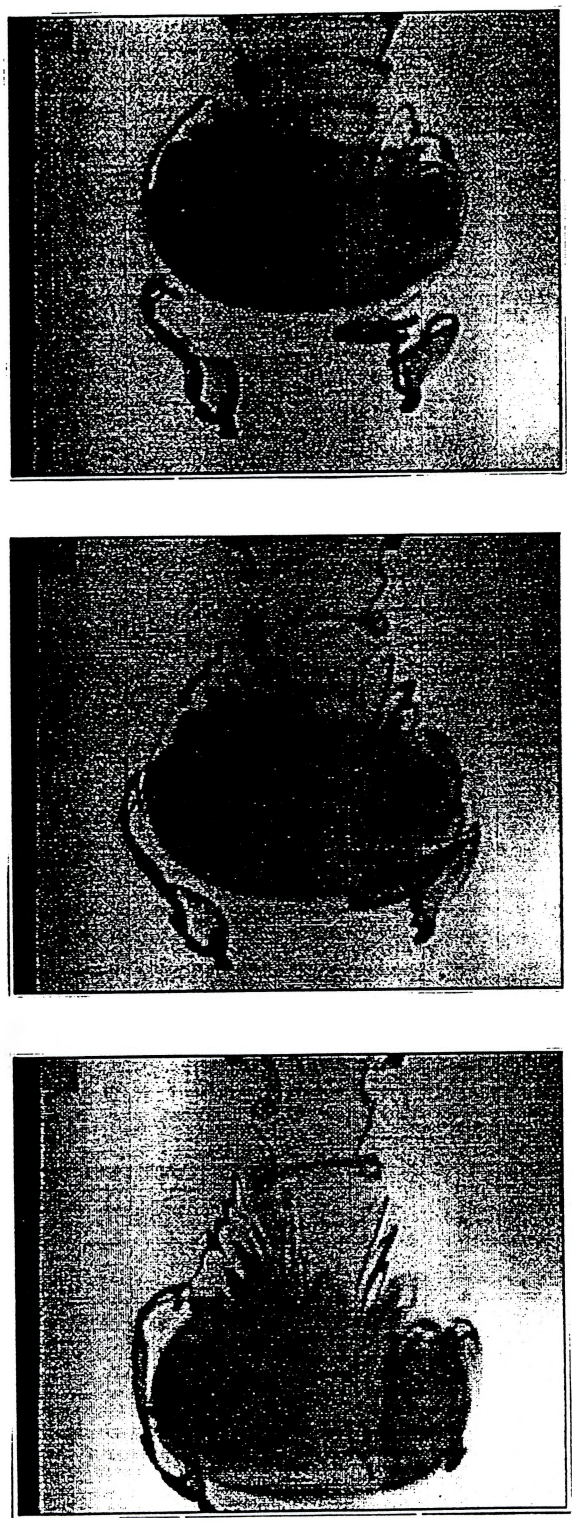

Figure 3.8 The change of the volume of a vortex ring as it travels downwards.

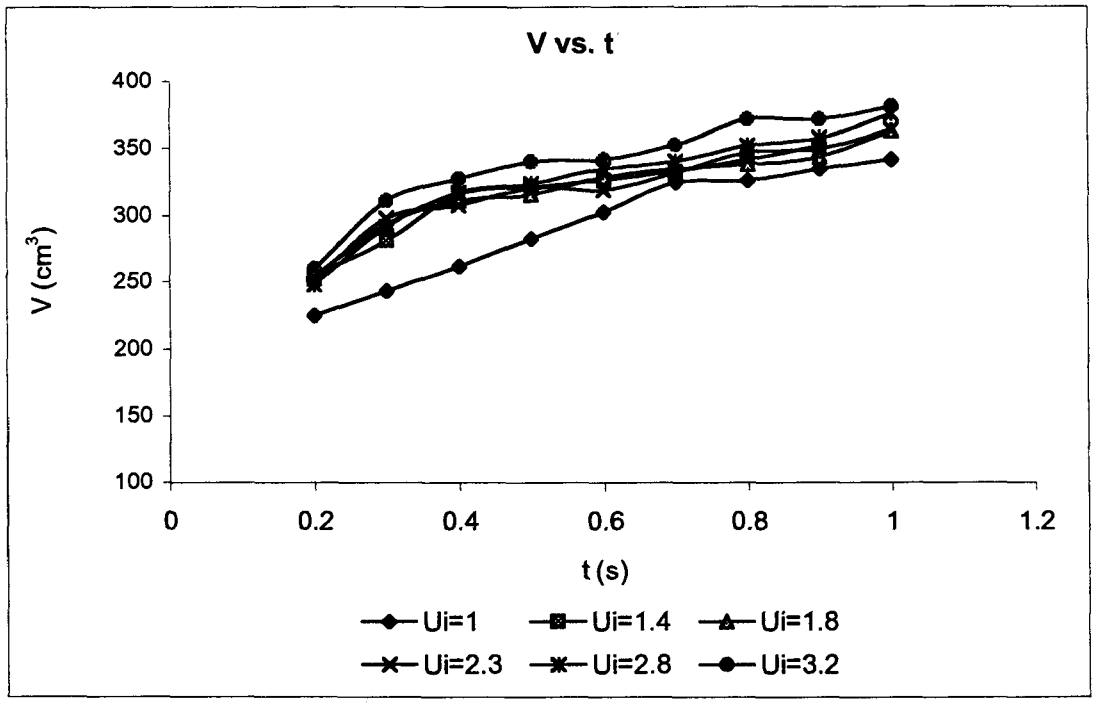

Figure 3.10 Volume of Vortex Rings vs. Time

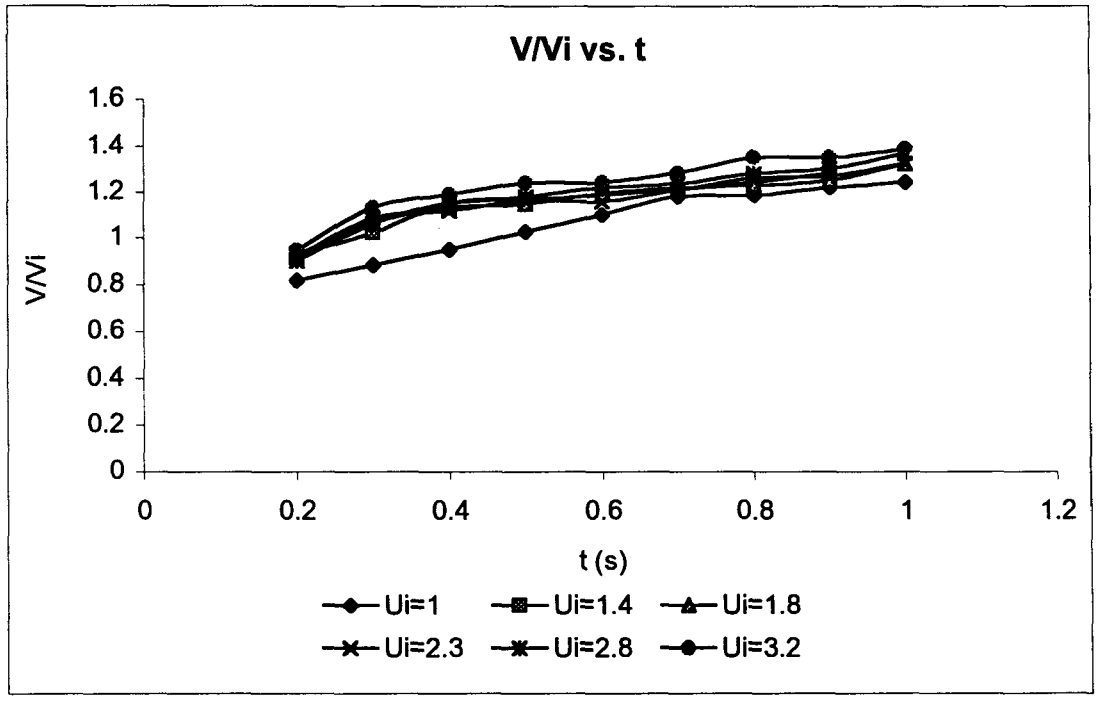

Figure 3.11 Dimensionless Volume vs. Time

CHAPTER 4

NUMERICAL SIMULATION OF VORTEX RINGS

4.1 Introduction

Numerical simulation of fluid flow has a considerable value in the prediction and understanding of the behavior of vortex rings and the fluid motion adjacent to a generating device. The Computational Fluid Dynamics (CFD) technique is becoming increasingly popular as a tool for some very good reasons. CFD numerical simulation gives a complete picture of the flow regime, which is not normally available from experimental measurements. Since they do not involve real plant systems and fluids, CFD numerical models are often cheaper, safer and more convenient to run than their physical equivalents, and once a model has been set up it is easy to make changes and run "what if ?" queries for various parameter changes.

As presented in Chapter 2, many previous efforts of numerical simulation of vortex rings have been achieved. Under the direction of Latto, Ho (1990) studied analytically the effect of the proximity of one wall on the path of a vortex ring; later Hua (1994) numerically simulated vortex ring behavior in both Newtonian and Non-

Newtonian stratified fluids, using a control volume based finite difference technique to solve the continuity, Navier-Stokes and energy equations in cylindrical coordinates; both Stapleton (1996) and Lumley (1997) simulated the relationship between basic vortex formation parameters and the resulting displacement using a numerical model in FLUENT (Version 3.03). Stapleton examined the motion of an orifice generated vortex ring by varying the injection profile, and Lumley investigated practical methods for causing premature vortex ring decay by introducing obstructions in the path of the vortex ring.

A number of CFD programs are commercially available, of which FLUENT is a well-known software package produced by Fluent Inc., which is a general purpose computer program for modeling fluid flow, heat transfer, and chemical reaction. FLUENT enables one to apply computer simulation methods to analyze and solve practical design problems. It incorporates up-to-date modeling techniques and a wide range of physical models for simulating numerous types of fluid flow problems. These are accessible to users through an interactive graphical user interface for problem definition, computation, and graphical postprocessing.

In this chapter the use of FLUENT to describe the processes of a vortex ring formation and propagation in an axis-symmetric pulse will be discussed.

4.2 Model Description

The majority of the numerical simulations of vortex rings were performed

using FLUENT (V 4.47), and were run on an Intel Pentium-75 MHZ computer with Windows 95, while some were done using a previous version of FLUENT (V3.03) with Windows 3.1.

4.2.1 Geometry Setup and Grid Generation

The basic model in this study used a polar model of a cylindrical tank with diameter 30 units and a length 100 units, and a stationary tube injector with diameter 5 units and length 5 units was located on the top of the tank. The fluid model was water at 25^0C. A 2D axial symmetric polar model of the tank with finite difference grid was considered, consequently only one radial slice was defined in the grid (Figure 4.1). The left end of the cylinder is closed except for the orifice which is an inlet, and the right end is modeled as an outlet to satisfy the mass balance requirements imposed by FLUENT.

To check for grid dependency, two grid sizes were tested: 100x30, and 171x43. No significant variations were found regarding the flow field result between different grids. Thus the majority of the calculation were performed on a 171x43 grid.

In order to reduce the computational time and improve the solution accuracy, a non-uniform grid was used, which permits the use of a more dense grid in areas where the flow is complex or of interest, and to use a less dense grid in regions that are of lesser interest. In this study, it is expected that most fluid motion occurs in the stage of vortex ring formation, that is in a axial region in approximate the first 15

units adjacent to the generation orifice, and a cylindrical region along the model axis with a diameter about twice that of the orifice, which corresponds to the path of a vortex ring. The physical domain is divided into a set of segments, which are four segments in the axial direction and three segments in the radial direction, therefor the computational nodes can be concentrated in the regions of highest change in the flow field. To yield a smoothly, mono-tonically varying grid spacing throughout each segment, weighting factors are defined to control the grid density at each endpoint of a segment. The grid segment information is shown as Table 4.1.

coordinate direction	segment	start-point	length	# cells	weighting factor start-point	weighting factor end-point
axial	1	0	0.05	10	0	2
"	2	0.05	0.1	40	1	1
"	3	0.15	0.45	80	2.25	0.9
"	4	0.6	0.4	40	1.6	0
radial	1	0	0.025	14	0	1
"	2	0.025	0.035	14	1.4	0.8
"	3	0.06	0.09	14	1.92	0

Table 4.1 Grid Segment Information

4.2.2 Physical Model Selection

In order to find a model having a good agreement with empirical observations, several basic physical models have been tested, which include

lamina, k-ε turbulence, and the RNG k-ε turbulence model. Three discretization interpolation schemes: power-law interpolation (PL), quadratic upwind interpolation (QUICK), and blended second order upwind/ central difference (B/C) were used in the models. Although in the injection stage the Re varied from 3.5×10^4 to 1.4×10^5 for an injection velocity variation from 0.7 m/s to 2.8 m/s which would imply a turbulent flow, Figure 4.2 shows that the computational result of using the lamina model appears to agree with empirical experiments better than a turbulent model. Figure 4.3 gives the results of using turbulence model with different discretization schemes. There is no noticeable difference among the three interpolation schemes, and it seems that the higher order schemes do not reduce the discrepancy between the empiric and numerical tests. Consequently, the laminar model with a power-law scheme was chosen for the simulation, since it did agree more favorably with empirical and numerical data and it may represent the fluid motion in a vortex ring better than the turbulence model.

The vortex ring formation and propagation is a time dependent flow problem. In each discrete solution, the maximum number of iterations per time step is 100 and the minimum residual sum is 0.001. Each calculation time step Δt is set from 0.001 to 0.01 gradually increasing as the calculation proceeds, to meet the ideal number of iterations per time step of 10 to 20. In each calculation, FLUENT automatically records the pressure and velocity change in the flow for each time step. The time steps between each save are changed with calculating time step.

The criteria used for convergence were: (1) The residual error in each iteration for each cell is not larger than 10^{-3}. (2) The total sum of the residual error for all cells is not larger than 10^{-3}.

4.2.3 Injection Velocity Profile

The injection profile including the magnitude and shape is one of the key parameters for vortex ring formation and propagation. The injection profile is the fluid velocity vs. time for the injected fluid. To observe clearly the effect of injection velocity profiles for vortex ring formation, only one injection pulse was examined in each test. The function of velocity was assumed to begin and end at zero over a finite interval of time length T_i, and the velocity was governed by certain function $U_i(t)$ for time interval from 0 to T_i. That is

$$\begin{cases} U_i(t) = f(t); & 0 \le t \le T_i \\ U_i(t) = 0; & t < 0,\ t > T_i \end{cases} \qquad (4.1)$$

Then an average velocity can be defined as

$$U_i^* = \int U_i(t)\, dt / T_i \qquad (4.2)$$

The injected fluid mass is expressed in terms of the length L of a theoretical cylinder of fluid, which has the same volume as the injected material and the diameter of the generating orifice, see Figure 4.4.

Now L is equal to:

$$L = T_i\, U_i^* \qquad (4.3)$$

and the ratio L/D is equal to:

$$L/D = T_i U_i^*/D \qquad (4.4)$$

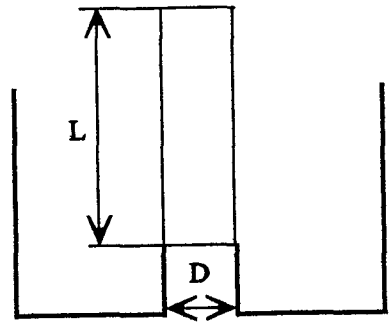

Figure 4.4 Diagram of the L/D ratio

Three injection profiles were used, namely rectangular, triangular and sinusoidal, as shown in Figure 4.5 (a), (b), (c). All profiles have an L/D ratio of 2.8, which was originally selected as the ideal optimal condition found by Latto (1989).

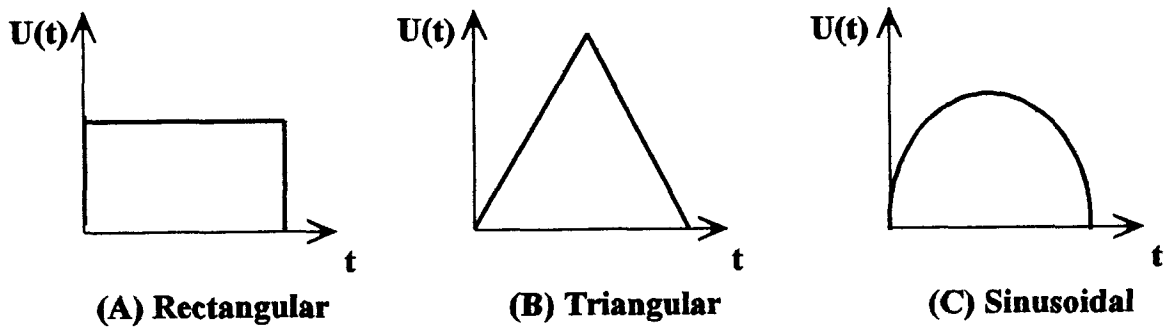

Figure 4.5 Injection Profiles

4.2.4 Graphics Tool

Graphics tools in FLUENT are very powerful which allow one to process the information contained in the results of the FLUENT model and make it very convenient to view the solution. Once a solution is calculated, a vortex ring displacement in both axial (X) and radial (R) directions vs. time profile can be generated by determining the location of the center of rotation of the vortex ring ("eye") in the flow solution for each time step. The "eye" of a vortex ring may be easily assessed in a plot of pressure contours, velocity vectors, or streaklines.

Figure 4.6 is a plot of pressure contours of a vortex ring. The core of the vortex ring is a low pressure area which provides the centripetal acceleration necessary to hold the fluid in rotation. Along the axis in front of the ring there is a high pressure region which corresponds to the stagnation point on the front surface of the vortex ring shell. There is also a high pressure region along the axis behind the vortex ring. This elevated pressure is due to the ingestion of fluid from the back of the vortex ring. The point of the lowest pressure is considered as the center of rotation of the vortex ring. The location of a vortex ring is measured from the end of the orifice to the "eye" in each time step.

Figure 4.7 displays the velocity vector field of a traveling vortex ring. The highest velocity area presents the main flow of a vortex ring, which leads the vortex ring traveling along the axis. The revolving vectors show the core of a vortex ring, which cause the rolling up of the vortex ring.

Figure 4.8 is a plot of streaklines. Streaklines are continuous lines joining all fluid particles that have originated from the same point in the fluid. FLUENT displays streaklines in steady-state problems by drawing the trajectory of particles as they travel through the continuous phase fluid. These trajectories display the flow patterns of a vortex ring during the propagation phase.

There appears to be a good agreement of the "eye" position in the above three plots. That is the flow patterns in the three plots give the same location of a vortex ring "eye" for each time step.

4.3 The Effect of Injection Profile

In an attempt to predict the movement mechanism of a vortex ring and offer a set of relatively simple equations for the applications of vortex rings, vortex ring trajectories were measured for a series of injection velocity profiles (including various values and shapes).

4.3.1 Variation of Injection Profile Magnitude

Three rectangular injection velocity profiles were used to examine the effect of injection velocity in this experiment. From equation (4.4), it is clear that the higher the injection velocity, the shorter the injection period required to maintain a constant L/D ratio. In order to compare the simulation solutions with empiric results, while keeping the ideal optimal L/D ratio of 2.8, specific injection periods and

velocities were selected as presented in Table 4.2.

test #	Injection Velocity (m/s)	Injection Period (s)
test 1	0.7	0.2
test 2	1.4	0.1
test 3	2.8	0.05

Table 4.2 Injection Parameters

The position and velocity of a vortex ring vs. time data for all three rectangular injection models are presented in Figure 4.9 and 4.10. From these figures it is easy to see that the travel velocity of a vortex ring increases as the injection velocity increases. Figure 4.10 also shows that a vortex ring attains a velocity approximately 1/3 of the injection velocity at the end of injection, and it decreases as the ring travels in the fluid. The higher the injection velocity, the faster the vortex ring translational velocity declines.

Figure 4.11 is a plot of dimensionless displacement (X/D) vs. dimensionless time (t/T_i) for all three injection velocities. This figure reveals that there is a good agreement among the three displacement profiles. This implies that the velocity of a vortex ring is directly proportional to the injection velocity, that is can be correlated with a specific L/D. Figure 4.12 is a dimensionless plot for U/U_i vs. t/T_i, and appears substantiated this observation.

The data can be correlated using a polynomial plot of the dimensionless data to give the following equation for a rectangle injection profile:

$$X/D = -0.0114\,(t/T_i)^2 + 0.9284\,(t/T_i) + 0.1004 \quad (4.5)$$

It is clear, (see Figure 4.11), that this polynomial function agrees very well with the experimental data, at least in the range $0 \le t/T_i < 35$.

4.3.2 Variation of Injection Profile Shape

The three injection profile shapes described in Section 4.2.3 have been used to test the influence of different injection profile. All profiles have a L/D ratio of 2.8, an average injection velocity U* of 0.7 m/s, and an injection period T_i of 0.2 s. The different injection profile functions are shown in Table 4.3. For triangular and sinusoidal profiles, the maximum U(t) occurs at $t/T_i = ½$.

Profile	Function		Umax (m/s)
rectangular	$U_i(t) = 0.7;$	$0 \le t \le T_i$	0.7
triangular	$U_i(t) = 14\,t;$ $U_i(t) = 2.8 - 14\,t;$	$0 \le t \le T_i/2$ $T_i/2 < t \le T_i$	1.4
sinusoidal	$U_i(t) = 1.1 \sin(\pi t/T_i);$	$0 \le t \le T_i$	1.1

Table 4.3 Injection Functions

Figures 4.13 through 4.15 give a series of results for the displacement and velocity of a vortex ring for rectangular, triangular and sinusoidal injection profiles. Although all three input profiles have the same average injection velocity of 0.7 m/s and an injection period of 0.2 s, it is clear that both triangular and sinusoidal profiles appear to give a higher vortex ring traveling velocity in the axial direction than the

rectangular profile, (see Figure 4.13 and 4.14). However, Figure 4.15 shows there is no noticeable difference in the radial direction of vortex ring movement for all three injection profiles.

Using a procedure similar to that used above, a polynomial equation was developed to express the relationship of non-dimensional displacement vs. non-dimensional time as a function of the injection profile:

$$X/D = a\,(t/T_i)^2 + b\,(t/T_i) + c \qquad (4.6)$$

Here a, b and c are constants. For the three injection profiles, the constants are given in Table 4.4. The empirical correlation equations are in good agreement with the experimental data, and for all three cases the $R^2 > 0.998$.

Profile	a	b	c
rectangular	-0.0114	0.9284	0.1004
triangular	-0.0277	1.4451	-0.1077
sinusoidal	-0.0260	1.4259	-0.1749

Table 4.4 The Constants for The Equation

4.4 The Effect of Geometry of Injection Tube

Some different types of injection tube exits have been used by different researchers in previous studies. There mainly are two typical tube exits, i.e. a tube with or without a lip at the exit (see Figure 4.16). In order to investigate the effect of a generator tube exit type in the formation and propagation phases of a vortex

ring, these two types of injection tube exit were tested.

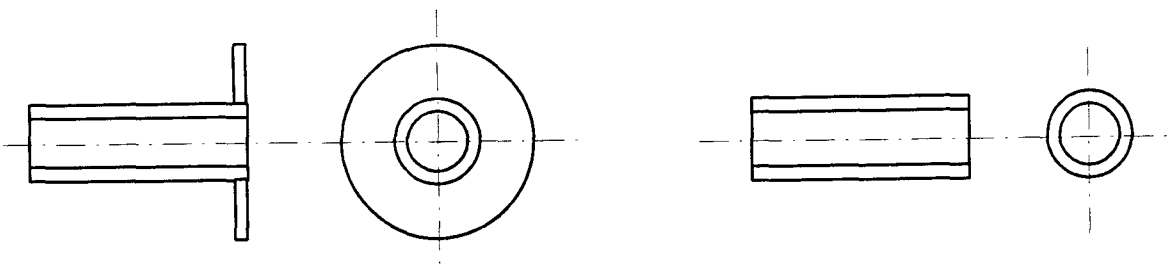

(A) The tube with a lip (B) The tube without a lip

Figure 4.16 Diagram of two typical tube exits

To compare these two types of tube, the same geometry and physical model described previously was used, except one generator has a plate with a diameter of 12 units at the tube exit , as shown in Figure 4.16 (A). The injection velocity profile was rectangular with U_i = 0.7 m/s, injection time T_i = 0.2 s, and L/D = 2.8.

The computational results of the two types of tube are shown in Figure 4.17 (A) to (C). The plot data were measured from the location or pressure of the "eye" of a vortex ring. The plots represent: (A) the axial displacement vs. time, (B) the radial displacement vs. time, and (C) the pressure vs. time. As indicated in Figure 4.17 (A) and (B), there is no noticeable difference being observed in the vortex ring formation and propagation stages between the two types of tube. This indicates that the type of a tube exit does not significantly affect the movement of a vortex ring in both axial and radial directions. However in Figure 4.17 (C), the plot shows that the core pressure for the tube with an end plate is about 15% lower (or higher

in absolute value) than that of the tube without a plate in the vortex ring generation stage (at t=0.1s), which implies the vortex ring from the tube (A) is stronger than that from the tube (B). But after the vortex ring formed, the pressure plots for the two orifices approach the same values in the vortex ring propagation stage.

These computational results reveal that although an injection tube exit type may have some influence on the vortex ring formation stage, there is no noticeable influence on the vortex ring propagation stage. Overall, the type of an injection tube exit does not have a significant effect for vortex ring transfer. Therefor, it is not a critical factor in the design of a vortex ring mixer.

4.5 The Effect of Obstructions in The Flow Field of A Vortex Ring

The empirical experiments by Latto have shown that vortex rings traveling upward toward the liquid surface often have considerable momentum when they reach the surface. In consequences, energy is wasted as the vortex rings erupt from the surface of the tank, and the splashing effect may introduce unwanted gases into the mixture (such as in the mixing of paint). To avoid this problem, an obstruction was placed in the path of a vortex ring , which may change the trajectory of the vortex ring.

Figure 4.18 gives the frames of color filled pressure contour plots which show the propagation process of a vortex ring with a baffle in the flow field. The diameter of the baffle was 0.69 D. The baffle was fixed on a shaft and located in the central line at X_b = 4.42 D. After it fully formed and traveled downwards from top, a vortex

ring initially encountered the shaft and slightly enlarged in diameter (see Figure 4.18 (a)). The ring kept approximate a constant diameter and pattern when it traveled though the shaft (Figure 4.18 (b), until it approached to the baffle, then its diameter and shape changed dramatically and it strayed from the original path (Figure 4.18 (c)). As the ring passed the baffle, its core separated to two pair of low pressure areas (Figure 4.18 (d) and (e)). After the ring left the baffle, the low pressure areas emerged into one and the diameter of the vortex ring increased continually (Figure 4.18 (f) and (g)). These frames revel that a baffle can significantly change the trajectory of a vortex ring.

In order to examine the effects of obstructions, various size and shape of baffles were tested with a rectangular injection profile with three different generation velocities (U_i = 0.7, 1.4, 3.0 m/s). All baffles were set on a shaft and located at X_b which is 4.42D from the exit plane of the generating tube orifice.

4.5.1 Varying Baffle Size

The varying sizes of baffles (D_d/D) were tested at different injection velocity (U_i). The test scenarios are shown as Table 4.5.

D_d/D U_i (m/s)	0.23	0.38	0.54	0.69	1.00	1.43	1.75
0.7	a1	b1	c1	d1	e1	f1	
1.4				d2	e2	f2	g2
3.0			c3	d3	e3	f3	g3

Table 4.5 Test Scenarios for D_d/D

The results of varying the baffle size are shown in Figure 4.19 through Figure 4.24. The injection velocities considered were 0.7 m/s, 1.4 m/s and 3.0 m/s respectively. These Figures clearly show that a baffle in the flow path can significantly change the direction and velocity of a vortex ring. In all the cases, when a vortex ring approaches a baffle, the baffle causes the vortex ring to expand outwards in the radial direction (i.e. R_r growing). The larger the baffle size is, the larger the diameter of vortex ring grows and the faster the axial velocity declines.

Figures 4.19, 4.21 and 4.23 show that if the diameter of a baffle is not large enough, e.g. at $D_d \leq D$, the core of the vortex ring passes over the baffle perimeter, and then continues to travel with the similar trajectory that it had before it encountered the baffle and some increase in diameter. When $D_d \geq 1.43$ D, the baffle significantly affects direction of travel of a vortex ring. Once the vortex ring encounters the baffle, the forward motion of the vortex stops immediately, but it radially expand until its shell approaches the wall of the vessel and then the vortex ring has no axial or radial motion. The graphs also show that the diameter of a baffle does not have remarkable effect on the location where a vortex ring begins to expand radially. For instance, in all the cases, the vortex ring starts to expand at approximately X = 3D, i.e. about 1.4D upstream of (prior to) the baffle. However, the size of a baffle certainly affects the extent of a vortex ring deflecting from the original path. Figures 4.20, 4.22 and 4.24 show that a baffle has a great influence upon the travel velocity of vortex rings, even a small baffle with a diameter of only

0.23D can cause the velocity of a vortex ring to moderately drop. As the diameter of the baffle increase, the axial velocity sharply declines. In Figure 4.20, for instance, at X/D = 5 for the baffle diameters of 0.23D, 0.38D, 0.54D, 0.69D, 1D and 1.43D, the axial velocities are 0.14 U_i, 0.13 U_i, 0.085 U_i, 0.025 U_i, and 0 respectively. When the baffle diameter $D_d \geq D$, the velocity decelerates to zero at or before X = 5.6 D. Furthermore, when $D_d \geq 1.43$ D, the vortex ring stops its forward motion (i.e. U = 0) just before it reaches the baffle.

Figure 4.25 (A) to (C) are plots of X/D, R_r/R and U/U_i vs. D_d/D at various time steps, which were converted from Figure 4.19 and 4.20. These plots directly give a correlation of a vortex ring displacement in both axial and radial directions and velocity versus the diameter of a baffle in the certain configuration and injection condition, (i.e. L/D = 2.8, X_b = 4.42D, U_i = 0.7 m/s). Similarly, a series of plots can be created according to different configuration and injection condition.

4.5.2 Varying Injection Velocity

Three injection velocities U_i = 0.7 m/s, 1.4 m/s and 3.0 m/s were tested with a rectangular injection profile. The results of varying the injection velocity are shown in Figures 4.26 and 4.27. Figure 4.26 shows that the trajectory of vortex rings are essentially the same when the baffles have the same size with a diameter of D_d = D, even though the injection velocities were varied from 0.7 m/s to 3.0 m/s. Figure 4.27 shows that before a vortex ring reaches the baffle, the ratio of the axial velocity of a vortex ring to the injection velocity (U/U_i) decreases as the injection

velocity increases.

4.5.3 Varying Baffle Shape

Three different shapes of baffles and configurations were tested with an injection velocity U_i = 1.4 m/s: (i) a solid disc with a diameter of 0.69 D (Figure 4.28 (A)) as employed in above cases; (ii) an annular disc with a central hole, whose inside diameter D_i = D and outer diameter D_o = 2.1 D (Figure 4.28 (B)); and (iii) a system combined the both solid and annular discs, in which the solid disc set at X_b = 3.34 D and the annular disc set at X_b = 4.42 D (Figure 4.28 (C)).

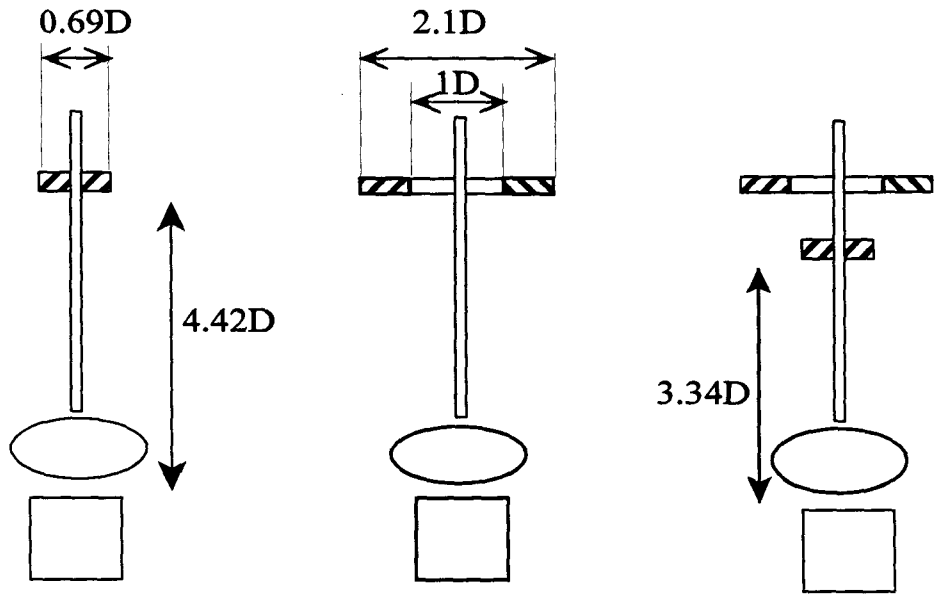

(A) A solid disc (B) An annular disc (C) A system combined both solid and annular discs

Figure 4.28 Diagram of baffles

The results of varying the obstruction shape are shown in Figures 4.29 and 4.30. Comparing the three test scenarios, one can see that the combined baffle system is better than a circular baffle or a annular baffle used alone. The reason is that the core of a vortex ring may pass over the circular baffle perimeter, or it may go through the orifice of the annular baffle, and then continue traveling in an axial direction. However, combining these two baffles together, the system significantly improves the obstructing effect. When a vortex ring reaches the circular baffle, it passes over the baffle with a growing diameter and continues its motion in both axial and radial directions. Then, when the vortex ring approaches the annular baffle with a relatively large diameter, it can not go through the orifice anymore, but can only travel along the baffle in an radial direction until reaches the vessel wall. Figure 4.29 shows that once a vortex ring goes through the baffle orifice, the axial velocity jumps up from 0.1 U_i to 0.14 U_i, and then declines in an axial direction. Using the system of combining two baffles, the axial velocity declines almost linearly and comes to zero just upstream of the annular baffle.

4.6 Discussion and Comment

From this study, it shows the computational result of using the laminar model is in a good agreement with the experimental result, which indicates that the laminar model is appropriate for the simulation of tube type vortex ring generator for injection velocities with rage from 0.7 m/s to 3 m/s. The result also implies that the

type of a injection orifice exit is not a critical fact in vortex ring mixer design.

These results demonstrate that the injection profile shape and value are important parameters of vortex ring formation and propagation. Different injection profiles resulted in different vortex ring displacement data. However, there exists a certain relationship between the injection profile and the subsequent motion of a vortex ring. For a given family of similar injection profiles, it appears possible to correlate the displacement data using non-dimension distance (X/D) versus non-dimension time (t/T_i). A polynomial equation was developed to express this relationship in variation injection profile as the following:

$$X/D = a\,(t/T_i)^2 + b\,(t/T_i) + c$$

where a, b and c are constants related to injection profile.

It is clear that putting obstructions into the path of a vortex ring can significantly change the trajectory and velocity of the vortex ring. The diameter of a obstruction has a pronounced affect on "eye" distance of a vortex ring traveled in both axial and radial directions, and the rate of deceleration of a vortex ring. As expected, the larger the obstruction, the greater the effect it has. As the size of the obstruction increases, the diameter of a vortex ring increases in the radial direction, but its axial velocity decreases. The obstruction begins to deflect the vortex ring at approximately 1.4 D upstream of it for giving baffle diameters from 0.23 D to 1.75 D. Moreover, the location that a vortex ring starts to stray from its original trajectory does not depend on the size of the obstruction. The injection velocity does not appear to noticeably affect the "eye" trajectory. By using several baffles with

different sizes and shapes together, the trajectory of a vortex ring can be controlled in a desirable way. A series of plots of the correlation of a vortex ring non-dimension displacement and velocity versus the non-dimension diameter of a baffle in the certain configuration and injection condition were generated.

The results of this research can be applied to the design vortex ring mixers using for the control of the mixing process. According to the content and shape of a vessel and the properties of a mixture, designers may use one or several baffles with different size and shape to control the zone of influence of a vortex ring. Therefore, the energy generated by vortex rings could be maximized for relatively violent mixing, and splashing could be avoided.

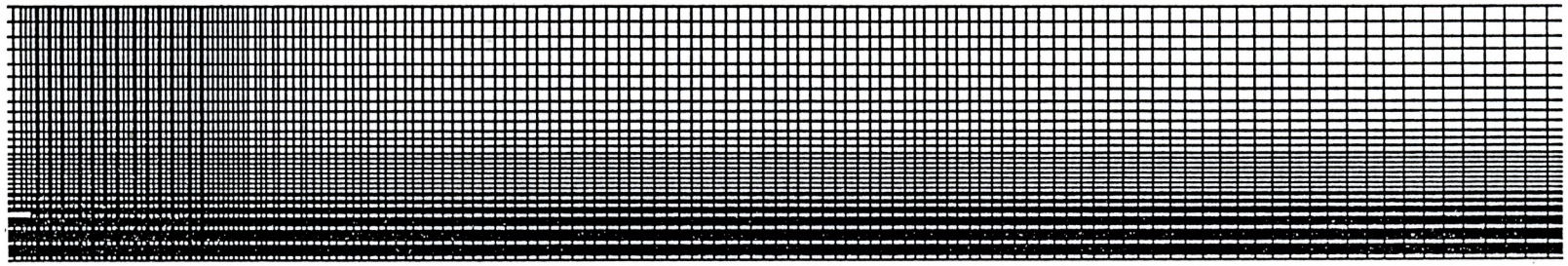

Figure 4.1

Grid (171 X 43)

Mar 11 1998
Fluent 4.47
Fluent Inc.

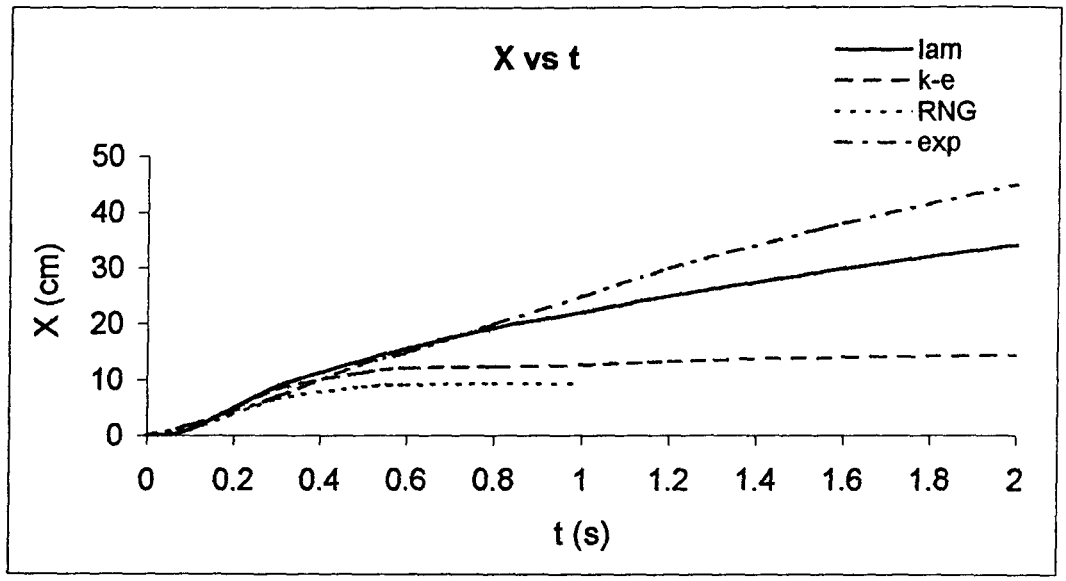

Figure 4.2 Plots of different models

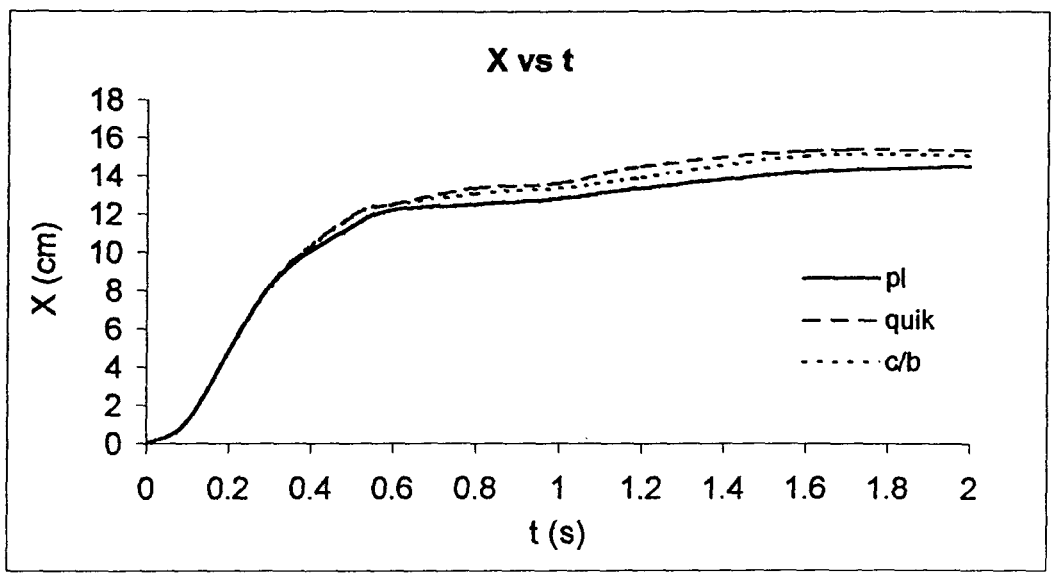

Figure 4.3 Plots of different discretization schemes

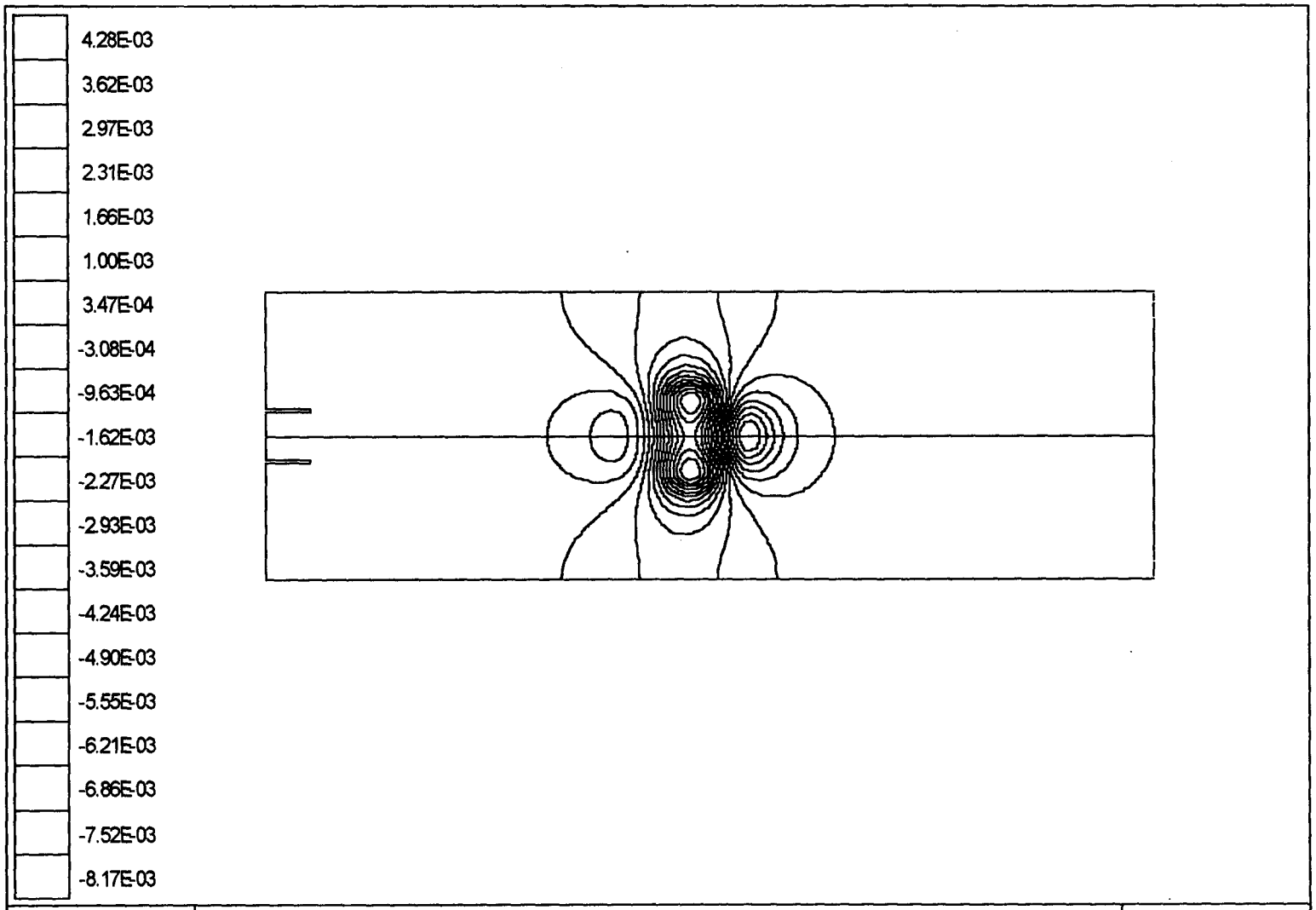
4.28E-03
3.62E-03
2.97E-03
2.31E-03
1.66E-03
1.00E-03
3.47E-04
-3.08E-04
-9.63E-04
-1.62E-03
-2.27E-03
-2.93E-03
-3.59E-03
-4.24E-03
-4.90E-03
-5.55E-03
-6.21E-03
-6.86E-03
-7.52E-03
-8.17E-03
Y
Z X
Figure 4.6
Static Pressure (Pa)
Max = 4.280E-03 Min = -8.173E-03 Time = 3.000E+00
Mar 08 1999
Fluent 4.48
Fluent Inc.

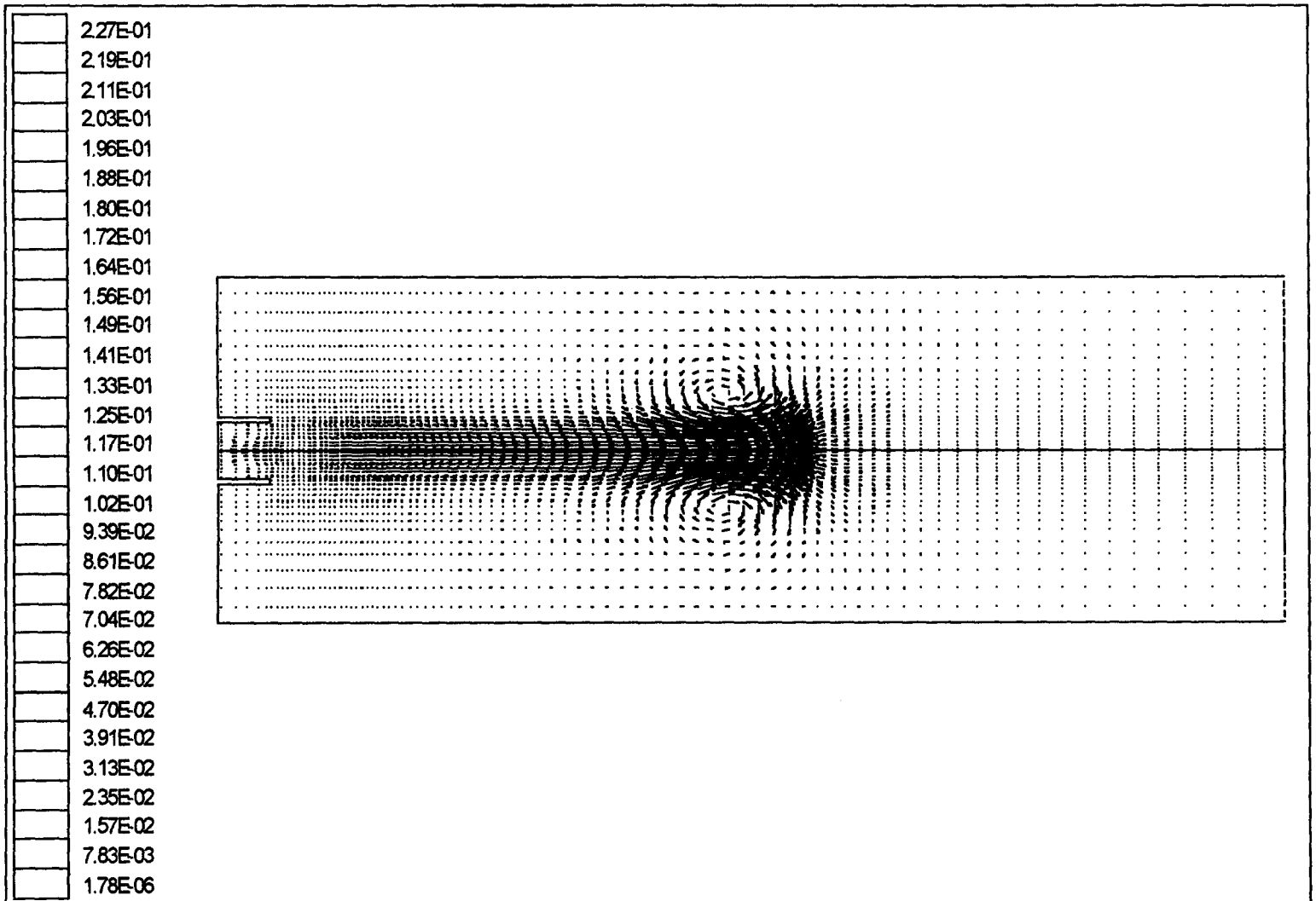
2.27E-01
2.19E-01
2.11E-01
2.03E-01
1.96E-01
1.88E-01
1.80E-01
1.72E-01
1.64E-01
1.56E-01
1.49E-01
1.41E-01
1.33E-01
1.25E-01
1.17E-01
1.10E-01
1.02E-01
9.39E-02
8.61E-02
7.82E-02
7.04E-02
6.26E-02
5.48E-02
4.70E-02
3.91E-02
3.13E-02
2.35E-02
1.57E-02
7.83E-03
1.78E-06
Y
Z X
Figure 4.7
Velocity Vectors (M/S)
Max = 2.269E-01 Min = 1.779E-06 Time = 3.000E+00
Mar 09 1999
Fluent 4.48
Fluent Inc.

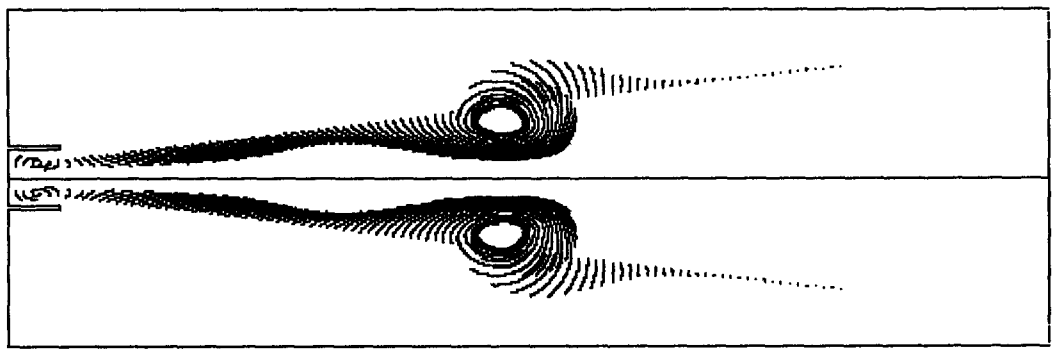

Y Z X	**Figure 4.8** Streaklines	Mar 08 1999 Fluent 4.48 Fluent Inc.

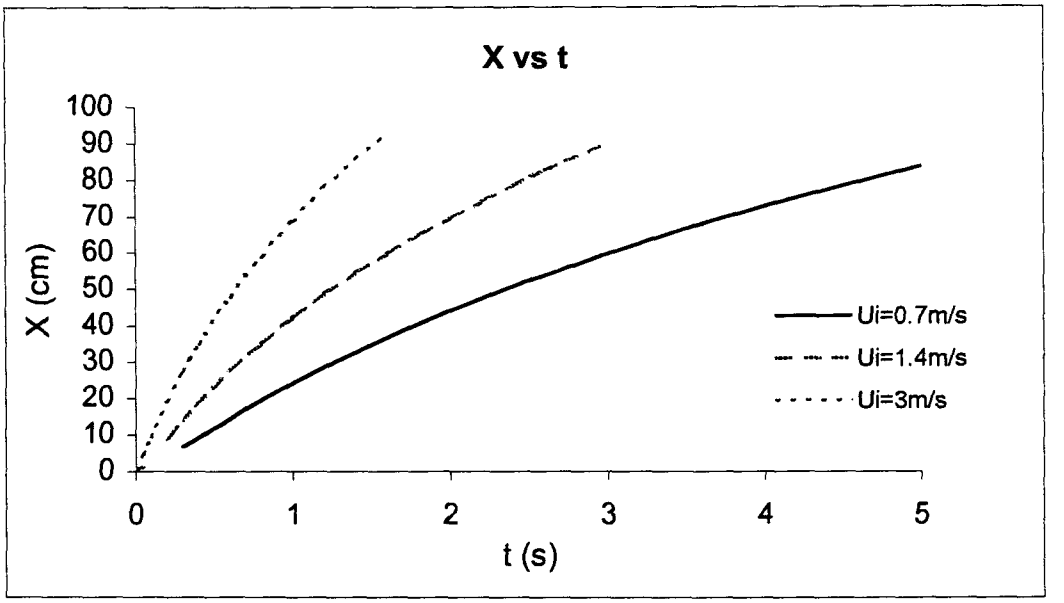

Figure 4.9 X vs t for variation of injection velocities

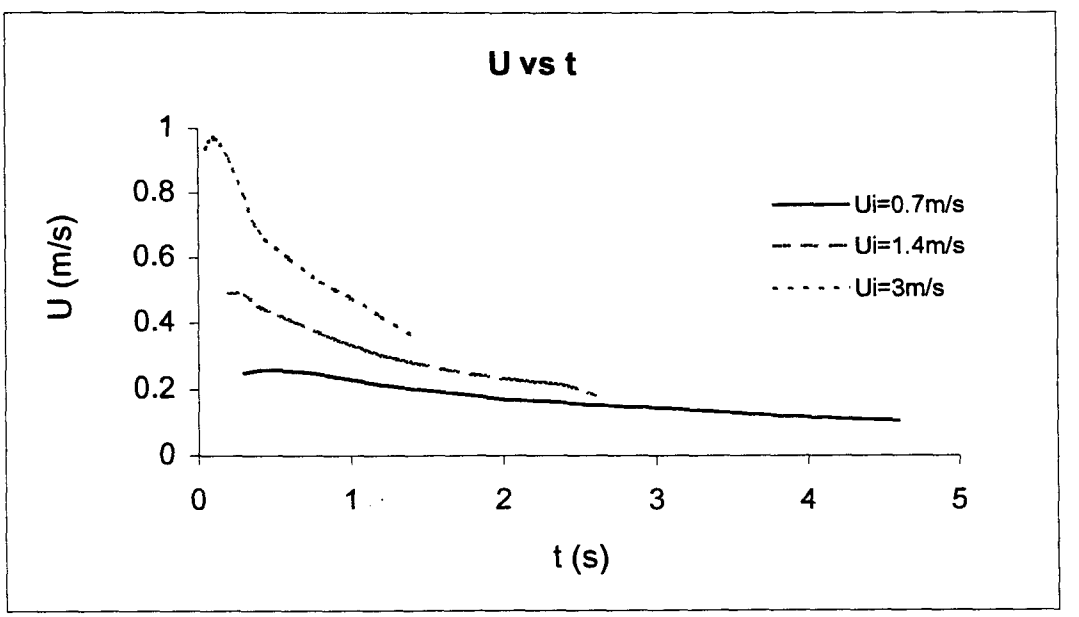

Figure 4.10 U vs t for variation of injection velocities

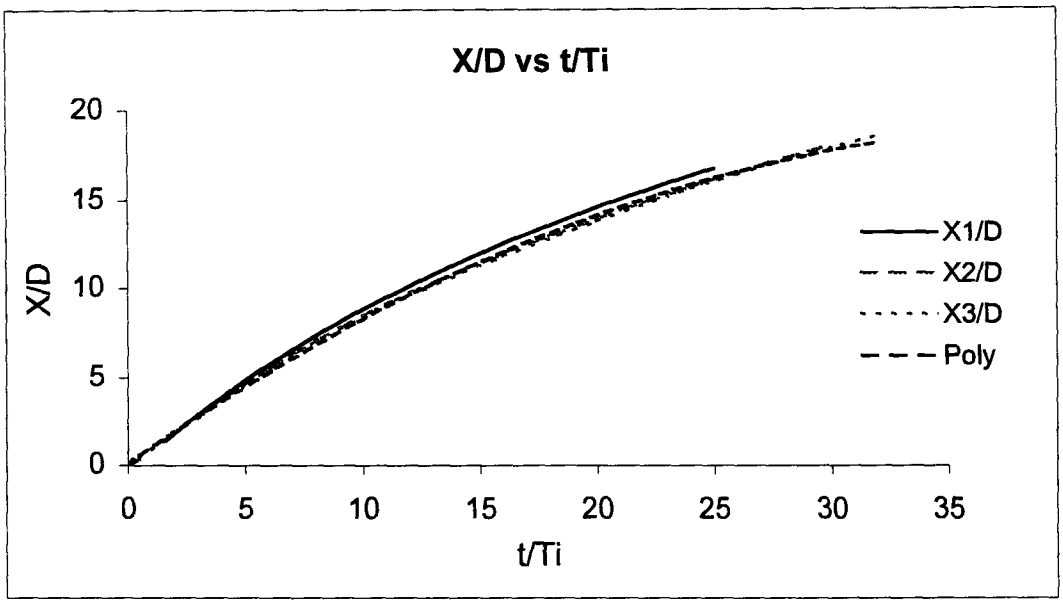

Figure 4.11 X/D vs t/Ti for variation of injection velocities

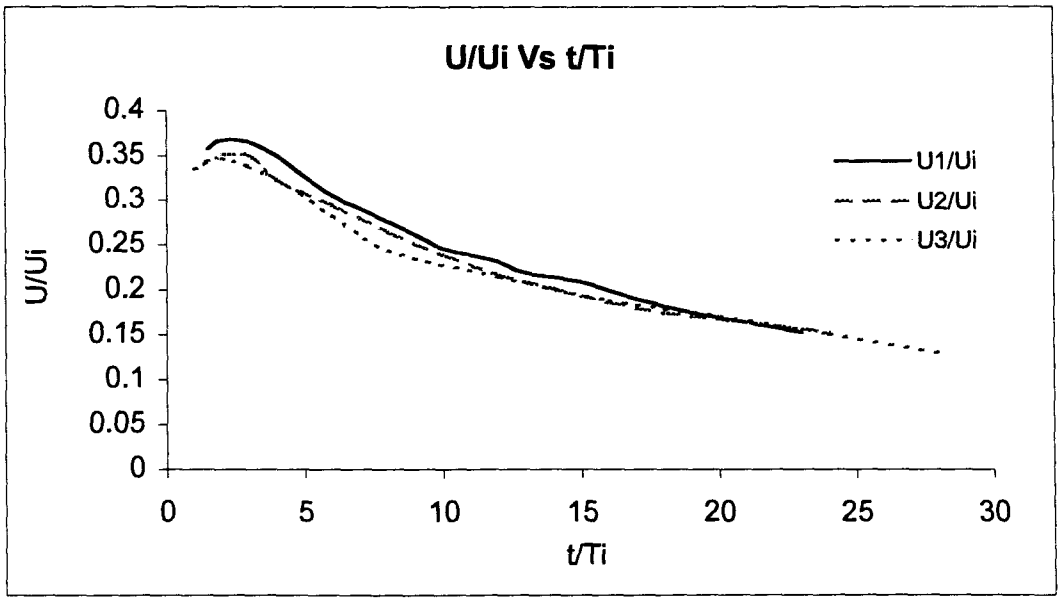

Figure 4.12 U/Ui vs t/Ti for variation of injection velocities

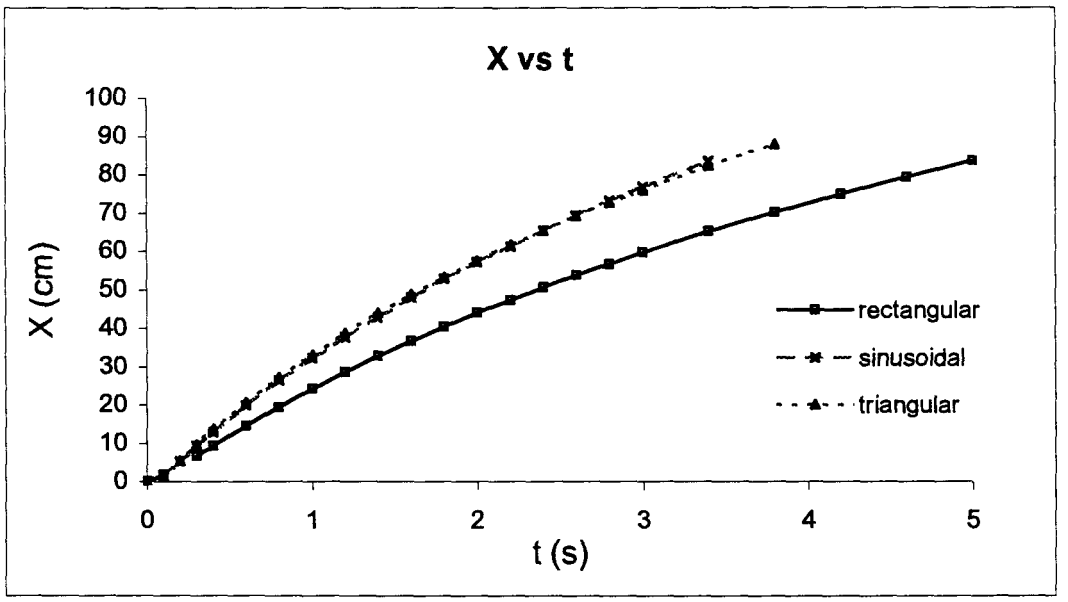

(a)

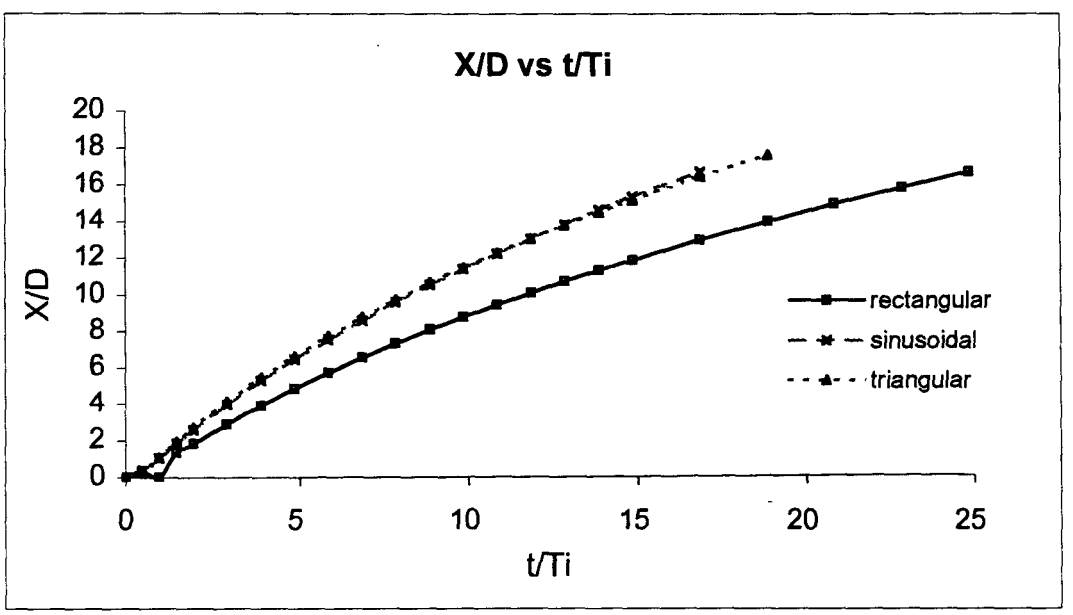

(b)

Figure 4.13 Displacement vs time for various injection profiles

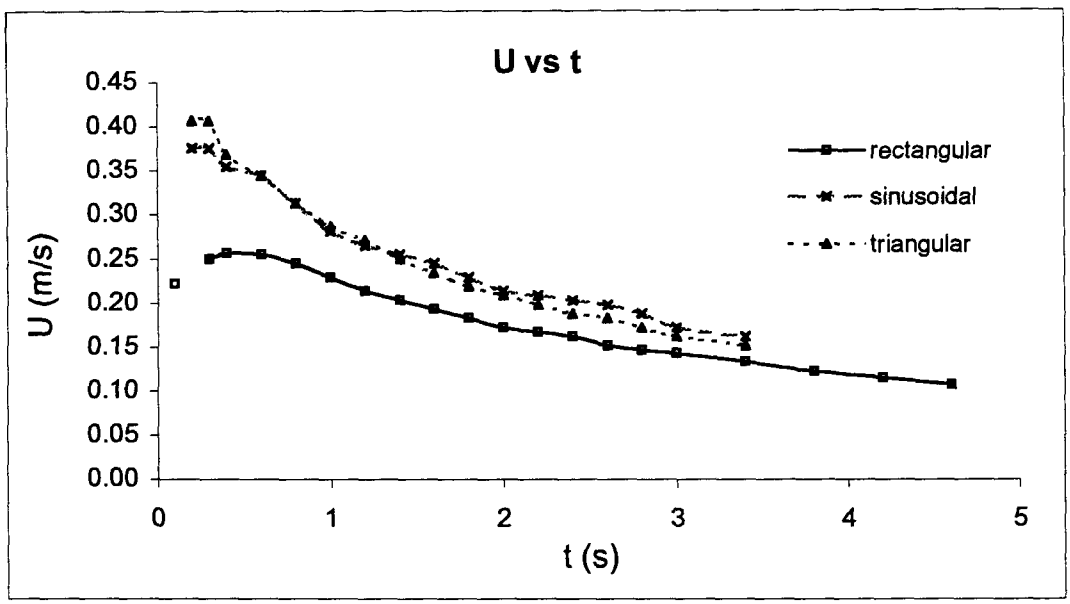

Figure 4.14 Velocity vs time for various injection profiles

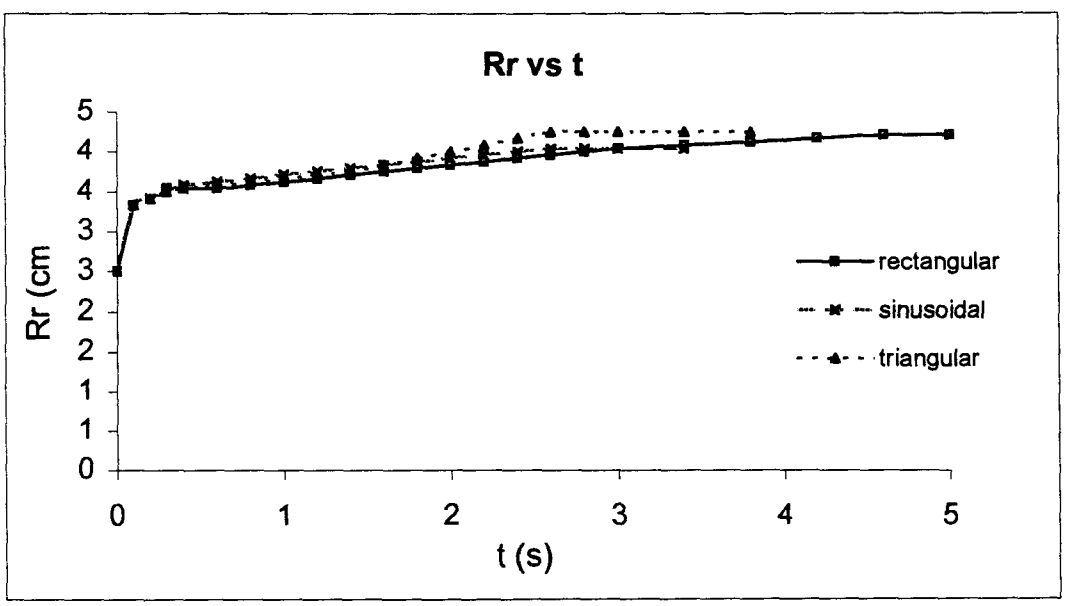

Figure 4.15 Radius vs time for various injection profiles

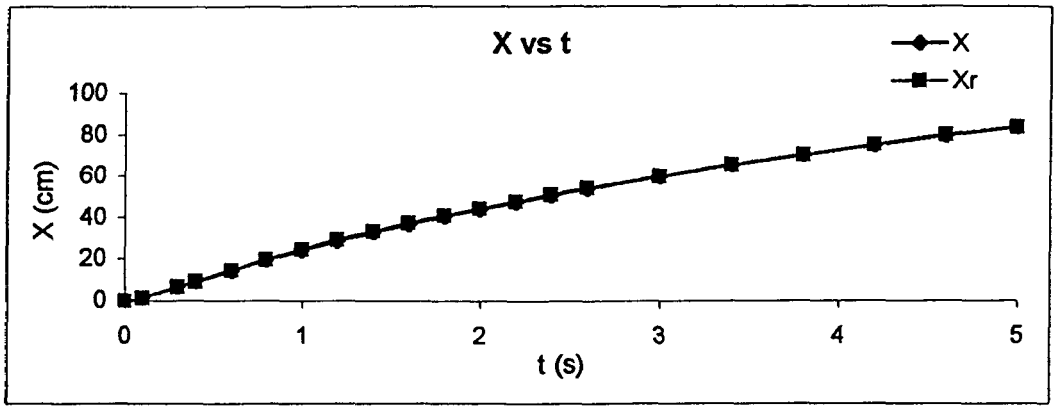

(A)

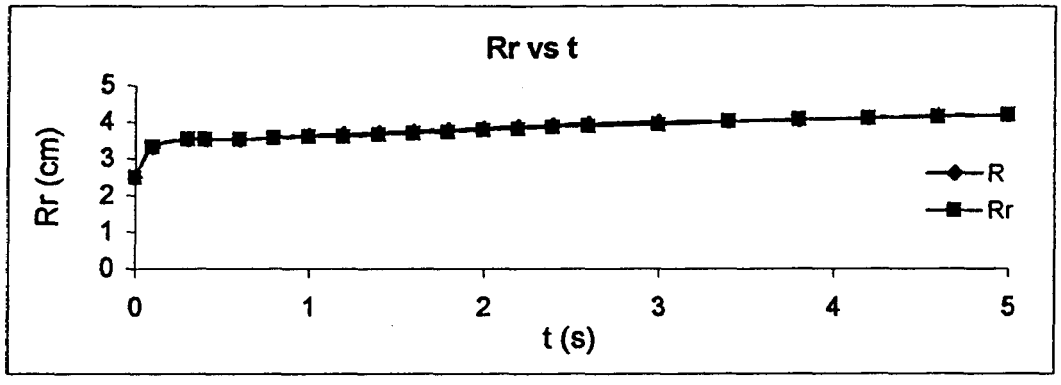

(B)

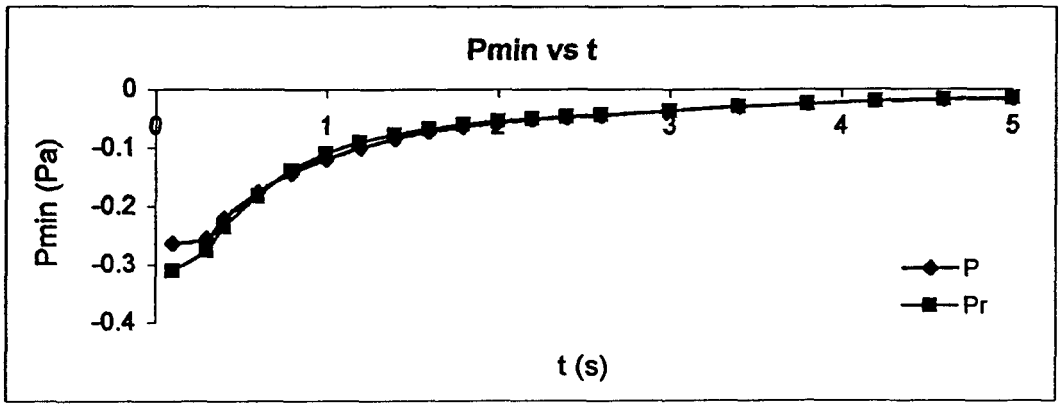

(C)

Figure 4.17 X, Rr and Pmin vs t

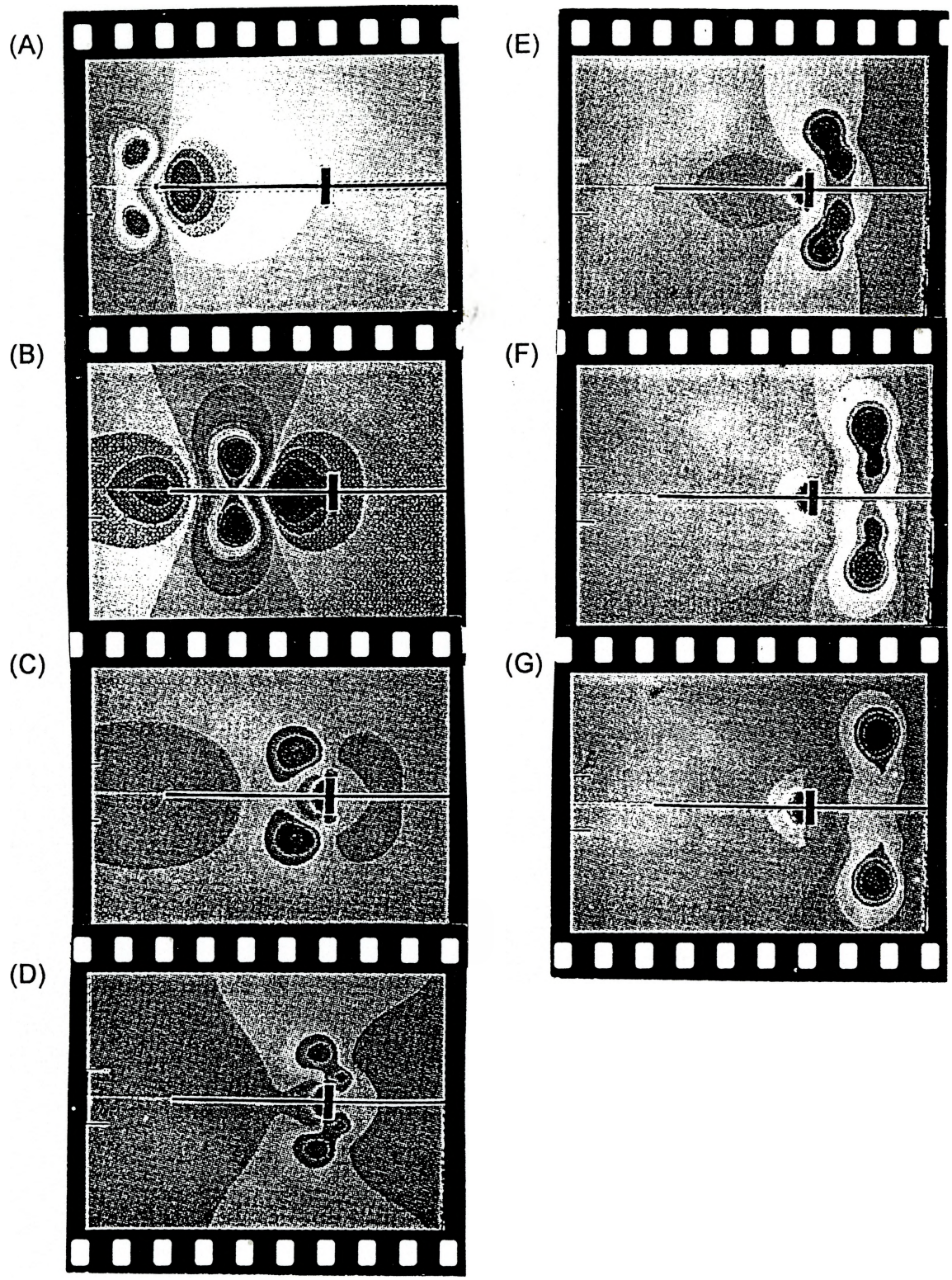

Figure 4.18 Frames of color filled pressure contour plots.

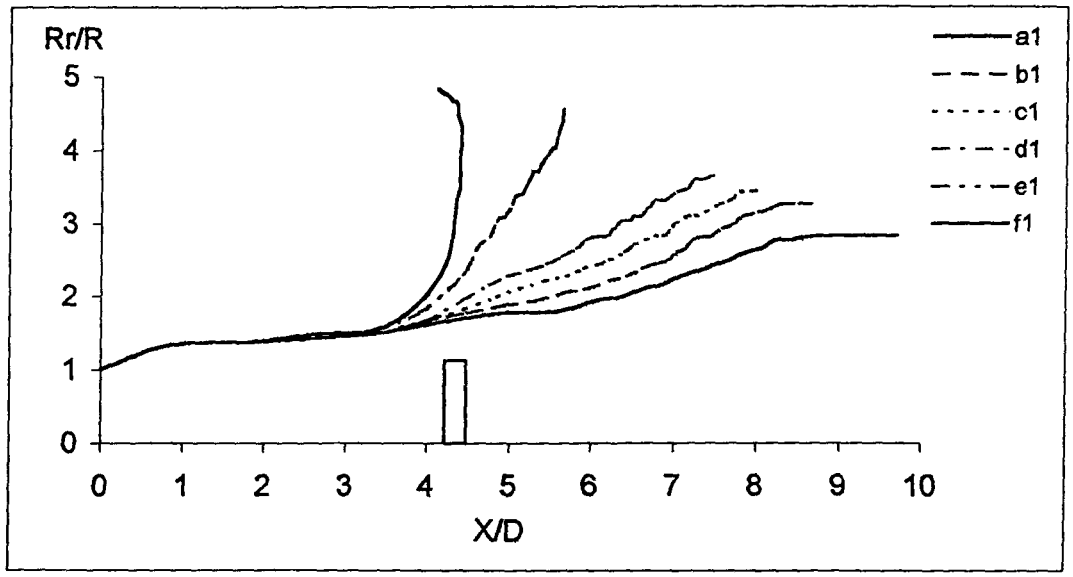

Figure 4.19 Rr/R vs X/D at Ui = 0.7m/s

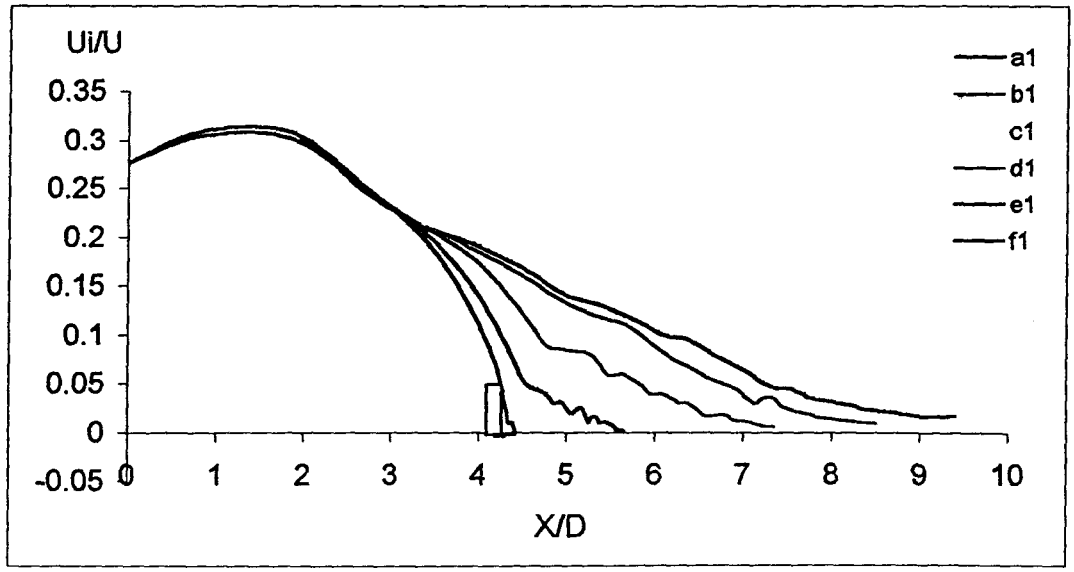

Figure 4.20 U/Ui vs X/D at Ui = 0.7 m/s

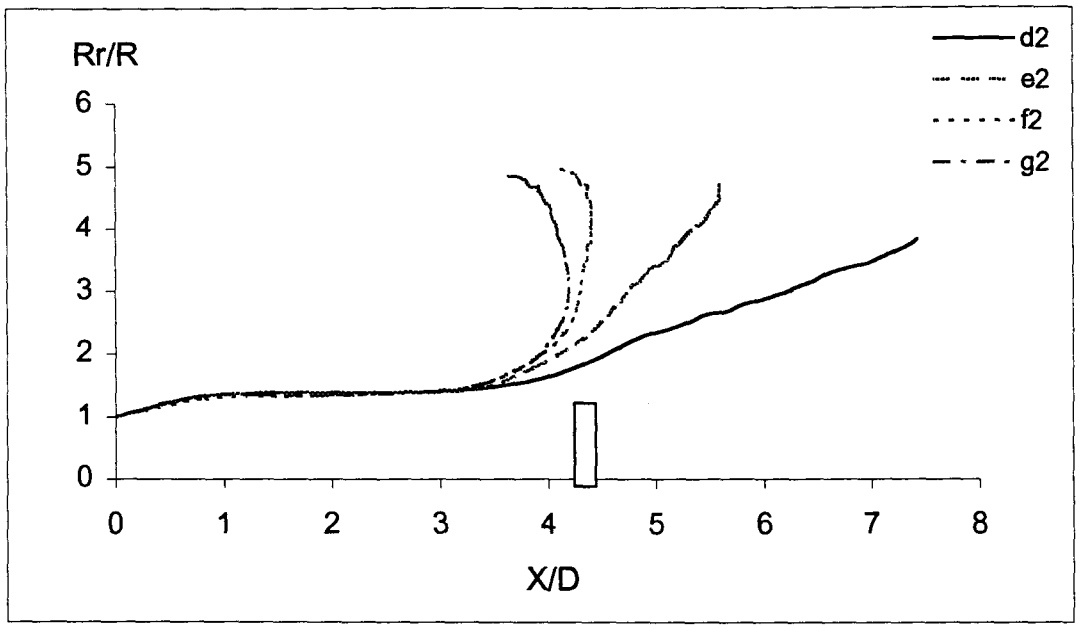

Figure 4.21 Rr/R vs X/D at Ui = 1.4 m/s

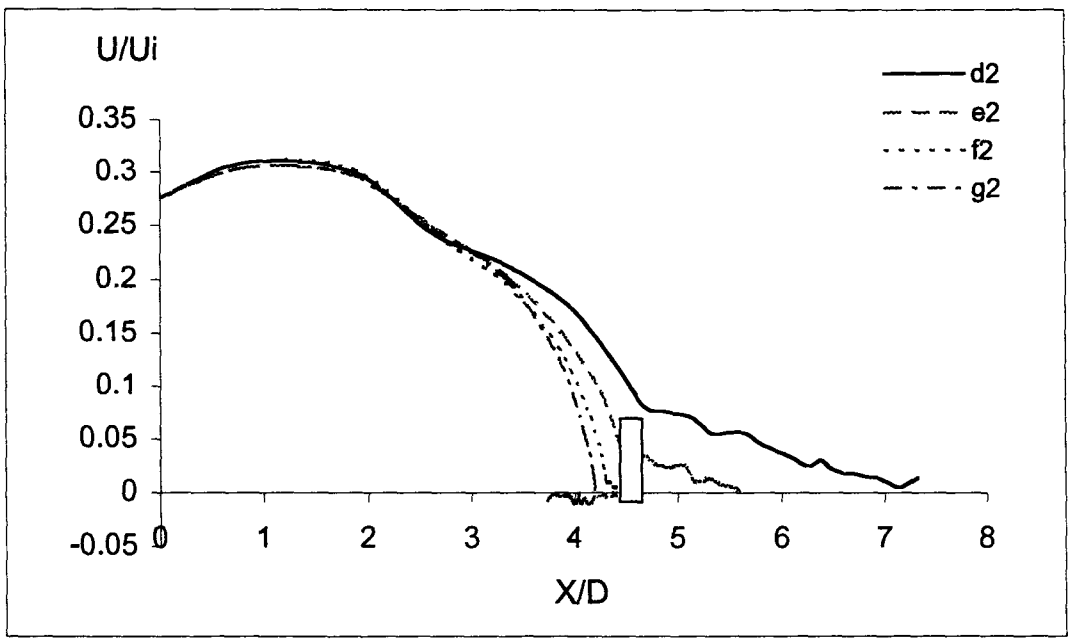

Figure 4.22 U/Ui vs X/D at Ui = 1.4 m/s

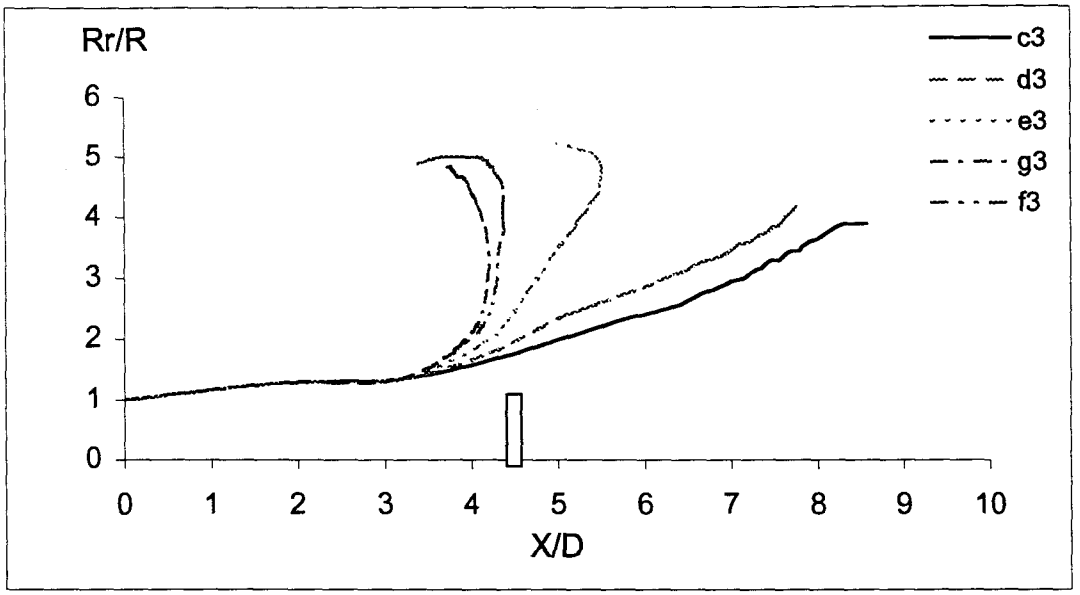

Figure 4.23 Rr/R vs X/D at Ui = 3 m/s

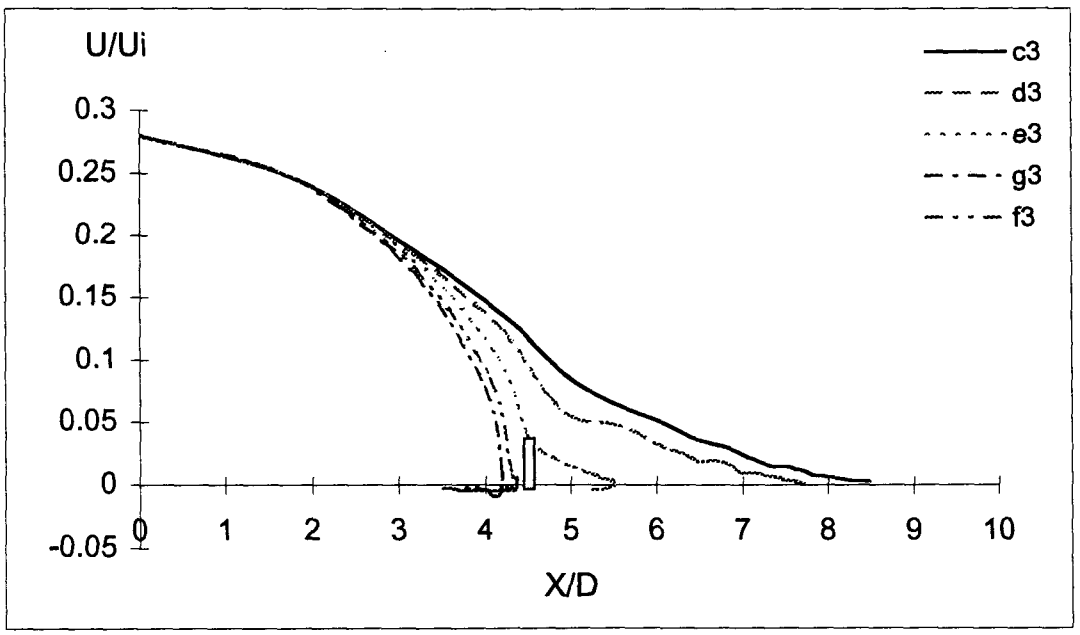

Figure 4.24 U/Ui vs X/D at Ui = 3 m/s

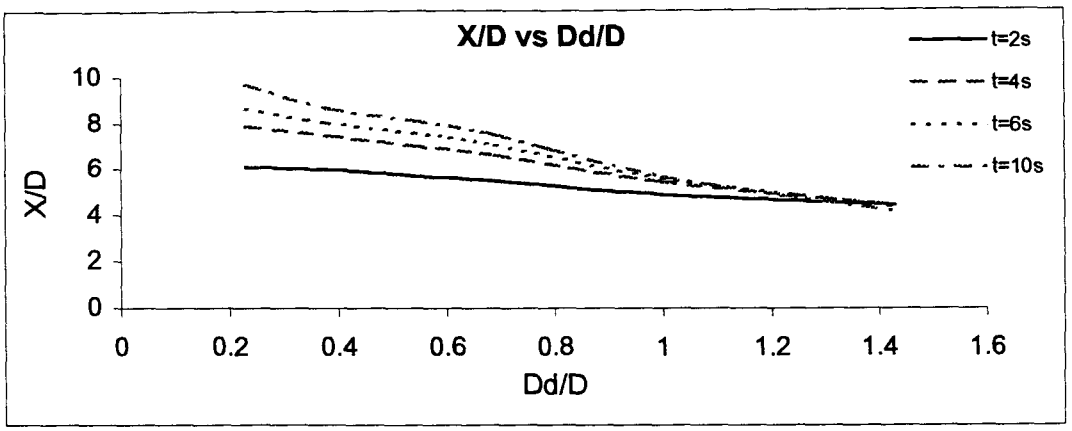

(A)

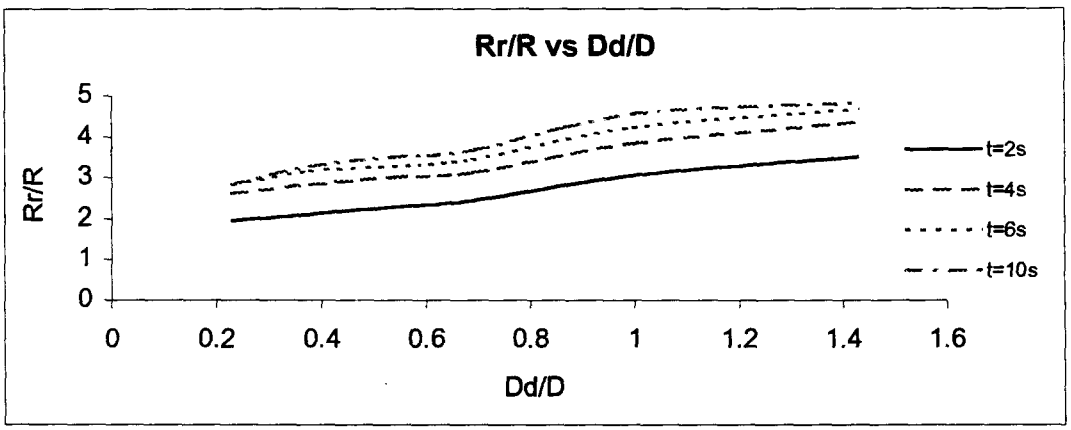

(B)

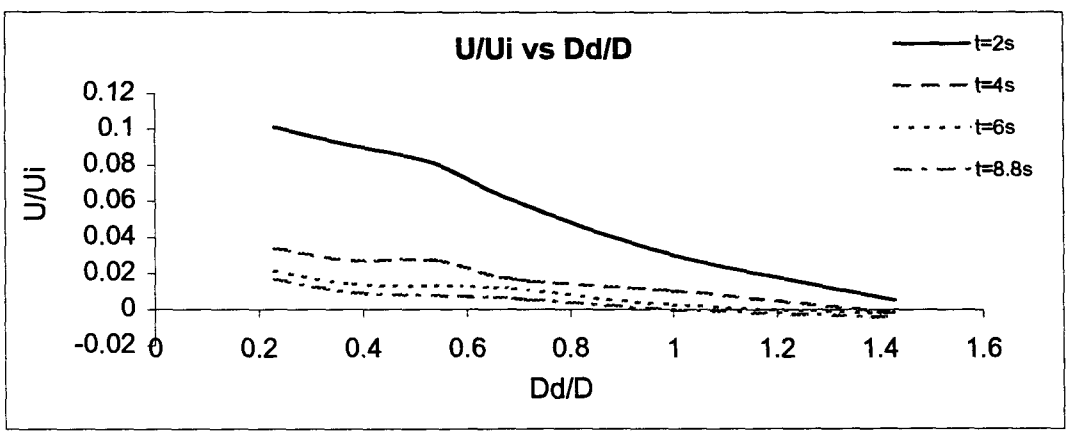

(C)

Figure 4.25 X/D, Rr/R and U/Ui vs Dd/D at different time steps

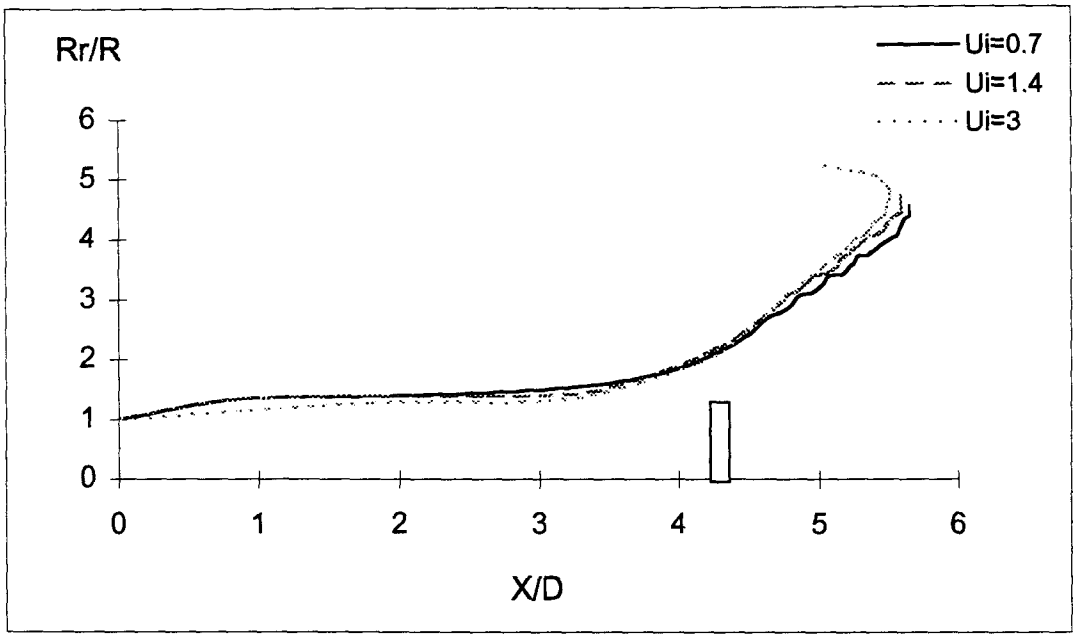

Figure 4.26 Rr/R vs X/D with Dd = D

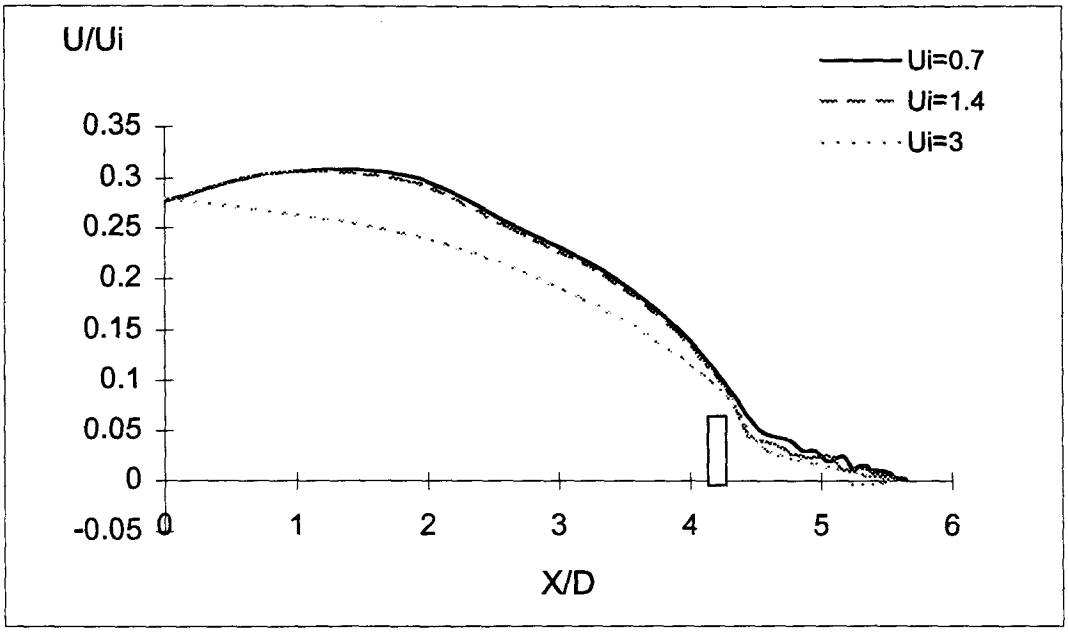

Figure 4.27 U/Ui vs X/D with Dd = D

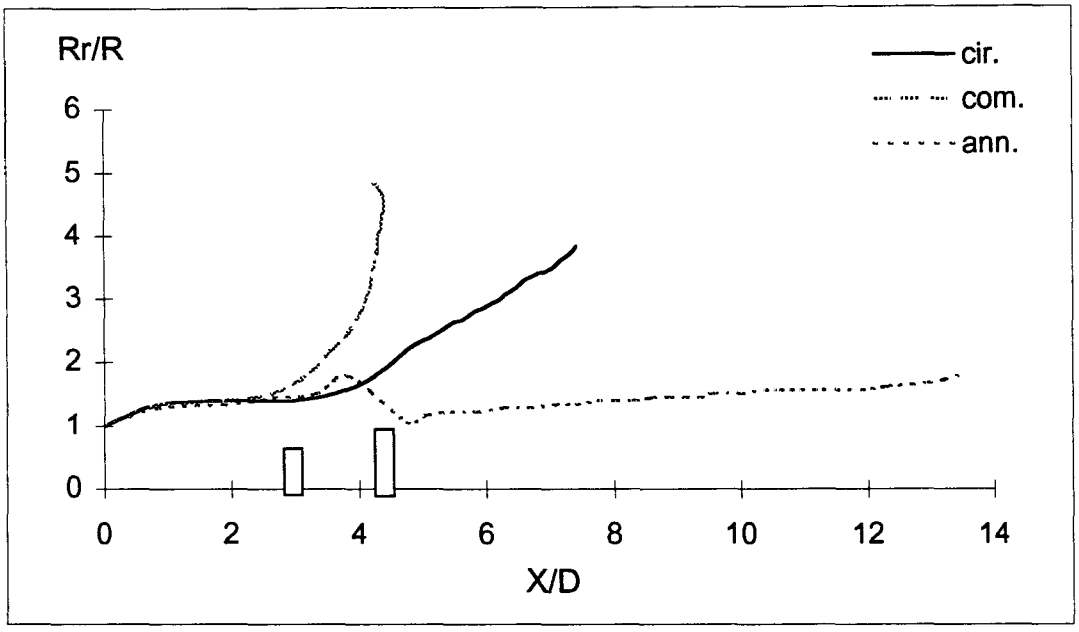

Figure 4.29 Rr/R vs X/D with varying baffles

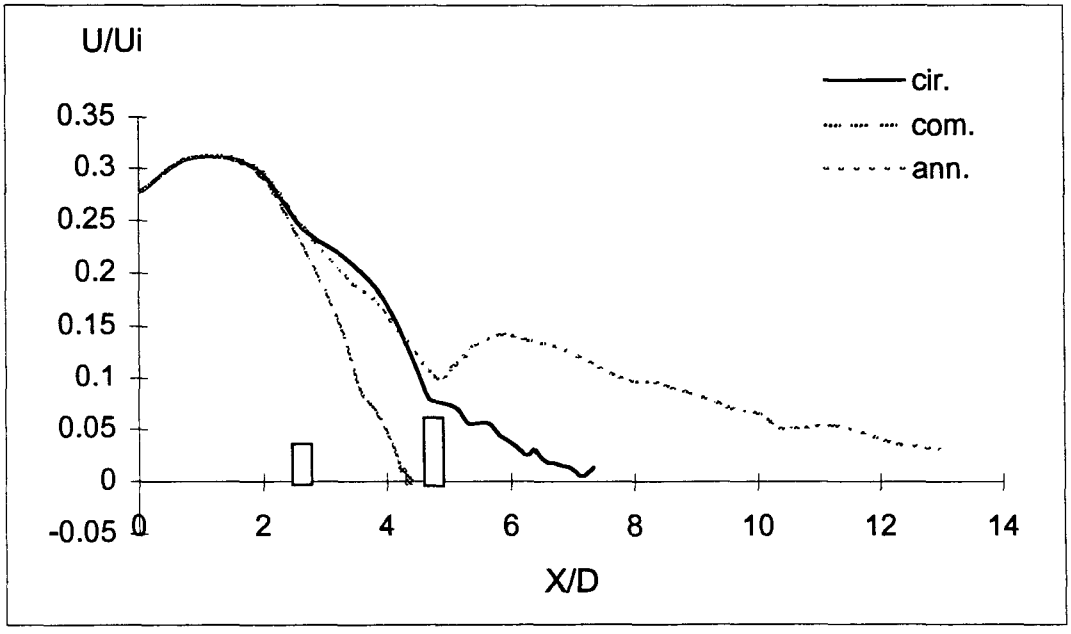

Figure 4.30 U/Ui vs X/D with varying baffles

CHAPTER 5

SIMULATION OF PLATE TYPE VORTEX RING MIXER

5.1 Introduction

In the prior studies the generating orifice was stationary and set just above the fluid surface. This is often impractical and a moving orifice is usually required for many practical applications. Therefore there is a need to investigate oscillating orifice plate generators. An introductory study on this matter was therefore conducted.

The orifice plate is usually located at a desirable depth in the fluid being agitated. The orifice plate is either impulsively moved or oscillated with a sinusoidal motion. When a generating plate stops and reverses its direction, a secondary vortex ring may be generated, due to inertial effects of the fluid following the plate, (see diagram in Figure 5.1). Thus as an orifice plate oscillates through one cycle, four vortex rings, two primary and two secondary vortex rings, may be generated depending on the motion of the plate. In a tube generator, only one primary vortex ring is emitted from the tube and relatively weak secondary ring travels into the generator tube in one cycle of liquid oscillation. Therefore, a plate type vortex ring mixer can have significantly higher mass transfer efficiency than a single tube type

vortex ring mixer, although the latter one produces a larger vortex ring than the former one.

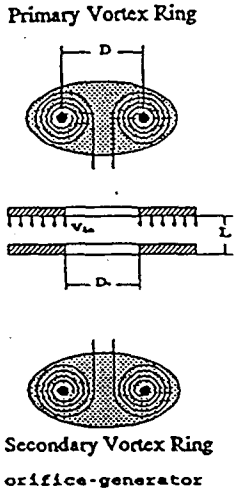

Figure 5.1 Primary & secondary vortex rings generated from an orifice plate. Hua (1994)

As previously stated, in order to efficiently design a vortex ring mixer, it is important to accurately assess vortex ring behaviour during the formation and propagation stages with a moving orifice plate. Moving mesh simulations using FLUENT (version 4.4) could permit the simulation of such flows in which physical boundaries are moving. The simulation of plate type vortex ring mixer using FLUENT to describe the vortex ring formation and propagation in a half cycle of the plate oscillation, will be discussed in this chapter.

5.2 Model Description

5.2.1 Geometry Setup and Grid Generation

Deforming mesh techniques may be used in dealing with an internal moving element, such as a vortex ring generator. The basic geometry outline is similar to the model previously described in chapter 4, which is an axis-symmetric polar model of a vessel having a radius 15 units and a length 100 units. However in this case the vortex ring generator is changed from a tube type to a plate type generator, and the orifice location is moved from the fluid surface to the middle of the fluid volume.

The deforming mesh model simulates flows in domains whose shape changes with time. In this model, a prescribed boundary and grid deformation is provided as part of the problem definition and the motion induced by the boundary motion contributes to the time varying flow prediction. The deforming mesh model requires that the time variation of the grid be prescribed as part of the problem definition. This domain discretization at each time step can be prescribed by reading a series of mesh files with interpolation between files. New control volumes are not created as the boundary moves and the basic grid topology remains unaltered throughout the calculation. Thus the initial grid must deform as the physical boundaries move. Each grid file or interpolated grid between files defines the geometry at successive time steps. The total number of instantaneous grid descriptions dictates the number of time values that can be considered.

Assuming that the orifice plate moves at an uniform velocity, U = constant, during the period of a half cycle ($0 \leq t \leq T_i$), two grid files are required for the simulation. The first grid is the plate initially at rest (t=0), and the second grid is when the plate has reached half its cycle ($t=T_i$), see Figure 5.2 (a) and (b). These two grid files were created using GeoMesh which is a CAD program of geometry creation and grid generation for the Fluent Inc. CFD software packages. A non-uniform grid is used and a more dense grid is constructed in the region of the moving plate orifice than the rest of the region. The total number of cells is 6080, which is 40 radially by 152 axially.

5.2.2 Physical Model Selection

Three basic flow models have been tested, which are (i) a laminar model, (ii) a standard k-ε turbulence model, and (iii) a RNG k-ε turbulence model. The computational results show that the computation using the laminar model is much more difficult to converge than the standard and the RNG k-ε turbulence models. However, no noticeable difference between these two turbulence models was observed.

Due to the extra terms and functions in the governing equations and a greater degree of non-linearity, computations with the RNG k-ε model tends to take more CPU time than with the turbulence standard model (about 10 - 15% increase). Furthermore compared to the turbulence standard model, the RNG model is more likely to be susceptible to instability and may lead to convergence difficulty.

Therefore, the k-ε turbulence model was selected for the simulation of plate type vortex ring mixer.

The default differencing scheme used in FLUENT is the power-law scheme, which is derived from the exact analytical solution of the one dimensional convection-diffusion equation. This scheme provides an accuracy between first and second order. The second-order upwind and QUICK schemes provide a higher order accuracy. When the flow is at an angle to the grid or higher numerical accuracy is required, these two schemes are recommended by FLUENT. The blended upwind/central scheme provides a blending of second-order-upwind and central differencing to calculate face values. The QUICK scheme involves a quadratic interpolation which provides higher numerical accuracy in the solution and can improve the interpolation when the flow is turning and is not aligned with the grid.

Having tested different schemes with the turbulence model, it was found that the model is very sensitive to the discretization interpolation schemes, and no vortex rings were formed when using the power-law scheme. Thus, the alternative QUICK scheme was chosen in this simulation.

5.2.3 Velocity Profile and L/D Ratio

A rectangular velocity profile for the plate was considered with U_i in the range 0.6 m/s to 2.5 m/s during $0 \leq t \leq T_i$, and varying T_i in the range from 0.1 to 0.02 seconds, for a given plate stroke or moving distance s.

Referring to Figure 5.3, for a plate type generator, the equivalent fluid slug length L may represent as:

$$L = (D_o/D_i)^2 s \qquad (5.1)$$

Where D_i is the orifice equivalent diameter, D_o is the overall diameter of the plate, and s is the plate stroke length. Assuming some amount fluid passes around the periphery of the plate, the fraction of the displaced volume passing through the orifice is k ($0 < k \leq 1$). The ratio of L/D is then:

$$L/D_i = k\, D_o^2 s/D_i^3 \qquad (5.2)$$

Since k is unknown and may vary with the geometry, size and velocity of a generating plate, the L/D ratios in the range from 3 to 7 were tested using FLUENT.

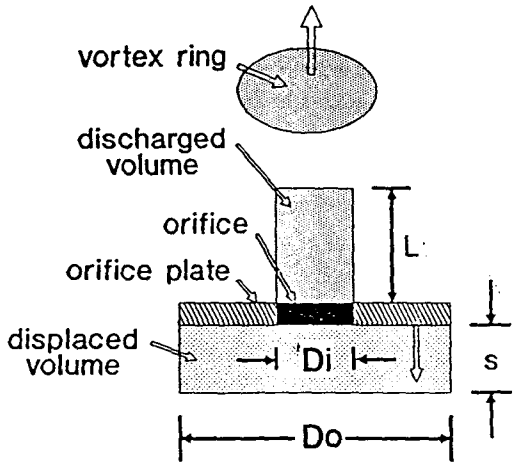

Figure 5.3 Generating parameters for a vortex ring at an orifice plate.

5.3 Result and Discussion

Figures 5.4 to 5.6 show the resulting pressure contour, velocity vectors and streaklines for primary and secondary vortex rings simultaneously generated through a generating orifice plate. As the orifice plate moved forwards, a primary vortex ring is ejected backwards; and when the plate was abruptly stopped, the inertial force of the fluid behind the generation plate produced a secondary vortex ring which travels in an opposite direction to that of the primary ring. Velocity vectors and streaklines show that the primary and secondary vortex rings have almost similar strength and approximately same trajectory. Thus, a plate type vortex ring generator could produce a pair of rings (primary and secondary ring) per stroke, and a total of four rings for a complete cycle of a plate oscillation. Consequently, a plate type generator could create higher mass transfer than a tube type generator. This may be particularly useful for the mixing of sedimentary slurries or stratified fluids, when a plate generator could be located near the interface, two pair of vortex rings, respectively containing dense and dilute phases, would be ejected upwards and downwards per cycle, which could cause rapid mix of the materials.

On the other hand, the Figures 5.5 and 5.6 also show that the primary and secondary vortex rings appear to be stationary adjacent to the generation plate, and not moving in the axial direction as fast as expected. This is not in agreement with the data for similar conditions which were generated using a numerical simulation

numerical simulation developed by Hua (1994).

Hua (1994) using a finite difference technique developed a computer model to solve the continuity, Navier-Stokes and energy equations in cylindrical coordinates with laminar model. His computational results show that both primary and secondary vortex rings traveled respectively from the orifice of the generation plate to the bottom of the tank and the surface (see Figure 5.7). Figure 5.8 presents Hua's computational and empirical data for the axial displacement of a vortex ring from the generation orifice, which shows relatively good agreement between the numerical simulation and empirical measurement.

Visual observations appear to indicate that a turbulent vortex ring is not truly turbulent. That is, there appears to be a distinct difference between a laminar vortex ring and what appear to a non-laminar ring, however, it cannot be definitively stated that the flow is totally turbulent throughout the entire volume vortex ring. It is observed a transition in the structure of a vortex ring occurs sometime after a vortex ring is generated and the central core around the "eye" of this ring becomes turbulent, but the outer region of the vortex ring does not appear to be so, see Figure 5.9. Therefore the use of a single hydrodynamic model may not accurately depict the behavior of a so-called turbulent vortex ring. However it is difficult to use different models in various time step and geometry during a computation with FLUENT. The FLUENT version 4 does not appear to be suitable for the simulation of plate type vortex ring generators, especially during the propagation phase.

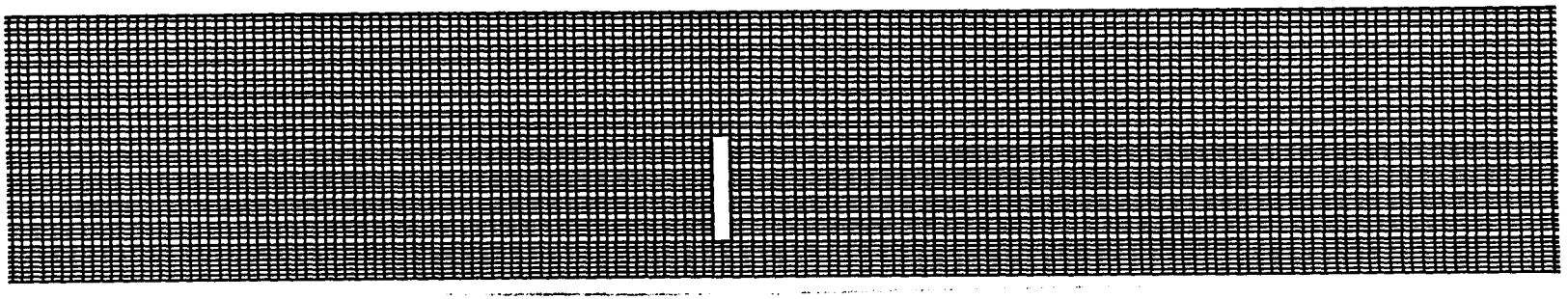

(a)

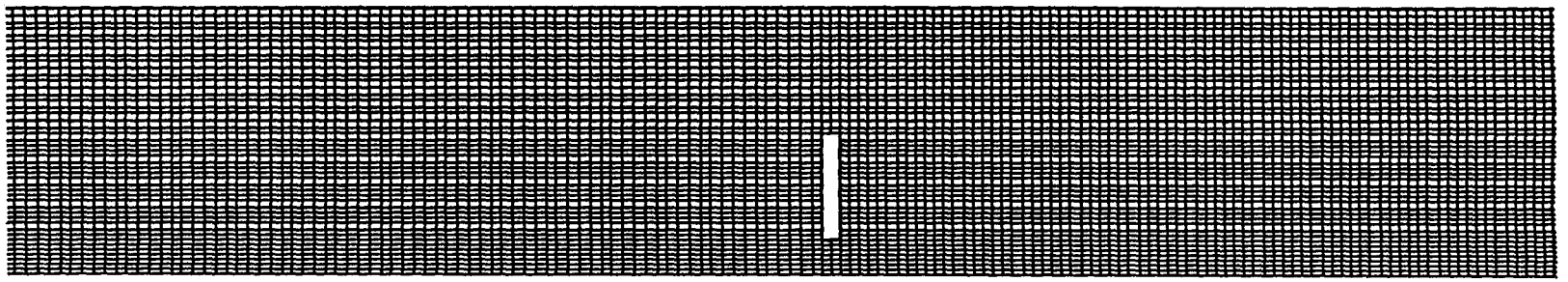

(b)

Figure 5.2

FLUENT Grid File /* CONFIGURATION = yy2 */

Grid (161 X 46) Time = 0.000E+00

Jan 11 1999

Fluent 4.47

Fluent Inc.

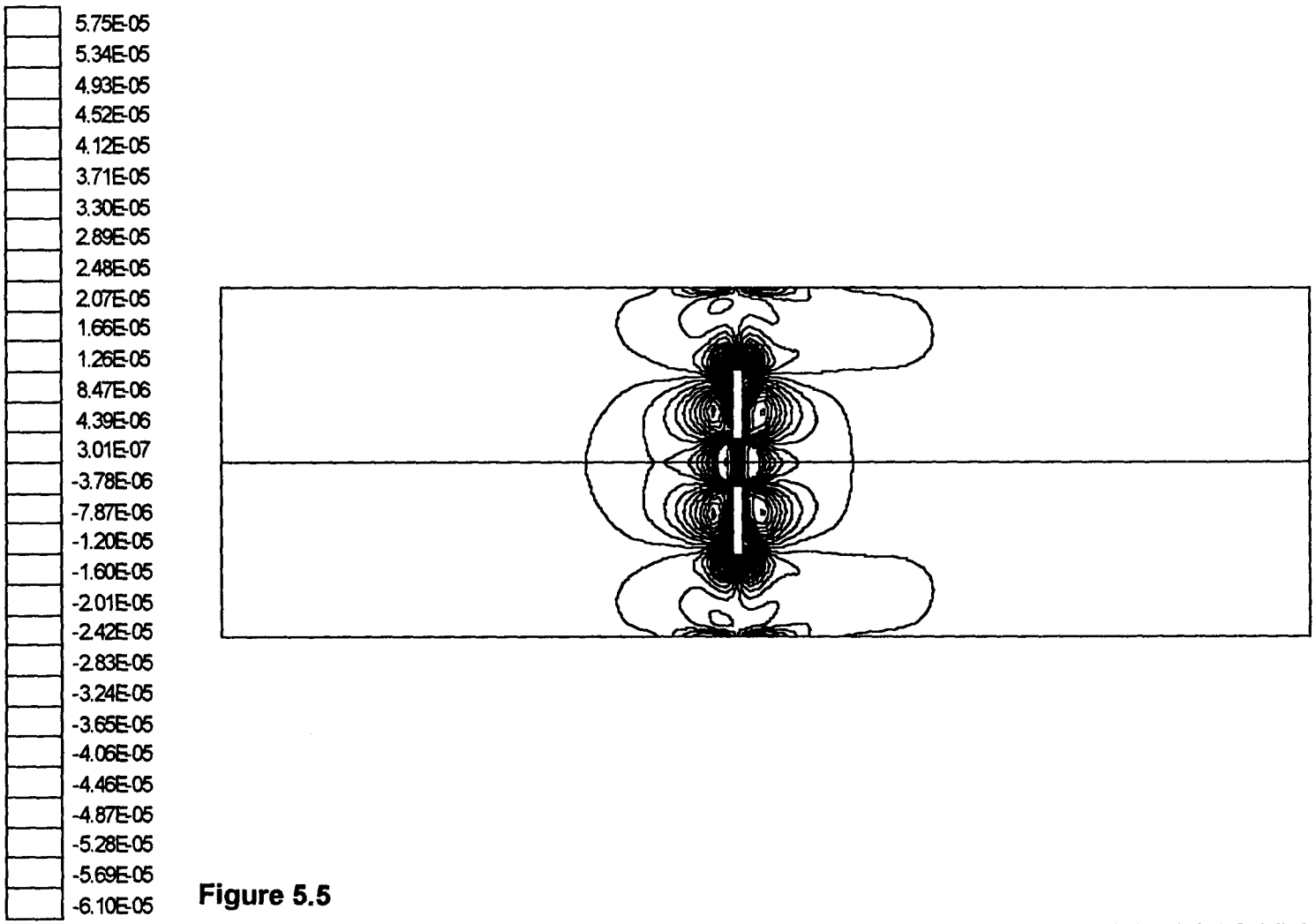
5.75E-05
5.34E-05
4.93E-05
4.52E-05
4.12E-05
3.71E-05
3.30E-05
2.89E-05
2.48E-05
2.07E-05
1.66E-05
1.26E-05
8.47E-06
4.39E-06
3.01E-07
-3.78E-06
-7.87E-06
-1.20E-05
-1.60E-05
-2.01E-05
-2.42E-05
-2.83E-05
-3.24E-05
-3.65E-05
-4.06E-05
-4.46E-05
-4.87E-05
-5.28E-05
-5.69E-05
-6.10E-05
Y
Z X
FLUENT Grid File /* CONFIGURATION = yy1 */
Static Pressure (Pa)
Max = 5.750E-05 Min = -6.098E-05 Time = 4.000E-01
Mar 08 1999
Fluent 4.48
Fluent Inc.

Figure 5.5

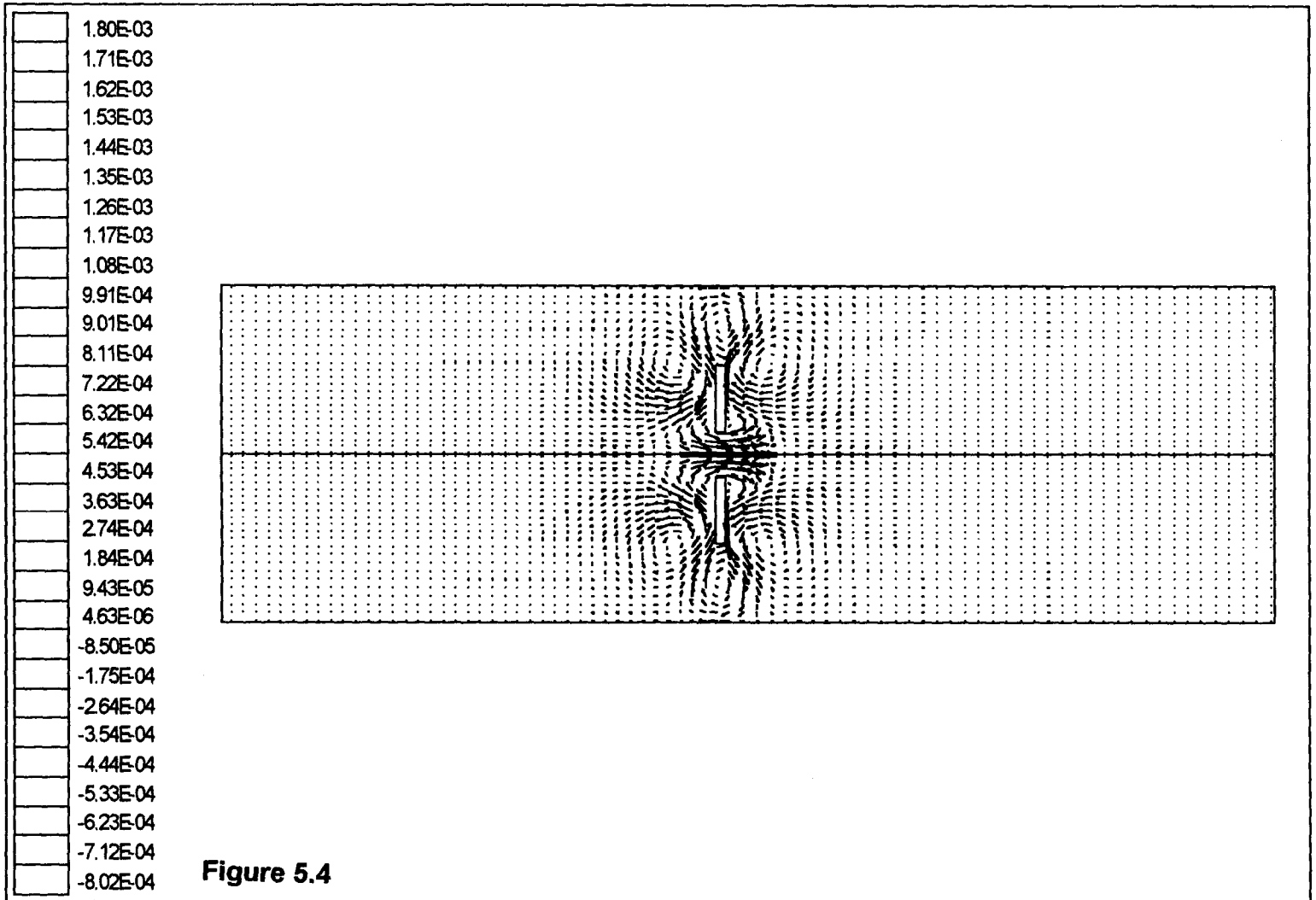
1.80E-03
1.71E-03
1.62E-03
1.53E-03
1.44E-03
1.35E-03
1.26E-03
1.17E-03
1.08E-03
9.91E-04
9.01E-04
8.11E-04
7.22E-04
6.32E-04
5.42E-04
4.53E-04
3.63E-04
2.74E-04
1.84E-04
9.43E-05
4.63E-06
-8.50E-05
-1.75E-04
-2.64E-04
-3.54E-04
-4.44E-04
-5.33E-04
-6.23E-04
-7.12E-04
-8.02E-04
Y
Z X
FLUENT Grid File /* CONFIGURATION = yy1 */
U-Velocity (M/S)
Max = 1.797E-03 Min = -8.021E-04 Time = 4.000E-01
Mar 08 1999
Fluent 4.48
Fluent Inc.

Figure 5.4

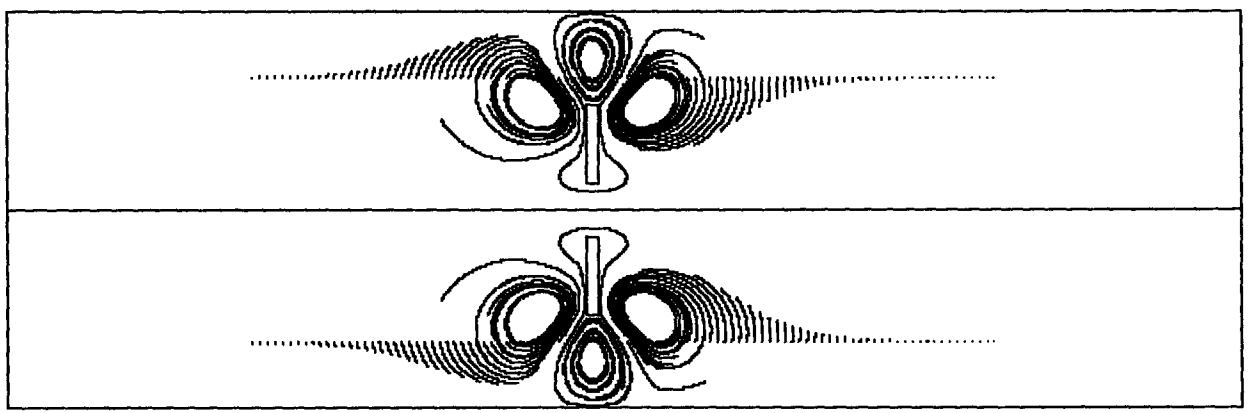

Figure 5.6

Y Z X	FLUENT Grid File /* CONFIGURATION = yy1 */ Streaklines	Mar 08 1999 Fluent 4.48 Fluent Inc.

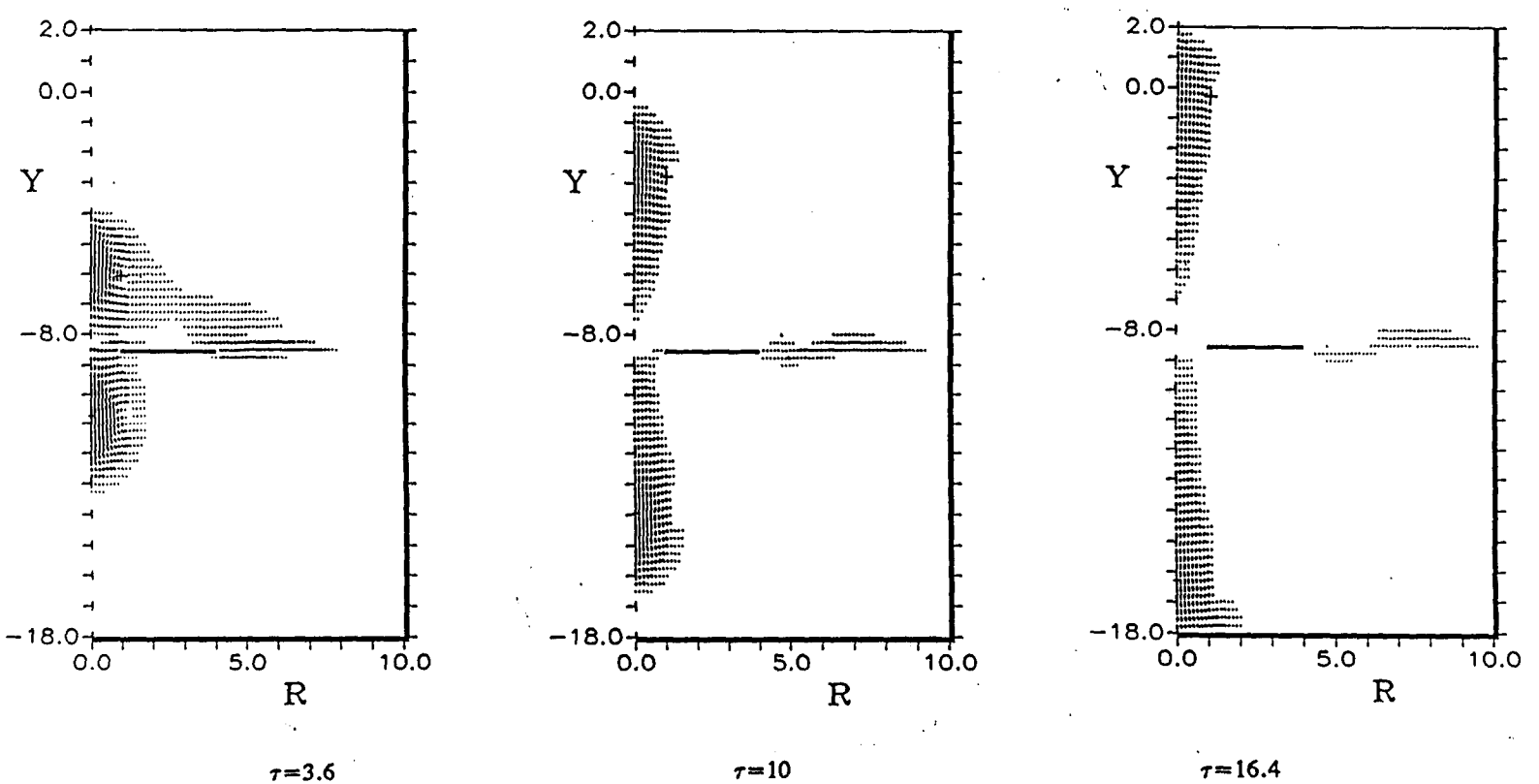

Figure 5.7 A series of velocity vector plots for a orifice plate. Hua (1994)

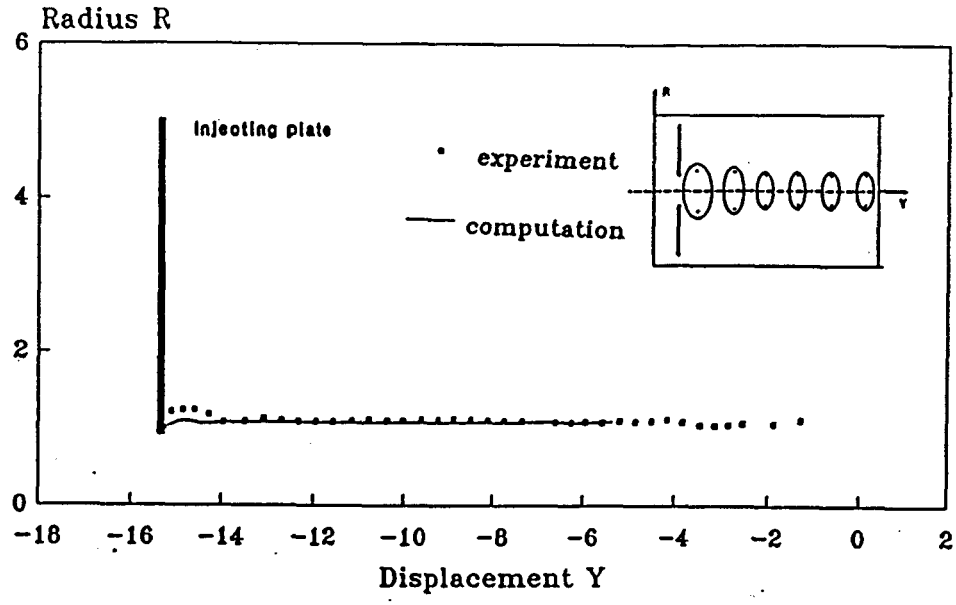

Figure 5.8 (a) Trajectory of vortex ring eye, Re = 2297. Hua (1994)

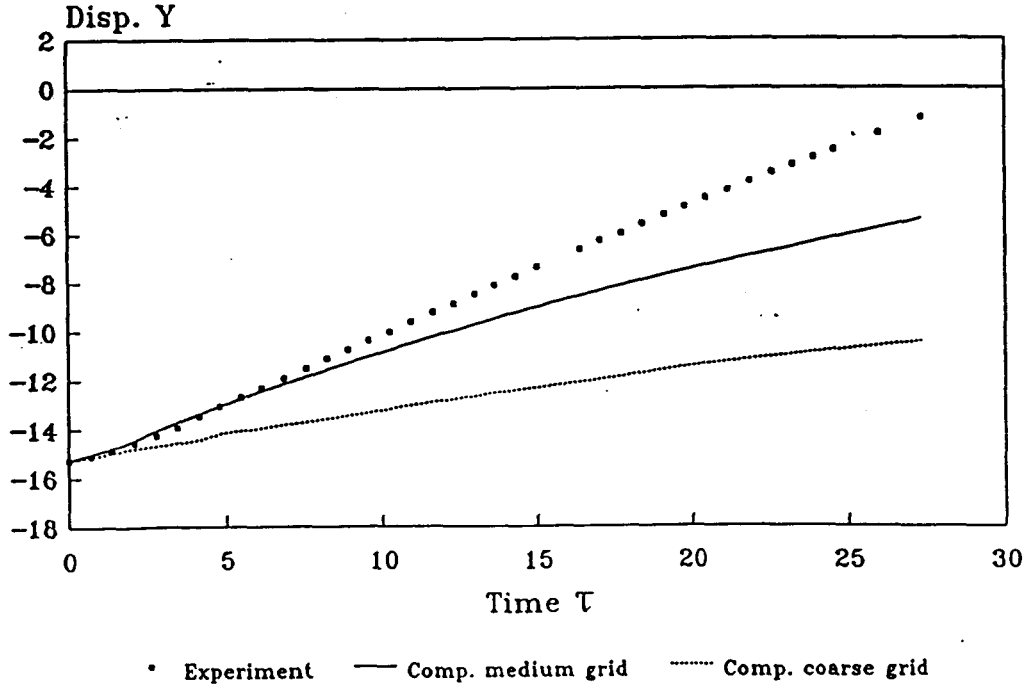

Figure 5.8 (b) Displacement of vortex ring vs. time, Re = 2297. Hua (1994)

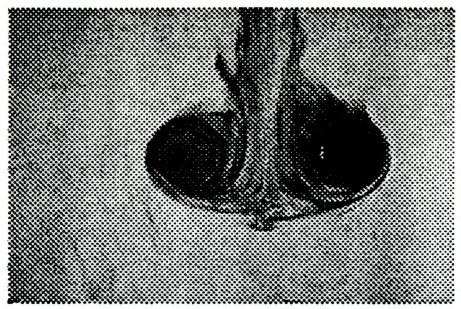

Laminar vortex ring immediately after generation clearly showing a wake

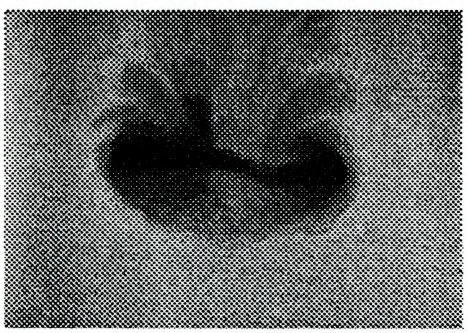

Vortex ring in transition from laminar to turbulent condition, showing wake and ingestion of ambient fluid

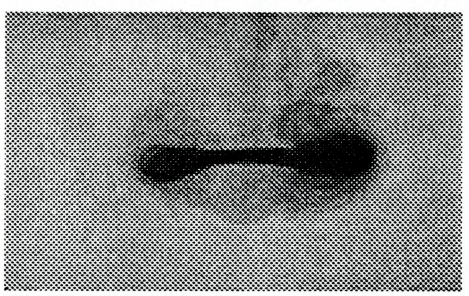

Turbulent vortex ring

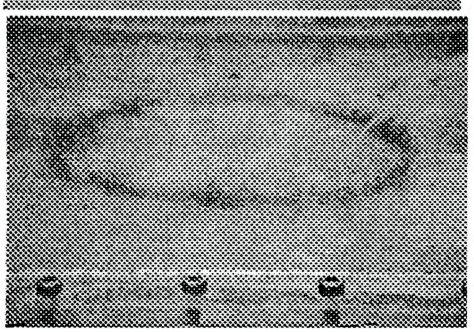

Impact of a vortex ring with a solid boundary(base of vessel)

Figure 5.9 Stages of a vortex ring development

CHAPTER 6

CONCLUSIONS AND RECOMMENDATIONS

6.1 Conclusions

This study was primarily concerned with factors which affect the efficient generation of vortex rings for the purpose of mixing. Of primary concern was the generation phase and the use of baffles to control the motion of a fully formed vortex ring. The results of this study can be summarised as follows:

Firstly, by using a flow visualisation technique which was an improvement over prior methods used in this particular laboratory, it was possible to relatively accurately measure the volume and forward velocity of a vortex ring. The empirical experiments indicated that the translational velocity of a vortex ring is a function of injection velocity. That is, the transnational velocity of a vortex ring increases as the injection velocity increases. However, the rate of increase of the velocity is lower than the rate of increase of the injection velocity and therefore there is not a linear relationship between a vortex ring velocity and the injection velocity. As observed elsewhere, the volume of a vortex ring increases as it travels forward, due to entrainment of ambient fluid into the vortex ring. The initial volume immediately after it is formed at an orifice, did not significantly change with increasing injection velocity. This may at first sight be expected

since the volume ejected from the generating tube is not a function of the injection velocity, however, entrainment from the ambient fluid outside the orifice was expected to occur.

Secondly, numerical simulation of vortex ring generation from a tube generator was done using a laminar model with a non-uniform grid. The simulation data appear to be in good agreement with empirical data. This simulation clearly indicated that the injection velocity profile is an important parameter in the formation and propagation of a vortex ring. It appears that there is a definite relationship between the injection velocity profile and the motion of a vortex ring. The data were fitted with a polynomial of non-dimensional distance versus non-dimensional time for specific injection profiles. It was also apparent from the simulation data that the type of orifice geometry, re-entrant or a tube with an entrance at a plane wall, does not significantly affect vortex ring behaviour. This is somewhat contrary to that expected since fluid is taken into a vortex ring at the generation phase from outside of the tube form which it is being generated. It was found that the FLUENT software will not properly simulate turbulent vortex rings, irrespective of the turbulence model used. In many cases a vortex ring simulated in this way did not form and/or quickly disintegrated, giving no feasible results. However, a laminar model appears to predict the behaviour of a vortex ring irrespective of its state. This may be because a vortex ring is not truly homogeneously turbulent. Visual observations indicate that there appears to be a turbulent central toroidal core

but outside of this region the flow may not be completely turbulent. The use of the laminar model appears to give more reasonable agreement with empirical data than turbulent model.

Thirdly, in order to investigate the possibility of controlling the motion and behaviour of vortex rings, various simple geometries were considered. This was partly done to enhance general mixing in the bulk of the fluid and also to avoid vortex rings erupting energetically from a free surface, which not only can introduce surface gases into the bulk of the fluid but also is a poor mixing mechanism. The simulation demonstrated that a disc type obstruction in the path of a vortex ring can either slow the forward motion of a vortex ring or actually deflect it radially which will greatly enhance the mixing process. The simulation showed that it is possible to control the trajectory of a vortex ring by diameter, location and number of baffles in the path of a vortex ring. Specific non-dimensional vortex ring trajectory graphs were produced which can be useful in the design of vortex ring mixers.

Lastly, the generation and propagation of vortex rings from a flat plate type mixer were simulated using a moving mesh technique. The results of this study explicitly demonstrate that a pair of vortex rings i.e. a primary and a secondary are generated in each half cycle of the plate oscillation. The simulation did not accurately predict the translation velocity, giving slower forward velocities than expected or measured empirically.

6.2 Recommendations

It is recommended that the research on flat plate mixers be continued for a wider range of injection conditions than considered in this study. Of particular interest is the affect of sinusoidal motion compared with a triangular or trapezoidal injection profile. This is because a sinusoidal profile is much more practical than the other types of profile. Also it is essential that the most recent version of FLUENT including GAMBIT should be investigate. These versions may be useful in predicting the effects of baffles oscillating with the drive shaft, which again is a practical configuration. Also, although various generator plat shapes such as conical are being used, these geometries have not been quantitatively investigated. Lastly, it is important to predict the effects of the generation of a stream of vortex rings or a series of cycles of the generator plate, which occurs in actual application. This would be the forerunner of a code for mixing vessels using vortex ring mixers.

REFERENCES

Baird, M. H. I., Wairegi, T. and Loo, H. J., (1977), "Velocity and Momentum of Vortex Rings in Relation to Formation Parameters", The Canadian J. of Chemical Engineering, Vol. 55, pp. 19-26.

Baird, M. H. I., Rohatgi, A. and Wairegi, T., (1979), "Mixing Effects and Hydrodynamics of Vortex Ring", The Canadian J. of Chemical Engineering, Vol. 57, pp. 19 - 26.

Baird (1992), M. H. I., Rama Rao, N. V. and Latto, B., (1992), "Liquid-Liquid Extraction Using vortex Rings in A Batch Cell", Trans. Inst. Chem. Eng., Vol. 70, Part A, pp. 323 - 332.

Carnevale, G. F., Velasco Fuentes, O. U. and Orlandi, P., (1997), "Inviscid Dipole - Vortex Rebound from A Wall or Coast", J. Fluid Mech., Vol. 351, pp. 75 - 103.

Didden, N., (1979), "On the Formation of Vortex Rings: Rolling and Production of Circulation", J. Appl. Math. Phys., Vol. 30, pp. 101 -116.

Eisengam A. H. M., Verzicco, R. and Van Heijst, G. J. F., (1998), "Dynamics of A Vortex Ring Moving Perpendicularly to the Axis of A Rotating Fluid", J. Fluid Mech., Vol. 354, pp. 69 - 100.

Fluent Inc., (1997), "FLUENT User's Manual".

Friebel, W. C. and Rath, H. J., (1987), "The Formation and Behaviour of Laminar Vortex Rings", PHOENICS Users Conference, #1987/56.

Gharib, M., Rambod, E. and Shariff, K., (1998), "A Universal Time Scale for Vortex Ring Formation", J. Fluid Mech., vol. 360, pp. 121-140.

Glezer, A., (1988), "The formation of Vortex Rings", Phys. Fluids, Vol. 31, No. 12, pp. 3532 - 3542.

Hecht, A. M., Bilanin, A. J., Hirsh, J. E., and Snedeker, R. S., (1980), "Turbulent Vortices in Stratified Fluids", AIAAJ., Vol. 18.

Heeg, R. S. and Riley, N., (1997), "Simulations of the Formation of An Axisymmetric Vortex Ring", J. Fluid Mech., vol. 39, pp. 199 - 211.

Ho, S. K., (1991), "An experimental and Numerical Study of the Effects of Surrounding Disturbances on Vortex Ring", M. Eng thesis, McMaster University.

Honji, H. and Tatsuno, M., (1976), "Vortex Rings in a Stratified Fluid", J. Phys. Soc. Japan, Vol. 41, No. 6, pp. 2121 - 2125.

Hua, F., (1994), "Numerical Simulation and Experimental Study of Vortex ring Behavior", Ph.D. Dissertation, McMaster University.

Irmusa, J. Z. and Garris, C. A., (1987), "Influence of Initial and Boundary Conditions on Vortex Ring Development", AIAA J., Vol. 25, No. 3, pp. 371 - 372.

James, S. and Madnia, K., (1996), "Direct Numerical Simulation of A Laminar Vortex Ring", Phus. Fluids, Vol. 8, pp. 2400 - 2414.

Kendig, F., (1972), "The Science of Smoke Rings and Doughnuts", Saturday Review, March 18, pp. 40 - 44.

Lamb, H., (1933), Hydrodynamics. Cambridge University Press.

Latto, B., (1987), "New Mixer for Slurries and Stratified Fluids", Proc. 12th. Int. Conf. on Slurry Tech., Ed. B. Sakkestad, March 1987, pp. 165 -173.

Latto, B., (1989), "The Mixing of Liquids and Slurries Using Novel Vortex Ring (VR) Mixers", LIQUITEC Exposition and Conference, Chicago, Sept. 1989.

Latto, B., M. L. C. Papple, M. Shoukri, and M. H. I. Baird, (1990), "Mixing of Thermally Stratified Fluids By Injecting A Series of Vortex Rings - A Numerical Simulation", Trans IChemE, Vol. 68, Part A, September 1990, pp. 457 - 463.

Latto, B., and Shoukri, M., (1990), Use of vortex Rings for Mixing", Proc. Symp. On Industrial Applications of Fluid Mechanics, ASME WAM Nov.

Latto, B., (1992), "vortex Ring Mixers for slurries and controlled Addition of Gases and Liquids", Proc. 19th Int. Conf. On coal and Slurry Tech.

Linden, P. F., (1973), "The Interaction of a Vortex Ring with a Sharp Density Interface: A Model for Turbulent Entrainment", J. Fluid Mechanics, Vol. 60, Pt. 3, pp. 467 - 480.

Lumley, T., (1997), "Numerical Simulation of Vortex Rings for Mixing Final Report", Baccalaureate Thesis, McMaster University.

Maxworthy, T., (1977), " Some Experimental Studies of Vortex Rings", J. Fluid Mech., Vol. 81, pp. 465 - 495.

Nitsche, M. and Krasny, R., (1994), "A Numerical Study of Vortex ring Formation at the Edge of A Circular Tube", J. Fluid Mech., vol. 276, pp. 139-161.

Papple, M. C. L., Shoukre, M., Latto, B., and Baird, M. H. I., (1991), "Numerical Simulation of The Transport of Vortex Rings in An Initially Stratified Fluid", Chem. Eng. Comm., Vol. 103, pp.167 - 179.

Perrons, R., (1995), "Vortex Ring Mixers: An Empirical Survey of Ring Properties", B. Eng thesis, McMaster University.

Pullin, D., (1979), "Vortex Ring Formation at Tube and Orifice opening", Phys. Fluids, Vol. 22, pp. 401 - 403.

Rao, N. V. R., Latto, B. and Baird, M. H. I. , (1994), "Liquid-Liquid Vortex Rings: Hydrodynamics and Mass Transfer", Trans IchemE, Vol. 72, Part A, July 1994.

Rogers, W. B., (1858), Amer. J. Sci., Vol. 26, pp. 246 - 258.

Saffman, P., (1978), "The Number of Waves on Unstable Vortex Rings", J. Fluid Mech., Vol. 84, pp. 625 - 639.

Stapleton, G., (1996), "Numerical Simulation of Vortex Rings", Baccalaureate Thesis, McMaster University.

Walker, J. D. A., Smith, C. R., Cerra, A. W. and Doligalski, (1987), "Impact of A Vortex Ring on A Wall", J. F. Mech., Vol. 181, pp. 99 - 140.

Weigand, A. and Gharib, M., (1997), "On the Evolution of Laminar vortex Rings", Exps. Fluids, Vol. 22, pp. 447 - 457.